Doctoral Thesis

Cooperative Vehicular Communications for High Throughput Applications

Akihito TAYA

Graduate School of Informatics, Kyoto University

September 2019

Preface

This thesis aims to realize high throughput vehicular communications by cooperation techniques. The development of electrification, artificial intelligence (AI), and diverse sensors have made vehicles highly automated to realize efficient and comfortable transportation, data collection of traffic and road conditions, unmanned construction and disaster relief, and other diverse services. Vehicular communication technologies play an important role in such systems because it is essential for vehicles to communicate with and access the Internet to share and collect data to recognize wide areas. This data sharing requires high-throughput communications and efficient resource sharing because the enormous data gathered by sensors are transmitted by many vehicles. This thesis focuses on cooperation techniques for high-throughput vehicular communications: cooperative multiple-input multiple-output (MIMO) with limited CSI and millimeter wave (mmWave) relay expansion. As an application of high-throughput vehicular communications, cooperative perception is introduced, and a scheduling technique of concurrent transmission is also proposed.

The first topic focuses on cooperative MIMO for vehicular communications. Although the channel capacity of cooperative MIMO increases with the number of cooperative transmitters and receivers, the feedback amount of the channel state information (CSI), which is required to overcome inter-receiver interference, also increases. To reduce the CSI feedback, this thesis proposes a precoding method with limited CSI at transmitters (CSIT) and an iterative MIMO detector, which can detect signals even if the signals interfere with each other. Transmitters with the proposed precoding method require CSIT that is related to only a single receiver. This method reduces the amount of CSI feedback drastically compared with conventional precoding methods. A novel receiver with semi-hard-input and soft-output (SHISO) iterative detecting is also proposed to detect MIMO signals including interfered signals, which cannot be removed by the proposed precoding. The proposed receiver improves the bit error rate (BER) performance by iteration between MIMO detection and Turbo decoding, which updates the log likelihood ratio of transmitted signals.

The second topic focuses on coverage expansion in mmWave multihop networks. It is expected that mmWave communications enable high-throughput vehicular communications. One of the challenges of mmWave communications is lengthening the communication range, because mmWave signals are strongly attenuated by oxygen absorption and severe blockage effects. In order to overcome these problems, this thesis proposes multihop relaying with a reinforcement-learning (RL)-based vehicle position control, which expands the communication range by lengthening mmWave relays. With these long relays, vehicles can access the Internet, even if they are out of coverage of road side units (RSUs). With this position-control system, fewer mmWave RSUs are required because multihop relaying enlarges the coverage. The proposed method can be realized by cooperating with connected and autonomous vehicles (CAVs). RL is a machine learning algorithm with which vehicles can obtain decision-making strategies through experience. Vehicles with the obtained strategy can change their relative positions intelligently to form long mmWave relays. Although each vehicle determines its movement using only the information of its surroundings, the resulting vehicular relay is cooperatively expanded.

The third topic is cooperative perception at intersections. Communication and cooperation between vehicles are important in intersections with poor visibility. One technology that enhances traffic safety is cooperative perception, with which vehicles share their perceptual sensor data (e.g., camera, radar, and light detection and ranging (LiDAR)) and recognize surroundings including blind spots by using the collected data. In order to meet the demand of sharing large amount of high-resolution data, mmWave communications can be utilized. This thesis proposes a concurrent mmWave data sharing with high spatial reuse efficiency. Vehicles cooperatively transfer their sensor data to the surrounding vehicles at an intersection, considering mmWave radio interferences, and send data concurrently if their signals are not interfered.

The chapters of this thesis are as follows. Chapter 1 explains the motivation and background and Chapter 2 introduces related technologies to this work. Chapter 3 proposes a precoding method and an iterative receiver for cooperative MIMO with reduced CSI feedback. Chapter 4 proposes a RL-based vehicle position control for mmWave relay expansion. Chapter 5 proposes a mmWave concurrent transmission scheduling for cooperative perceptions. Finally, Chapter 6 concludes this thesis.

Acknowledgements

First of all, I would like to express my sincere gratitude to my supervisor, Professor Masahiro Morikura, for his continuous support and guidance in my research. Without his persistent help and constant encouragement, this work would have never been completed.

I would like to offer my special thanks to Associate Professor Koji Yamamoto and Assistant Professor Takayuki Nishio, who are members of Integrated-Media Communications Laboratory of Graduate School of Informatics, Kyoto University. Their constructive feedbacks and discussions have helped my work.

I am deeply grateful to Professor Satoshi Denno of Graduate School of Natural Science and Technology, Okayama University and Professor Daisuke Umehara of Faculty of Information and Human Sciences, Kyoto Institute of Technology. Their constructive discussions and insightful comments have made enormous contribution to my work.

I would like to express my deep appreciation to Professor Hiroshi Harada and Professor Ken Umeno of Graduate School of Informatics, Kyoto University for valuable advice and incisive comments. Their advice and comments have been a great help in improving this thesis.

I am also very grateful to laboratory secretaries and student members of Integrated-Media Communications Laboratory of Graduate School of Informatics, Kyoto University. Their considerable support and comments were invaluable.

Finally, I would like to thank my parents and family for their support and encouragement throughout my work.

Contents

1 Introduction **1**

1.1 Motivation 1

1.2 Background 2

1.2.1 Applications with Connected Vehicles 2

1.2.2 Vehicular Communication Techniques and Open Issues . . 3

1.3 Research Challenges 6

1.3.1 Cooperative MIMO with Limited CSI 6

1.3.2 Cooperative mmWave Relay Expansion 8

1.3.3 Cooperative Perception with mmWave Concurrent Transmission 8

1.4 Contributions of This Thesis 9

2 Related Technologies **11**

2.1 Current Vehicular Communications 11

2.1.1 WLAN Based Vehicular Communications 11

2.1.2 Cellular Technology for Vehicular Communications 13

2.2 Technologies toward High-Throughput Vehicular Communications 13

2.2.1 MIMO 14

2.2.2 mmWave Communications 16

2.3 Reinforcement Learning 18

3 Cooperative MIMO with Limited CSI **19**

3.1 Background 19

3.2 System Model 21

3.2.1 MU-MIMO with Cooperating Transmitters 21

3.3 Proposed Method for Reducing CSI 22

3.4 Architecture of Proposed Receiver with Virtual Channels 25
3.4.1 Signal Decomposition with Virtual Channels 25
3.4.2 LLR Calculation of SISO Iterative Receiver 27
3.4.3 LLR Calculation of Proposed SHISO Iterative Receiver . . 29
3.4.4 Extended MAP Estimation for Virtual Channel Detection . 33
3.4.5 Procedure of Proposed SHISO Receiver 34
3.5 Analysis of Proposed Receiver in SU-MIMO Environments 35
3.5.1 SHISO Iterative Receiver 35
3.5.2 Receiver with Proposed Extended MAP Estimation 38
3.6 Simulation Evaluations of Proposed Precoding with Limited CSI . 44
3.7 Conclusions 46

4 Cooperative mmWave Relay Expansion 49
4.1 Background 49
4.2 Related Works 52
4.3 System Model 54
4.4 Distributed Vehicle Movement Controls 57
4.4.1 Motivation for Using Reinforcement Learning 57
4.4.2 Deep-Reinforcement-Learning-Based Algorithm 58
4.4.3 State Designs and Network Models 62
4.5 Simulation Evaluations 64
4.5.1 Simulation Setup 64
4.5.2 Performance of Reinforcement-Learning-Based Method . 66
4.5.3 Comparisons with Other RL Algorithm 73
4.6 Conclusions and Future Works 73

5 Cooperative Perception with mmWave Concurrent Transmission 75
5.1 Background 75
5.2 Related Works 77
5.3 System Model 79
5.4 Data-Sharing Algorithm 82
5.4.1 Vehicular Network Graphs 83
5.4.2 Scheduling Graph and Data-Sharing Scheduling 84
5.4.3 Priority of Transmissions 86

5.4.4 Conflict Rule of Interference 87
5.4.5 Required Time Slot for Complete Data Sharing 89
5.5 Simulation Evaluations 90
5.6 Conclusions and Future Works 97

6 Conclusions **99**

List of Figures

1.1 Cooperative V2X communications. 6
1.2 Iterative MIMO detection and error correction decoding. 7
1.3 Chapter overview. 9

2.1 Protocol stack for DSRC/WAVE. 12
2.2 Cooperative MIMO systems. 14

3.1 System model of cooperative MIMO. 21
3.2 Configuration of the SHISO iterative receiver. 25
3.3 BER performance of the proposed receiver with the different number of iterations. 36
3.4 Empirical CDF of misestimated extrinsic bit LLR. 37
3.5 BER performance of the extended MAP estimation with the different numbers of iterations. 39
3.6 Empirical CDF of misestimated extrinsic bit LLR with the extended MAP estimation. 39
3.7 Performance comparison with Turbo coded detectors. 40
3.8 Performance comparison with conventional detectors. 41
3.9 BER convergence performance of the proposed receiver with the extended MAP estimation when $E_\mathrm{b}/N_0 = 12\,\mathrm{dB}$. 42
3.10 Complexity in terms of the number of multiplications. 43
3.11 Complexity in terms of the number of additions. 43
3.12 BER Performance of the proposed precoding method where $(N_\mathrm{out}, N_\mathrm{in}) = (6, 8)$. 45
3.13 BER performance with various numbers of iterations. 46

4.1 Concept of mmWave relaying with vehicle position controls. . . . 50
4.2 System model of coverage expansion by mmWave relays. 54
4.3 Example of coverage expansion by vehicle movements. 57
4.4 Actor-critic reinforcement learning model. 59
4.5 DNN models of policy and value functions. 63
4.6 Coverage of different state designs when $\lambda = 0.02$ veh/m/lane and $R_{\mathrm{mm}} = 0.4$. 66
4.7 Coverage for different discount factors γ when $\lambda = 0.02$ veh/m/lane, $R_{\mathrm{mm}} = 0.4$, and PTCL is used as the state type. 67
4.8 Accumulated reward for different discount factors γ when $\lambda = 0.02$ veh/m/lane, $R_{\mathrm{mm}} = 0.4$, and PTCL is used as the state type. . 67
4.9 Coverage and accumulated reward as functions of time steps when $\lambda = 0.02$ veh/m/lane, $R_{\mathrm{mm}} = 0.4$, $R_{\mathrm{c}} = 0.5$, and PTCL is used as the state type. 68
4.10 Moving average of coverage and accumulated reward as functions of the number of training episodes. 69
4.11 Coverage performance of models learned in different learning conditions R_{mm} and R_{c} when $\lambda = 0.02$ veh/m/lane. 70
4.12 Coverage of different movable methods when $\lambda = 0.02$ veh/m/lane, $R_{\mathrm{mm}} = 0.4$ and uncontrollable vehicles move at constant velocities. 71
4.13 Coverage of different movable methods when $\lambda = 0.02$ veh/m/lane, $R_{\mathrm{mm}} = 0.4$ and uncontrollable vehicles move at random velocities. 71
4.14 Coverage of different movable methods when $\lambda = 0.01$ veh/m/lane, $R_{\mathrm{mm}} = 1$ and uncontrollable vehicles move at constant velocities. . 72

5.1 System model of data sharing with mmWave concurrent transmissions. 80
5.2 Time frame for data sharing. 81
5.3 Example of scheduling graph. 84
5.4 Normalized perceivable area as a function of the number of time slots when $\left(l_{\mathrm{avg}}, N_{\mathrm{v}}\right) = (40\,\mathrm{m}, 20)$ and beam width is 15°. 92
5.5 Empirical CDF of normalized perceivable area when $\left(l_{\mathrm{avg}}, N_{\mathrm{v}}\right) = (40\,\mathrm{m}, 20)$. 93

5.6 Normalized perceivable area when $\left(l_{\mathrm{avg}}, N_{\mathrm{v}}\right) = (20\,\mathrm{m}, 40), (20\,\mathrm{m}, 20), (40\,\mathrm{m}, 20), (40\,\mathrm{m}, 10)$ and the beam width is 15°. 94
5.7 Normalized perceivable area when $\left(l_{\mathrm{avg}}, N_{\mathrm{v}}\right) = (40\,\mathrm{m}, 20)$ and the beam width is 15° and 30°. 95
5.8 Normalized perceivable area with the different priority designs, when $\left(l_{\mathrm{avg}}, N_{\mathrm{v}}\right) = (40\,\mathrm{m}, 20)$ and beam width is 15°. 95
5.9 Empirical CDF of the number of time slots required to share all data. 96

List of Tables

2.1 Supported PHY data rates in IEEE 802.11p. 12

3.1 Simulation parameters for receiver evaluation in SU-MIMO systems. 36
3.2 Simulation parameters for the precoding method evaluation in MU-MIMO systems. 45

4.1 Parameters of DeepRL-based vehicle position control simulations. 65

5.1 Parameters of mmWave concurrent transmission simulations. . . . 91

Notations

Notation	Description
$\mathbb{R}$	Real numbers
$\mathbb{R}^+$	Positive real numbers
$\mathbb{C}$	Complex numbers
e	Napier's constant
j	Imaginary unit
$\mathrm{Re}[x]$	Real part of x
$\mathrm{Im}[x]$	Imaginary part of x
$\mathbf{O}$	Zero matrix
$\mathbf{I}$	Unit matrix
$\mathbf{A}^{\mathrm{T}}$	Transpose of a matrix $\mathbf{A}$
$\mathbf{A}^{\mathrm{H}}$	Hermitian transpose of a matrix $\mathbf{A}$
$\mathrm{diag}\,[\cdots]$	Diagonal matrix with entries of $[\cdots]$
$\backslash$	Difference of sets
$\emptyset$	Empty set
$\mathcal{N}_{\boldsymbol{G}}(v)$	Neighborhood of a vertex v in a graph $\boldsymbol{G}$
$\min\limits_{\text{constraint}} \{\ldots\}$	Minimum value among $\{\ldots\}$ under the indicated constraint
$\max\limits_{\text{constraint}} \{\ldots\}$	Maximum value among $\{\ldots\}$ under the indicated constraint
$\mathbb{P}\,(A \mid B)$	Conditional probability of A given B
$\mathrm{sgn}[x]$	Sign function, $\mathrm{sgn}[x] = \begin{cases} +1 & (x \geq 0) \\ -1 & (x < 0) \end{cases}$

Abbreviations

Abbreviation	Description
3GPP	Third Generation Partnership Project
5G	fifth generation
A3C	asynchronous advantage actor-critic
AI	artificial intelligence
ARIB	Association of Radio Industries and Businesses
AWGN	adaptive white Gaussian noise
BD	block diagonalization
BER	bit error rate
BPSK	binary phase-shift keying
BRP	beam refinement protocol
CAV	connected and autonomous vehicles
CDF	cumulative distribution function
CNN	convolutional neural network
CSI	channel state information
CSIT	channel state information at transmitters
CSMA/CA	carrier sense multiple access with collision avoidance
C-V2X	cellular vehicular to everything
D2D	device to device
DeepRL	deep reinforcement learning
DNN	deep neural network
DQN	deep Q network
DSRC	dedicated short range communications
EA	evolutionary algorithm
E-SDM	eigenbeam-space division multiplexing

Abbreviation	Description
FC	fully connected
FFT	fast Fourier transform
Gorila	general reinforcement learning architecture
GPS	global positioning system
IFFT	inverse fast Fourier transform
i.i.d	independently and identically distributed
ITS	intelligent transportation system
LiDAR	light detection and ranging
LLR	log likelihood ratio
LOS	line of sight
LTE	long term evolution
LLC	logical link control
MAC	medium access control
MAP	maximum *a posteriori* probability
MDP	Markov decision process
MIMO	multiple-input multiple-output
MIS	maximum independent set
MLD	maximum likelihood detection
MMSE	minimum mean square error
mmWave	millimeter wave
MU-MIMO	multi-user MIMO
MWIS	maximum weighted independent set
NLOS	non line of sight
OFDM	orthogonal frequency division multiplexing
OSD	ordered successive detector
PHY	physical
PT	state design with vehicle position and type
PTCL	state design with vehicle position, type, and continuous relay length
PTDL	state design with vehicle position, type, and discrete relay length
QAM	quadrature amplitude modulation
QPSK	quadrature phase-shift keying
QRM-MLD	QR decomposition and M-algorithm

Abbreviation	Description
RL	reinforcement learning
RoI	region of interest
RSU	road side unit
SC	single carrier
SHISO	semi-hard-input and soft-output
SINR	signal-to-interference plus noise power ratio
SISO	soft-input and soft-output
SLS	sector-level sweep
SODAD	segment-oriented data abstraction and dissemination
SOTIS	self-organizing traffic-information system
SSW	sector sweep
SU-MIMO	single-user MIMO
SVD	singular value decomposition
TDMA-FDD	time division multiple access-frequency division duplex
V2I	vehicle to infrastructure
V2V	vehicle to vehicle
V2X	vehicle to everything
VANET	vehicular adhoc network
V-BLAST	vertical Bell laboratories layered space-time
VFA	virtual force algorithm
WAVE	wireless access in vehicular environment
WLAN	wireless local area network
WSN	wireless sensor networks

Chapter 1

Introduction

1.1 Motivation

Connected and autonomous vehicles (CAVs) not only achieve safe and efficient transportation but also have the potential to provide diverse intelligent services, such as real-time detailed maps, vehicular cloud computing, cooperative perception, and infotainment [1–3]. Many sensors implemented on vehicles help the vehicles perceive and recognize their surrounding environments, such as their positions, objects, and pedestrians around them, as well as traffic signals and information. Vehicular communications enable vehicles to collect information over a wider area, and artificial intelligence (AI)-assisted driving systems leverage the collected data to drive efficiently and safely. Vehicles connected to the Internet not only download data, but also upload their sensor data, which can be a part of big data. The uploaded vehicular big data are used to diagnose road conditions, analyze traffic flows, and enhance the transportation system.

Two well-known protocols are standardized for vehicular communications. One is dedicated short range communications (DSRC) [4, 5], which is based on IEEE wireless local area networks (WLAN) protocols, and the other is cellular vehicle-to-everything (C-V2X) standardized in the third generation partnership project (3GPP) Release 14 [6]. These protocols, however, cannot provide a sufficient data rate for upcoming applications using high-resolution perception data, because they assume small data, such as positions and velocities. In addition, considering that the number of sensors implemented on vehicles is increasing, more efficient communication protocols with higher throughput should be developed. In order to realize these future requirements of vehicular communications, cooperative methods play an important role: data dissemination and relaying to overcome radio attenuation and resource sharing and interference management for effective communications. Moreover, network designs for some cooperative applications should be studied to demonstrate what vehicular communications can achieve. This thesis proposes cooperative V2X communications from the perspective of applications and communication techniques.

1.2 Background

1.2.1 Applications with Connected Vehicles

One of the most important roles of vehicular communication is the realization of much safer driving. Vehicles can avoid traffic accidents by sharing information of their positions, velocities, and other recognized objects (e.g., pedestrians and parked vehicles in blind spots) with each other [7]. Such information can also be used to enhance traffic efficiency. In addition, the control of traffic flows, navigation, and many other services using the vehicle probe data have been studied for a long time.

Another demand of vehicular communication is support for self-driving vehicles. Platooning is an energy efficient self-driving technique with which several vehicles are coordinated into a platoon that follows a leading vehicle within a very close inter-vehicle distance [8, 9]. Coordination techniques can be efficient for intersection management and lane changing in autonomous vehicles, as well [10–12].

Sharing sensor data with surrounding vehicles is called cooperative perception [13]. Autonomous vehicles have many sensors, such as camera, radar, and light detection and ranging (LiDAR) to perceive their surroundings. If a vehicle receives sensor data obtained by other vehicles, it can perceive not only its surroundings, but also the areas around the vehicles that sent the sensor dat; thus, vehicles can recognize other vehicles, pedestrians, and traffic signs in blind spots. For example, see-through systems provide following vehicles with front views of the platoon leader, and bird's-eye-view systems generate top views of surrounding areas by aggregating the perceptual data of multiple vehicles [14, 15]. Such techniques enable vehicles to perceive wide areas accurately, and thus improve traffic safety. Although sharing raw sensor data requires much greater communication capacity than sharing only processed data, such as the positions of recognized objects, sharing raw data has advantages of accurate and detailed recognition.

[2] introduces the concept of vehicular cloud, which provides connected vehicles with computing resources and enables diverse services from routing to content searching, spectrum sharing, dissemination, attack protection, etc. Sensor data collected by vehicles can be also provided by the vehicular cloud and are utilized to analyze vehicular mobility and diagnose road conditions.

Many more applications that require high-capacity communication are listed in [13], e.g., map download, live perceptual data broadcast, sending data for cloud processing, media downloading, and video streaming. Some of the applications mentioned above require high-throughput communication because the shared data size is very large and many vehicles cooperate. Therefore, high-throughput vehicular communication techniques should be developed.

1.2.2 Vehicular Communication Techniques and Open Issues

Vehicular communication has been developed for traffic safety and efficiency. IEEE 802.11p [4,5], also known as DSRC, is an amendment to the IEEE 802.11 standard to add wireless access in vehicular environments (WAVE). IEEE 802.11p uses the 5.9-GHz band and provides a maximum data rate of 27 Mbit/s to support intelligent transportation system (ITS) applications. In contrast to DSRC based on WLAN protocols, another vehicular communication protocol is standardized in 3GPP Release 14, referred to as C-V2X, long-term-evolution (LTE)-V, or LTE-V2X [6]. This standard provides reliable vehicle-to-vehicle (V2V) communications based on LTE sidelink, which was originally standardized as device-to-device (D2D) communication in Release 12. However, these protocols cannot provide sufficient throughput for the upcoming vehicular communication demand. Cooperative perception requires 50–100 Mbit/s per vehicle, and the required total throughput increases with the number of vehicles [13, 16], which exceeds the maximum data rate of DSRC. Therefore, higher-throughput vehicular communications should be developed, such as using cooperative multiple-input multiple-output (MIMO) and millimeter-wave (mmWave) communications.

Cooperative MIMO

Cooperative MIMO (also known as virtual MIMO or distributed MIMO) can be applied to vehicular communications [17,18]. Cooperative MIMO, which increase the total number of antennas in MIMO systems by treating a group of multiple nodes as a single node with many antennas, achieves higher system throughput than single-user MIMO (SU-MIMO) because the channel capacity of the MIMO system increases with the number of antennas [19].

However, cooperative MIMO requires much amount of channel state information (CSI) feedback from receivers to transmitters. In the downlink of cooperative MIMO systems, road side units (RSUs) (i.e., transmitters) precode the signals using CSI to avoid interference. However, CSI can be basically estimated at vehicles (i.e., receivers), and thus, vehicles should feed CSI back to transmitters. The amount of feedback CSI increases rapidly with the number of RSUs when the RSUs require the CSI of whole systems. Therefore, it is very important to reduce the amount of feedback CSI [20].

mmWave Communications

In order to expand bandwidth, mmWave are considered to be a candidate of high-throughput vehicular communications [13, 16, 21, 22]. The IEEE 802.11ad standard uses the unlicensed 60-GHz band. The 28-GHz band is allocated to the fifth generation (5G) mobile communication systems and spectra around 38 GHz and 73 GHz are under consideration. Sub-6-GHz assisted mmWave vehicular communications are also studied in [16].

Although mmWave communications can achieve high-throughput data transmission, their communication ranges tend to be shorter than microwave communications because of their large path losses. This shortens the communication coverage of RSUs. For microwave vehicular communications, multihop relaying has been studied to extend the coverage of RSUs [23–25]. Multihop relaying is significantly more important for mmWave communications because of their short communication range. However, mmWave relaying presents a major challenge in the form of its disconnection problem. In mmWave V2V relaying, the line-of-sight (LOS) path is easily blocked by other vehicles, particularly those without the capability of mmWave relaying. Therefore, mmWave V2V relay networks can be disconnected and fragmented frequently because mmWave signals are severely attenuated by blockages. The disconnection induced by the blockage is critical, particularly in the early diffusion phase of mmWave-available vehicles, where not all vehicles have mmWave communication devices. In such situations, mmWave relays are fragmented and long relays cannot be established, which decreases the efficiency of RSU coverage extensions based on relaying. Hence, relay-expansion techniques should be developed considering blockage effects.

Cooperative Perception with mmWave Communications

One of the most important traffic safety applications facilitated by mmWave communications is cooperative perception. Cooperative perception is particularly important at intersections with poor visibility to avoid car crashes. By sharing information regarding their surroundings, the region that autonomous vehicles can perceive is enlarged based on the shared information. Computer-vision systems enable vehicles to recognize other vehicles, pedestrians, and traffic signs, even if they cannot be seen directly because buildings or other obstacles block the LOS. To cover the entire area surrounding an intersection, vehicles near the intersection should send their massive data to the other vehicles within a short period, in particular 100 ms for safety applications [26]. For example, assume 20 vehicles attempt to share compressed camera images within 100 ms. Data sizes of the images range from 1–9 Mbit because they are generated at rates of 10–90 Mbit/s [21]. Therefore, 20–180 Mbit of data must be transmitted within 100 ms by 20 vehicles, meaning each datum must be transmitted at a rate of 0.2–1.8 Gbit/s. Because DSRC and C-V2X cannot support such high-throughput systems, mmWave communications can be a candidate of cooperative perceptions.

Although mmWave communications enable high-throughput transmission, it is difficult to broadcast data to all vehicles, compared with microwave communications, because few vehicles can receive the transmitted signals because of narrow-beam directional antennas and severe attenuation by blockage effects. In order to increase areas that vehicles can recognize, as much data as possible should be shared among many vehicles. Hence, development of an efficient data-sharing scheme is needed.

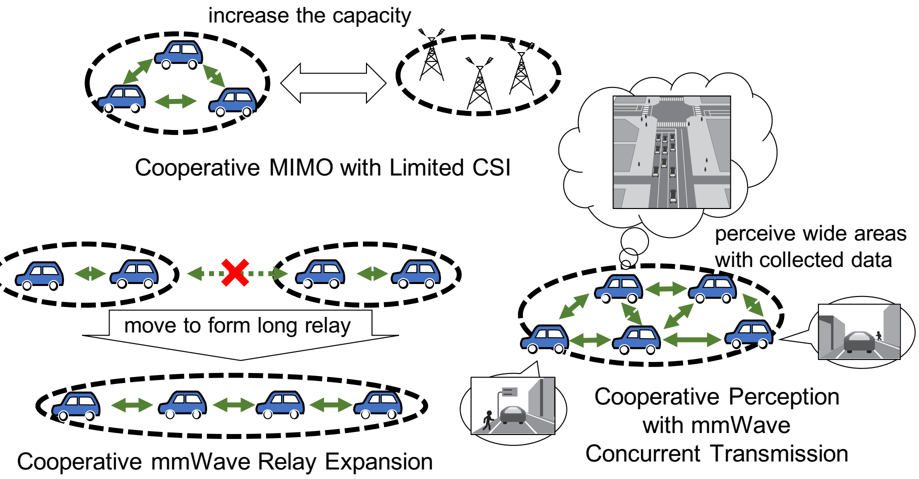

Figure 1.1: Cooperative V2X communications.

1.3 Research Challenges

To solve the problems described in the previous section, three topics shown in Figure 1.1 are discussed in this thesis. Two techniques for cooperative V2X networking to realize high-throughput communications are proposed. One is cooperative MIMO with reduced CSI feedback, and the other is a cooperative relay expansion for mmWave networks. This thesis also proposes a mmWave communication technique for a specific cooperative application: cooperative perception.

1.3.1 Cooperative MIMO with Limited CSI

As described in Section 1.2.2, CSI feedback from the receivers to transmitters is required to avoid interference in a common cooperative MIMO system. The amount of CSI feedback increases with the number of transmitters, which makes it difficult to increase the capacity of cooperative MIMO systems. In order to achieve high-throughput communications, this thesis provides a precoding scheme with limited CSI that allows interference and a receiver that can decode the desired signals, even if the signals interfere with each other. In the proposed system, each receiver selects a transmitter and the receiver feeds back partial CSI only to the associated transmitter to reduce a feedback overhead, while the all transmitters require CSI of whole systems in common cooperative MIMO to prevent inter-

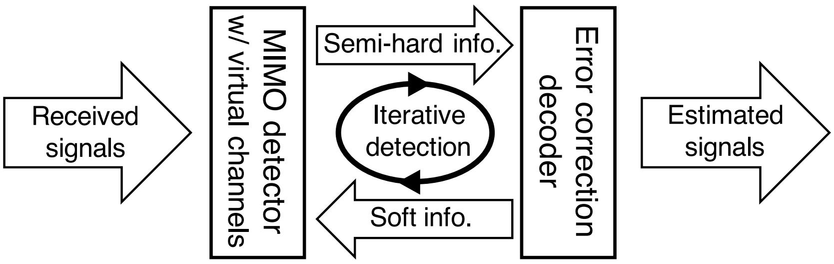

Figure 1.2: Iterative MIMO detection and error correction decoding.

receiver interference.

Because the received signals include inter-receiver interference, the receivers should remove the interference. The proposed receivers regard the interference signal for other receivers as the desired signals, which means the system can be considered as an overloaded MIMO system, where the number of spatially multiplexed streams is greater than that of receive antennas. Although, many MIMO detectors has been developed, e.g., minimum mean square error (MMSE) filters, ordered successive detectors (OSDs), eigenbeam-space division multiplexing (E-SDM), and the maximum likelihood detection (MLD) with QR decomposition and M-algorithm (QRM-MLD) [27], these schemes with linear filters cannot detect MIMO signals when the number of streams is greater than the number of receive antennas. To overcome overloaded environments, the concept referred to as "virtual channels" is applied. Virtual channel detection is a non-linear MIMO signal detection that can detect signals even when the number of transmitted streams is greater than the number of receiver antennas.

The proposed receiver also adopts an iterative scheme to improve signal-estimation accuracy. The iterative-detection scheme is shown in Figure 1.2. The MIMO detector estimates MIMO signals using log likelihood ratios (LLRs) as *a priori* information and outputs detected signals to the error correction decoder. The error correction decoder calculates LLRs of data bits and feeds them back to the MIMO detector, which detects MIMO signals again using the updated LLRs. Although common iterative detecting schemes, which are called soft-input and soft-output (SISO), transfer LLRs between the MIMO detector and the error correction decoder, SISO receivers do not achieve high performance with virtual channels; thus, the MIMO detector with virtual channels output detected signals and they are inputted into the error correction decoder. This iterative scheme is referred to as a semi-hard-input and soft-output (SHISO) in this thesis.

1.3.2 Cooperative mmWave Relay Expansion

This thesis proposes a distributed vehicle position control method that expands coverage by establishing long relay paths. This is realized by a scheme through which autonomous vehicles can change their relative positions to communicate with each other via LOS paths. Even though vehicles with the proposed method do not use all the information of the environment and do not cooperate with each other, they can decide their actions (e.g., lane changing and overtaking) and form long relays using only information of their surroundings (e.g., surrounding vehicle positions). The decision-making problem is formulated as a Markov decision process, such that autonomous vehicles can learn a practical movement strategy for developing long relays via a reinforcement learning (RL) algorithm. This thesis designs a learning algorithm based on a sophisticated deep reinforcement learning algorithm, asynchronous advantage actor-critic (A3C), which enables vehicles to learn a complex movement strategy quickly through its deep neural network (DNN) architecture and multi-agent-learning mechanism. Once the strategy is well trained, vehicles can move independently to establish long relays and connect to the RSUs via the relays.

1.3.3 Cooperative Perception with mmWave Concurrent Transmission

This thesis proposes an efficient data-sharing algorithm based on mmWave concurrent transmissions for cooperative perception. In order to realize high system throughput and short delay, concurrent transmission and forwarding with cached data are applied to the proposed algorithm. Concurrent transmission, where many transmitters send data to different receivers simultaneously, promotes efficient spatial reuse, which is realized by leveraging the antenna directionality and high attenuation. On the other hand, forwarding with cached data reduces redundant transmissions for data sharing in multihop networks because each datum is requested to be sent to many different vehicles. In multihop networks, if relay vehi-

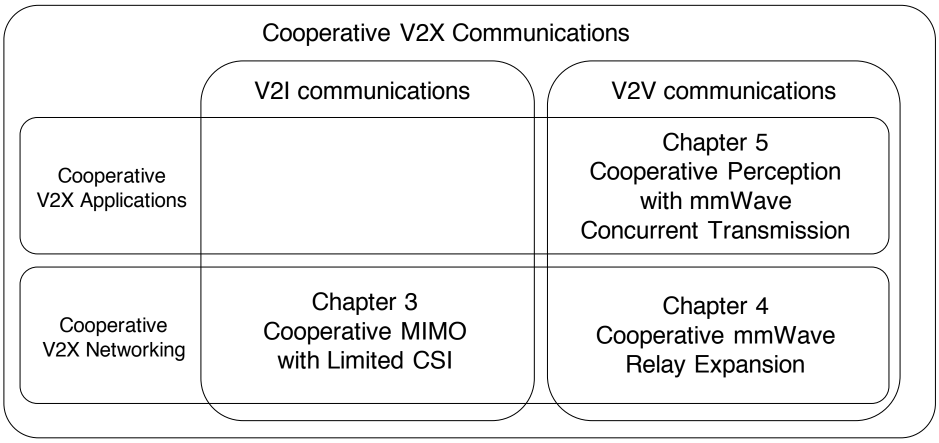

Figure 1.3: Chapter overview.

cles store the forwarded data, the source vehicles do not need to transmit the same data many times. Leveraging the geographical information in perceptual data also helps enlarge the perceivable regions. Therefore, a data-sharing algorithm that employs a graph-based concurrent transmission scheduling is developed. To realize concurrent transmission and improve spatial reuse, "conflict rules" are designed to determine whether the two pairs of transmitters and receivers interfere with each other by considering the radio propagation characteristics of narrow-beam antennas. A prioritization method that considers the geographical information in perceptual data is also designed to enlarge perceivable areas in situations where data-sharing time is limited and not all data can be shared.

1.4 Contributions of This Thesis

The chapter overview of this thesis is shown in Figure 1.3. Chapter 3 proposes a precoding method with limited CSI and a receiver with an iterative MIMO detecting scheme for cooperative MIMO systems. With the proposed method, the amount of CSI feedback can be reduced. The simulation results verify that the proposed receiver can detect MIMO signals, even if the signals are interfering with each other and the number of received signal streams exceeds the number of receivers.

A cooperative mmWave relay expansion is tackled in Chapter 4. It enables vehicles to change their relative positions to expand relays avoiding blockages. The simulation results confirm that the proposed RL-based algorithm achieve higher performance than conventional algorithms. The proposed algorithm is also robust to the traffic conditions (e.g., vehicle density and the ratio of mmWave-communicable vehicles).

A cooperative sharing with mmWave concurrent transmissions is discussed in Chapter 5. The proposed algorithm realizes concurrent transmission considering antenna directionality, and thus improves the spatial reuse efficiency. This chapter proves that all the sensor data can be shared among the participating vehicles in finite steps with the proposed algorithm. The simulation results verify that the proposed algorithm enlarges the area that vehicles can perceive through the shared sensor data more rapidly than conventional algorithms that do not consider antenna directionality. The prioritization method also improves the rate of enlarging the perceivable area.

Chapter 2

Related Technologies

2.1 Current Vehicular Communications

Vehicular communication protocols have been studied for traffic safety and efficient transportation. Although the currently available standards do not support multi-Gbit/s communications, they enable sharing small data, such as positions, velocities, destinations, and control messages. This section describes two categories of vehicular communications.

2.1.1 WLAN Based Vehicular Communications

WLAN realizes the direct communication among vehicles which is suitable for V2V applications. DSRC is designed to support a variety of vehicular communication applications. The IEEE 802.11p standard, which is an amendment to the IEEE 802.11 standards, is employed for the physical (PHY) and the medium access control (MAC) layers of DSRC in the United States. The IEEE 1609.x series of standards supports the higher layers, e.g., security management, networking, and multi-channel operations, for WAVE [5, 28, 29]. The protocol stack for DSRC/WAVE is shown in Figure 2.1. Because IEEE 802.11p uses a 10-MHz bandwidth, which is half that of IEEE 802.11a, the data rate is also half that of IEEE 802.11a. The supported PHY data rates in IEEE 802.11p is shown in Table 2.1. The supported modulation schemes on each sub-carrier which constitutes orthogonal frequency division multiplexing (OFDM) are binary phase-shift

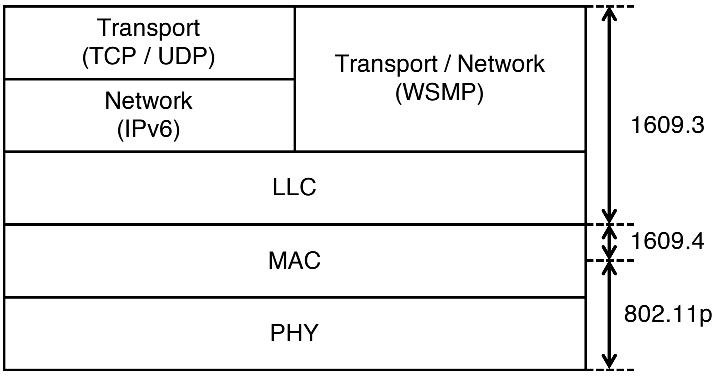

Figure 2.1: Protocol stack for DSRC/WAVE.

Table 2.1: Supported PHY data rates in IEEE 802.11p.

Modulation	Code rate	Data rate
BPSK	1/2	3 Mbit/s
BPSK	3/4	4.5 Mbit/s
QPSK	1/2	6 Mbit/s
QPSK	3/4	9 Mbit/s
16-QAM	1/2	12 Mbit/s
16-QAM	3/4	18 Mbit/s
64-QAM	2/3	24 Mbit/s
64-QAM	3/4	27 Mbit/s

keying (BPSK), quadrature phase-shift keying (QPSK), 16-quadrature amplitude modulation (QAM), and 64-QAM for modulation. The 5.9-GHz band is allocated for IEEE 802.11p in the United States. With the IEEE 1609.4 standard, vehicles can exchange safety messages every 100 ms in the default value [4]. Therefore, vehicles know the information of their surrounding vehicles, e.g., positions and velocities, which can be utilized by the high-throughput communicate systems introduced in Chapter 4.

The Association of Radio Industries and Businesses (ARIB) standardized the vehicle-to-infrastructure (V2I) protocol, STD-T75, which utilizes the 5.8-GHz band [30] in Japan. STD-T75 uses a time division multiple access-frequency division duplex (TDMA-FDD) scheme for the multiple access method and an adaptive slotted ALOHA for the access control method. Two data rates are supported: 1 Mbit/s and 4 Mbit/s. ARIB STD-T109, which uses the 700-MHz band, is also available for ITS in Japan [31]. ARIB STD-T109 supports both V2I and V2V communications by using carrier sense multiple access with collision avoidance (CSMA/CA) for the access method. The maximum data rate is 18 Mbit/s.

2.1.2 Cellular Technology for Vehicular Communications

Using the licensed radio bands, cellular-assisted vehicular communication systems realize managed resource scheduling. Therefore, they suit for safety applications, e.g., avoiding traffic accidents. The 3GPP standardized vehicular communication protocols, called C-V2X, LTE-V, or LTE-V2X [6]. C-V2X supports both V2I communications using a cellular interface and V2V communications based on LTE sidelink, which was introduced for safety-related D2D communications in 3GPP Release 12. Because V2X applications require more reliable and low-latent protocols than D2D communications, Release 14 introduces additional two communication modes. In mode 3, two vehicles directly communicate with each other, but resource scheduling is managed by cellular infrastructure, i.e., eNodeB. In mode 4, vehicles manage resources by themselves and thus, communication can be performed in the absence of cellular network coverages. V2X application-layer services are also discussed in 3GPP Release 16, which is currently studied.

2.2 Technologies toward High-Throughput Vehicular Communications

Although communication standards described in the previous section can be applied to some V2X applications, they cannot support high-throughput applications, e.g., cooperative perceptions. This section explains two technologies that can be applied to high-throughput vehicular communications.

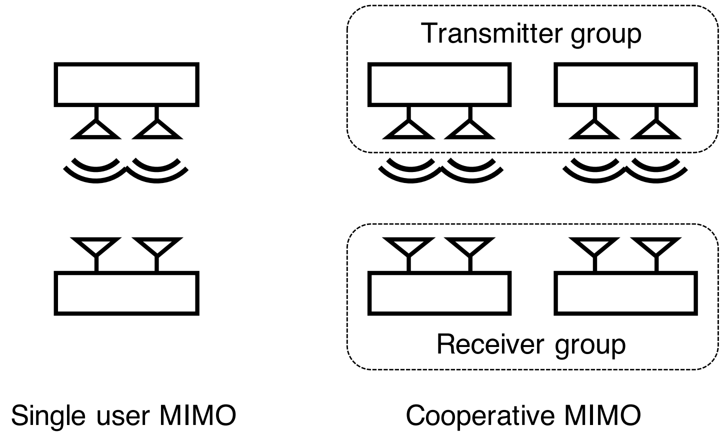

Figure 2.2: Cooperative MIMO systems.

2.2.1 MIMO

MIMO is a fundamental technique employed in Wi-Fi (IEEE 802.11n/ac) and cellular networks (LTE, WiMAX, and 5G) because of its high throughput and spectral efficiency. In MIMO systems, transmitters send multiplexed data streams from multiple transmit antennas and receivers separate them using multiple receive antennas to increase the system throughput by leveraging diversity gain of multiple antennas.

Cooperative MIMO

In order to further increase the system throughput, cooperative MIMO, which is also called distributed MIMO, has been developed. Models of cooperative MIMO are shown in Figure 2.2. Both multiple transmitters and receivers constitute groups, each of which can be regarded as a single node. Because the resulting virtual MIMO system has more antennas than single-user systems, the system throughput is increased. Multi-user MIMO (MU-MIMO) systems can be regarded as a specific case of cooperative MIMO, where there is a single transmitter and a receiver group consists of multiple receivers.

Block Diagonalization Precoding

Block diagonalization (BD) precoding is a technique introduced in MU-MIMO systems of avoiding inter-receiver interference [32], which is also applied to co-operative MIMO, where there are multiple transmitters. Let M_{T}, M_{R}, n_{T}, and n_{R} denote the number of transmitters and receivers and the number of antennas of each transmitter and receiver, respectively. A receive signal vector $\mathbf{Y}_i \in \mathbb{C}^{n_{\mathrm{R}}}$ at receiver i is expressed as follows:

$$\mathbf{Y}_i = \sum_{j=1}^{M_{\mathrm{T}}} \mathbf{H}_{ij}\mathbf{X}_j + \mathbf{N}_i, \tag{2.1}$$

or

$$\begin{bmatrix} \mathbf{Y}_1 \\ \vdots \\ \mathbf{Y}_{M_{\mathrm{R}}} \end{bmatrix} = \begin{bmatrix} \mathbf{H}_{11} & \cdots & \mathbf{H}_{1M_{\mathrm{T}}} \\ \vdots & \ddots & \vdots \\ \mathbf{H}_{M_{\mathrm{R}}1} & \cdots & \mathbf{H}_{M_{\mathrm{R}}M_{\mathrm{T}}} \end{bmatrix} \begin{bmatrix} \mathbf{X}_1 \\ \vdots \\ \mathbf{X}_{M_{\mathrm{T}}} \end{bmatrix} + \begin{bmatrix} \mathbf{N}_1 \\ \vdots \\ \mathbf{N}_{M_{\mathrm{R}}} \end{bmatrix}, \tag{2.2}$$

where $\mathbf{X}_j \in \mathbb{C}^{n_{\mathrm{T}}}$, $\mathbf{H}_{ij} \in \mathbb{C}^{n_{\mathrm{R}} \times n_{\mathrm{T}}}$, and $\mathbf{N}_i \in \mathbb{C}^{n_{\mathrm{R}}}$ represent a transmitted signal vector from transmitter j, a channel matrix from transmitter j to receiver i, and an adaptive white Gaussian noise (AWGN) vector at receiver i, respectively. Here, define $\mathbf{H}_i$ and $\mathbf{H}^{(i)}$ as follows:

$$\mathbf{H}_i \coloneqq \begin{bmatrix} \mathbf{H}_{i1} & \cdots & \mathbf{H}_{iM_{\mathrm{T}}} \end{bmatrix}, \tag{2.3}$$

$$\mathbf{H}^{(i)} \coloneqq \begin{bmatrix} \mathbf{H}_1^{\mathrm{T}} & \cdots & \mathbf{H}_{(i-1)}^{\mathrm{T}} \; \mathbf{H}_{(i+1)}^{\mathrm{T}} & \cdots & \mathbf{H}_{M_{\mathrm{R}}}^{\mathrm{T}}, \end{bmatrix}^{\mathrm{T}} \tag{2.4}$$

where $[\cdot]^{\mathrm{T}}$ is the transpose of $[\cdot]$. In the BD precoding, data signals are precoded to transmission signals using precoding matrices $\tilde{\mathbf{V}}_i \in \mathbb{C}^{M_{\mathrm{T}} n_{\mathrm{T}} \times n_{\mathrm{S}}}$ lying in the null space of $\mathbf{H}^{(i)}$, where $n_{\mathrm{S}} = M_{\mathrm{T}} n_{\mathrm{T}} - M_{\mathrm{R}} n_{\mathrm{R}} + n_{\mathrm{R}}$. Precoding matrices can be obtained using singular value decomposition (SVD). Data signal vector $\mathbf{D}_i \in \mathbb{C}^{n_{\mathrm{S}}}$, which is sent to receiver i, is precoded to $\mathbf{X}$ by $\tilde{\mathbf{V}}_i$ as $\mathbf{X} = \begin{bmatrix} \tilde{\mathbf{V}}_1 & \cdots & \tilde{\mathbf{V}}_{M_{\mathrm{R}}} \end{bmatrix} \begin{bmatrix} \mathbf{D}_1^{\mathrm{T}} & \cdots & \mathbf{D}_{M_{\mathrm{R}}}^{\mathrm{T}} \end{bmatrix}^{\mathrm{T}}$, and the transmission signals from each transmitter are defined to satisfy $\mathbf{X} = \begin{bmatrix} \mathbf{X}_1^{\mathrm{T}} & \cdots & \mathbf{X}_{M_{\mathrm{T}}}^{\mathrm{T}} \end{bmatrix}^{\mathrm{T}}$. Because $\tilde{\mathbf{V}}_i$ lies in the null space of $\mathbf{H}^{(i)}$, $\mathbf{H}_i \tilde{\mathbf{V}}_{i'} = \mathbf{O}$ for $i \neq i'$, where $\mathbf{O}$ is a zero matrix. Therefore, (2.2) is rewritten as follows:

$$\begin{bmatrix} \mathbf{Y}_1 \\ \vdots \\ \mathbf{Y}_{M_\mathrm{R}} \end{bmatrix} = \begin{bmatrix} \mathbf{H}_1 \\ \vdots \\ \mathbf{H}_{M_\mathrm{R}} \end{bmatrix} \begin{bmatrix} \tilde{\mathbf{V}}_1 & \cdots & \tilde{\mathbf{V}}_{M_\mathrm{R}} \end{bmatrix} \begin{bmatrix} \mathbf{D}_1 \\ \vdots \\ \mathbf{D}_{M_\mathrm{R}} \end{bmatrix} + \begin{bmatrix} \mathbf{N}_1 \\ \vdots \\ \mathbf{N}_{M_\mathrm{R}} \end{bmatrix} \tag{2.5}$$

$$= \begin{bmatrix} \mathbf{H}_1\tilde{\mathbf{V}}_1 & & \mathbf{O} \\ & \ddots & \\ \mathbf{O} & & \mathbf{H}_{M_\mathrm{R}}\tilde{\mathbf{V}}_{M_\mathrm{R}} \end{bmatrix} \begin{bmatrix} \mathbf{D}_1 \\ \vdots \\ \mathbf{D}_{M_\mathrm{R}} \end{bmatrix} + \begin{bmatrix} \mathbf{N}_1 \\ \vdots \\ \mathbf{N}_{M_\mathrm{R}} \end{bmatrix}, \tag{2.6}$$

$$\mathbf{Y}_i = \mathbf{H}_i\tilde{\mathbf{V}}_i\mathbf{D}_i + \mathbf{N}_i. \tag{2.7}$$

Regarding $\mathbf{H}_i\tilde{\mathbf{V}}_i$ as a channel matrix, each receiver can detect data signal $\mathbf{D}_i$ with common MIMO detection schemes. When using precoding schemes, including the BD precoding, transmitters require channel matrices, which is referred to as CSI, which is estimated at receivers. Therefore, the estimated CSI should be fed back in uplink before data is transmitted in downlink. This feedback process can be an overhead for cooperative MIMO systems. Chapter 3 tackles this problem using the precoding method with limited CSI.

2.2.2 mmWave Communications

MmWave communications enable high-throughput transmission because wide bandwidth can be allocated to the mmWave bands. Therefore, it can be applied to high-throughput V2X applications. The characteristics of mmWave propagation is provided in this section.

Characteristics of mmWave Propagation

In free space, the received power can be derived from the Friss transmission formula [33]. Assume that there are transmission and receive antennas with gain G_t and G_r, respectively, and that the distance of these antennas is denoted by d. If these antennas have LOS and face with each other, the received power P_r is derived as follows:

$$P_\mathrm{r} = P_\mathrm{t}G_\mathrm{t}G_\mathrm{r}\left(\frac{c}{4\pi df}\right)^2, \tag{2.8}$$

where P_t, f, and c denote the transmission power, carrier frequency, and the speed of light, respectively. Because mmWave communications utilize higher carrier frequency f than that of microwave communications, the received power P_r becomes smaller if the transmission power and antenna gains are fixed.

There are some effects that cause attenuation in mmWave propagation. Blockage is an important effect because mmWave radio has the poor diffraction capability and high penetration loss. Therefore, it is better to establish LOS path between the transmitter and receiver to achieve high-data-rate transmission. Oxygen absorption also causes mmWave propagation loss. The oxygen absorption level depends on the frequency and it peaks at around 60 GHz.

In order to overcome these attenuation, directional beamforming can be leveraged. Because of the short wavelength, high-gain array antennas with beam steerable capability are utilized. In addition, the high mmWave propagation loss and directional antennas achieve high spatial reuse. Chapter 5 aims to take advantages of spatial reuse by concurrent transmissions.

Current mmWave Standards

IEEE 802.11ad is a currently available mmWave communication standard that uses the 60-GHz band. It was developed to support high-throughput applications, such as uncompressed video streaming. Data rates up to 4.6 Gbit/s with single carrier (SC) and 6.7 Gbit/s with OFDM are supported. Differential BPSK, $\pi/2$-BPSK, $\pi/2$-QPSK, and $\pi/2$-16QAM are utilized as modulation schemes in SC mode. Four channels with 2.16-GHz bandwidth each are available in Japan.

In IEEE 802.11ad, narrow-directional antenna is used to obtain high gain because the path loss of mmWave radio is very large. Beamforming training consists of two phases in IEEE 802.11ad: sector-level sweep (SLS) and beam refinement protocol (BRP). SLS is performed at first using the transmitting sector sweep (SSW) frame. Then, BRP may follow to train a receiver with iterative refinement between the transmitter and the receiver, whereas only the transmitter is trained in SLS.

2.3 Reinforcement Learning

RL, which is one of the machine learning schemes, has been developed to solve the problem of mapping from situations to actions so as to maximize a reward in an environment [34, 35]. In RL, an agent learns the mapping, referred to as a strategy or a policy, by performing actions and observing the results of the actions in the environment, and finally obtain a good strategy to maximize the cumulative rewards. In other words, an agent learns the optimal strategy through a trial-and-error process.

Table-based Q-learning is a basic and the most widely used RL algorithms because it is guaranteed to solve the simple Markov decision process (MDP). However, it cannot be applied to large-scale problems due to the limitation of computational memory capacity. In order to solve this problem, function approximations can be leveraged. Although convergence is not guaranteed when nonlinear function approximation is used to represent the strategy, recent studies revealed that RL using a DNN for function approximation can solve large-scale problems, such as video games [36] and the ancient board game Go [37]. Deep Q Network (DQN) [36] is one of the most famous deep RL (DeepRL) algorithms. DQN utilizes DNN to approximate an action-value function, whose outputs are an expectation of cumulative rewards. Moreover, multi-process learning algorithms, such as general reinforcement learning architecture (Gorila) [38] and A3C [39], have been developed to improve the convergence efficiency and learning speed of DeepRL. In A3C, multiple agents learn their strategies in independent environments and asynchronously share the strategies.

Chapter 3

Cooperative MIMO with Limited CSI

3.1 Background

A high-speed wireless access network is needed for CAVs to download wide-area traffic information via the Internet. Cooperative MIMO systems have been studied for realizing high-data-rate vehicular communication [17, 18]. In cooperative MIMO, CSI, which is required at transmitters to avoid interference, is fed back from the receivers to the transmitters, and the amount of feedback CSI increases rapidly with the number of cooperating transmitters when the transmitters need full CSI. Because the wireless channel resources are limited, it is very important to reduce the amount of feedback CSI [20]. Another problem of cooperative MIMO is that all transmitters need to share data and send them in the same frame. It becomes more difficult to solve this problem when the number of transmitters increases.

In order to overcome the above-mentioned problems, this chapter proposes a method for reducing the amount of feedback CSI. When this method is used, receivers selects some of the transmitters and feed back partial CSI that is relevant to the selected transmitter. Because limited CSI at transmitters (CSIT) causes signal interference, this chapter also proposes a novel receiver using the concept of a "virtual channel" in order to overcome the interference. A "virtual channel," which divides signals into real-signal elements and phase elements, has been developed for SU-MIMO systems so that signals can be detected even when the number of their streams exceeds the number of receive antennas [40]. Some receivers have been proposed that can be applied in MIMO systems where the number of the spatially multiplexed streams is more than that of receive antennas [41,42]. These non-linear detectors achieve superior performance in contrast with linear detectors where the number of spatially multiplexed streams is more than that of the receive antennas. The detector with "virtual channels" is one of the non-linear detectors that achieves superior performance with reasonable complexity even when the number of the streams is twice as many as that of the receive antennas [40,43,44].

In addition, this chapter proposes an iteration scheme for improving the bit error rate (BER) performance. In the iterative scheme, virtual channel detectors estimate signals by using the LLR of coded bit streams calculated at error correction decoders, and output the LLR of transmitted signals. Although the SISO iterative receiver composed of the MIMO detector with virtual channels and the convolutional decoder has been proposed [40], Turbo codes [45] is applied to the proposed receiver to further improve the BER performance. Turbo codes have been considered to combine with MIMO detectors in [46–49], because Turbo codes are powerful to improve transmission performance. However, even if Turbo decoders are applied to the SISO iterative receiver with the MIMO detector with the virtual channel detection, the performance is not improved, which is shown by the simulation evaluation. Therefore, a semi-hard-input soft-output (SHISO) iterative scheme which fully exploits the potential gain of Turbo decoders is designed in order to achieve superior performance.

Basically, the SHISO iterative receiver comprises a MIMO detector with virtual channel detection and the Turbo decoder, between which signals are exchanged iteratively. In the SHISO receiver, the extrinsic information is fed back from the Turbo decoder to the MIMO detector, and the MIMO detector estimates the phase on the maximum *a posteriori* probability (MAP) estimation with the extrinsic information. However, the hard decision signal of the phase is provided to the Turbo decoder, whilst the OSD output signals are fed to the decoder. This SHISO iteration is a key idea to improve the performance. Moreover, a new criterion,"Extended MAP estimation," is developed for the proposed receiver to select the most likely virtual channel for further improving the transmission performance with little additional complexity.

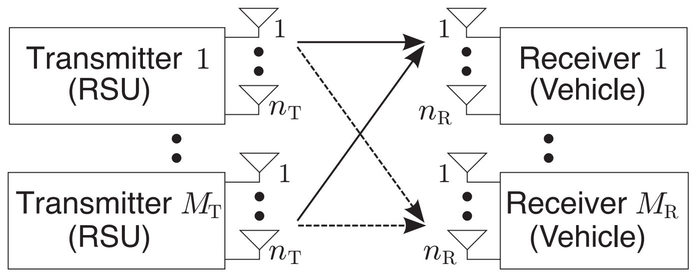

Figure 3.1: System model of cooperative MIMO.

The rest of this chapter is structured as follows: Section 3.2 introduces a model of a cooperative MIMO system. Section 3.3 proposes a precoding method with limited CSI and Section 3.4 describes a configuration of the proposed iterative receiver with virtual channels. The performance of the proposed receivers is evaluated in SU-MIMO environments in Section 3.5, and then, the performance of the proposed precoding method for cooperative MIMO is evaluated in Section 3.6. Finally, Section 3.7 presents concluding remarks.

3.2 System Model

3.2.1 MU-MIMO with Cooperating Transmitters

A system with M_T transmitters and M_R receivers is shown in Figure 3.1. This thesis considers the downlink of the system. Each transmitter has n_T antennas, and each receiver has n_R antennas. The sum of the transmission and receive antennas is represented as $N_T = M_T n_T$ and $N_R = M_R n_R$, respectively, and the sum of the transmitted streams to one of the receiver is represented as n_S.

At the transmitters, data bit streams are encoded using a Turbo code, interleaved, and modulated to QPSK signals. The signals are then precoded and are OFDM-modulated by inverse fast Fourier transform (IFFT). Finally, the transmitters send the OFDM signals to the receivers. The receivers demodulate these OFDM signals by FFT, and detect them using a virtual channel detector. The detected signals are then QPSK-demodulated and inputted into de-interleavers. Finally, the coded bit streams are decoded by Turbo decoders.

Let $\mathbf{Y}_i \in \mathbb{C}^{n_\mathrm{R}}$ represent a received signal vector at receiver i; $\mathbf{X}_j \in \mathbb{C}^{n_\mathrm{T}}$, a transmitted signal vector from transmitter j; $\mathbf{H}_{ij} \in \mathbb{C}^{n_\mathrm{R}\times n_\mathrm{T}}$, a channel matrix from transmitter j to receiver i; and $\mathbf{N}_i \in \mathbb{C}^{n_\mathrm{R}}$, an AWGN vector. The above signals are the subcarrier signals. Here, the received signal vector at receiver i is written as follows:

$$\mathbf{Y}_i = \sum_{j=1}^{M_\mathrm{T}} \mathbf{H}_{ij}\mathbf{X}_j + \mathbf{N}_i. \tag{3.1}$$

If the conventional BD algorithm described in Chapter 2 is utilized, each vehicle receives following signals:

$$\mathbf{Y}_i = \mathbf{H}_i\tilde{\mathbf{V}}_i\mathbf{D}_i + \mathbf{N}_i, \tag{3.2}$$

where $\mathbf{D}_i \in \mathbb{C}^{n_\mathrm{S}}$ and $\tilde{\mathbf{V}}_i \in \mathbb{C}^{n_\mathrm{T}\times n_\mathrm{S}}$ denote data signal vector and precoding matrix for receiver i, respectively. The number of data signal streams n_S satisfies $n_\mathrm{S} = N_\mathrm{T} - N_\mathrm{R} + n_\mathrm{R}$ when the BD algorithm is used.

Conventionally, each transmitter requires CSI of the entire system, denoted by $\mathbf{H}_{ij}$ for all $i = 1, \cdots, M_\mathrm{R}$ and $j = 1, \cdots, M_\mathrm{T}$. Therefore, receiver i feeds back $\mathbf{H}_{i1}, \cdots, \mathbf{H}_{iM_\mathrm{T}}$ to all the transmitters. The amount of such feedback information is equal to $2QLM_\mathrm{T}^2 M_\mathrm{R} n_\mathrm{T} n_\mathrm{R}$ bits for L-path Rayleigh fading channels, where Q represents a quantization bit number per real element of the channel matrix. This amount increases rapidly with the number of transmitters. Therefore, a method for reducing CSI is needed.

There is another problem in conventional BD algorithm. For detecting data signal $\mathbf{D}_i$, receiver i requires transmission signals $\mathbf{X}_1, \cdots, \mathbf{X}_{M_\mathrm{T}}$. Therefore, all the transmitters need to share same signal $\mathbf{D}_i$ and send its precoded signal $\mathbf{X}_j$ in the same frame. This synchronization is considered to be very difficult to achieve. Precoding methods for reducing feedback CSI described in the following section can overcome these problems. When these methods are used, transmitters can precode signals independently without sharing data signals with each other.

3.3 Proposed Method for Reducing CSI

This section explain precoding methods where only partial CSI is fed back to the transmitters. Receiver i can estimate CSI denoted by $\mathbf{H}_{ij}$ for all $j = 1, \cdots M_\mathrm{T}$, but only $\mathbf{H}_{ij}$ is fed back only to the related transmitter j with the proposed methods. In other words, $\mathbf{H}_{ij}$ is not fed back to transmitter j' where $j' \neq j$. In this section, a cooperative MIMO system with two transmitters and two receivers is assumed for simplicity, although the proposed precoding method can be extended to the systems with more transmitters and receivers. The proposed method allows receivers to select transmitters that CSI is fed back to and three types of precoding methods are designed for three cases: all receivers select all transmitters, all receivers select the same transmitter, and receivers select the different transmitters.

Case: All transmitters are selected

The first method allows receivers to fed back CSI to all transmitters. Because the fed back CSI is limited, the amount of such feedback information is reduced to $2QLM_{\mathrm{T}}M_{\mathrm{R}}n_{\mathrm{T}}n_{\mathrm{R}}$ bits, which is less than that when the conventional method is used by $1/M_{\mathrm{T}}$.

In this case, each transmitter knows CSI related to all receivers and thus, each transmitter precode signals by BD algorithm as in single-transmitter MU-MIMO system. Transmitter j can utilize CSI $\mathbf{H}_{1j}$ and $\mathbf{H}_{2j}$ that represent the channel impulse responses from transmitter 1 to receiver 1 and receiver 2, respectively. Therefore, transmitters precode data signals as $\mathbf{X}_j = \begin{bmatrix}\tilde{\mathbf{V}}_{1j} & \tilde{\mathbf{V}}_{2j}\end{bmatrix}\begin{bmatrix}\mathbf{D}_{1j}^{\mathrm{T}} & \mathbf{D}_{2j}^{\mathrm{T}}\end{bmatrix}^{\mathrm{T}}$, where $\tilde{\mathbf{V}}_{ij} \in \mathbb{C}^{n_{\mathrm{T}}\times(n_{\mathrm{T}}-n_{\mathrm{R}})}$ and $\mathbf{D}_{ij} \in \mathbb{C}^{n_{\mathrm{T}}-n_{\mathrm{R}}}$ represent a precoding matrix and data signal vector from transmitter j to receiver i, respectively. $\tilde{\mathbf{V}}_{ij}$ is defined to lie in the null space of $\mathbf{H}_{kj}$ and satisfies $\mathbf{H}_{kj}\tilde{\mathbf{V}}_{ij} = \mathbf{O}$, where $k \neq i$. Received signal vectors $\mathbf{Y}_i$ is expressed as follows:

$$\mathbf{Y}_i = \begin{bmatrix}\mathbf{H}_{i1}\tilde{\mathbf{V}}_{i1} & \mathbf{H}_{i2}\tilde{\mathbf{V}}_{i2}\end{bmatrix}\begin{bmatrix}\mathbf{D}_{i1}^{\mathrm{T}} & \mathbf{D}_{i2}^{\mathrm{T}}\end{bmatrix}^{\mathrm{T}} + \mathbf{N}_i. \tag{3.3}$$

Although inter-receiver interference can be avoided by this method, receivers should detect signals from different transmitters $\mathbf{D}_{i1}$ and $\mathbf{D}_{i2}$ which are received at the same time.

Case: Same transmitter is selected

When the receivers feed CSI back to one of the transmitters, the amount of such feedback information is reduced to $2QLM_{\mathrm{R}}n_{\mathrm{T}}n_{\mathrm{R}}$ bits, which is less than that when the conventional method is used by $1/M_{\mathrm{T}}^2$.

If both receivers select same transmitter 1, transmitter 1 knows CSI $\mathbf{H}_{11}$ and $\mathbf{H}_{21}$. Therefore, transmitter 1 can precode signals by BD algorithm as $\mathbf{X}_1 = \begin{bmatrix}\tilde{\mathbf{V}}_{11} & \tilde{\mathbf{V}}_{21}\end{bmatrix}\begin{bmatrix}\mathbf{D}_{11}^{\mathrm{T}} & \mathbf{D}_{21}^{\mathrm{T}}\end{bmatrix}^{\mathrm{T}}$. On the other hand, at transmitter 2, which has no CSI, data signals are transmitted without precoding as $\mathbf{X}_2 = \begin{bmatrix}\mathbf{D}_{12}^{\mathrm{T}} & \mathbf{D}_{22}^{\mathrm{T}}\end{bmatrix}^{\mathrm{T}}$. Here, the dimension of $\mathbf{D}_{ij}$ is equal to $n_{\mathrm{T}}/2$. In this case, received signal vector $\mathbf{Y}_i$ is expressed as

$$\mathbf{Y}_i = \begin{bmatrix}\mathbf{H}_{i1}\tilde{\mathbf{V}}_{i1} & \mathbf{H}_{i2}\end{bmatrix}\begin{bmatrix}\mathbf{D}_{i1}^{\mathrm{T}} & \mathbf{D}_{12}^{\mathrm{T}} & \mathbf{D}_{22}^{\mathrm{T}}\end{bmatrix}^{\mathrm{T}} + \mathbf{N}_i. \tag{3.4}$$

Case: Different transmitters are selected

In the other case in which the receivers select different transmitters, both transmitters can use partial CSI. Assume that receivers 1 and 2 select transmitters 1 and 2, respectively. At transmitter 1, the null space of the channel for receiver 1 can be calculated but the null space of the channel for receiver 2 cannot be calculated because only CSI denoted by $\mathbf{H}_{11}$ is available. Therefore, data signal vector $\mathbf{D}_{21}$ can be precoded with $\tilde{\mathbf{V}}_{21}$ for not being received at receiver 1, but $\mathbf{D}_{11}$ cannot be avoided from being received at receiver 2. In this case, $\mathbf{D}_{11}$ is precoded with $\mathbf{V}_{11} \in \mathbb{C}^{n_{\mathrm{T}}\times n_{\mathrm{R}}}$, which is right singular matrix of $\mathbf{H}_{11}$. The transmission signal vector is calculated as $\mathbf{X}_1 = \begin{bmatrix}\mathbf{V}_{11} & \tilde{\mathbf{V}}_{21}\end{bmatrix}\begin{bmatrix}\mathbf{D}_{11}^{\mathrm{T}} & \mathbf{D}_{21}^{\mathrm{T}}\end{bmatrix}^{\mathrm{T}}$ and the received signal vector is written as

$$\mathbf{Y}_i = \begin{bmatrix}\mathbf{H}_{ii}\mathbf{V}_{ii} & \mathbf{H}_{ik}\mathbf{V}_{kk} & \mathbf{H}_{ik}\tilde{\mathbf{V}}_{ik}\end{bmatrix}\begin{bmatrix}\mathbf{D}_{ii}^{\mathrm{T}} & \mathbf{D}_{kk}^{\mathrm{T}} & \mathbf{D}_{ik}^{\mathrm{T}}\end{bmatrix}^{\mathrm{T}} + \mathbf{N}_i. \tag{3.5}$$

In the above equation, $k = 2$ if $i = 1$ and $k = 1$ if $i = 2$.

In cases where receivers select one of the transmitters, receiver i receives signals $\mathbf{D}_{kj}$, which are intended for the other receiver k ($\neq i$). Therefore, receiver i must detect these interfered signals in addition to the signals intended for receiver i.

In all cases (3.3), (3.4), and (3.5) can be rewritten as follows:

$$\mathbf{Y}_i = \mathbf{H}_i\mathbf{D}_i + \mathbf{N}_i, \tag{3.6}$$

where $\mathbf{H}_i$ and $\mathbf{D}_i$ represent a channel matrix including precoding matrices at receiver i and a data signal vector including interfered signals at receiver i, respectively. When receivers fed CSI back to all transmitters, the number of streams

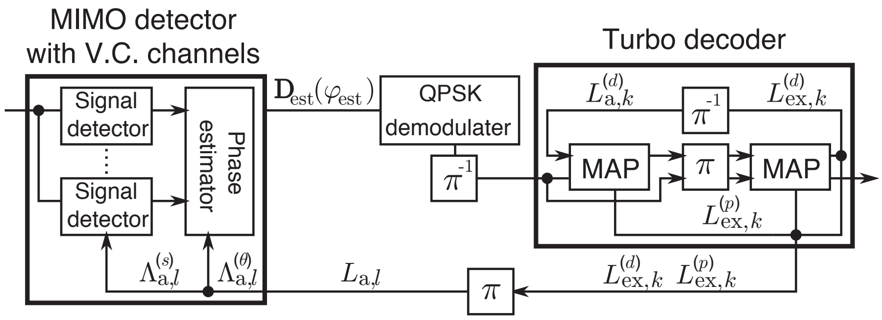

Figure 3.2: Configuration of the SHISO iterative receiver. ©2012 IEEE

of data signal vectors $\mathbf{D}_i$ is $n_S = 2(n_T - n_R)$. When receivers select one of the transmitters, the numbers of streams are $n_S = 2n_T - n_R$ and $n_S = n_T + n_R$, respectively for cases where the same transmitter is selected and different transmitters are selected. Because n_S is greater than n_R, linear-filter-based schemes cannot detect MIMO signals $\mathbf{D}_i$. Therefore, a novel receiver using the concept of a "virtual channel" and SHISO iterations is proposed in the following section.

3.4 Architecture of Proposed Receiver with Virtual Channels

3.4.1 Signal Decomposition with Virtual Channels

The architecture of the proposed receiver is shown in Figure 3.2. First, virtual channel detectors estimate data signal vectors from received signal vectors. The estimated signals are QPSK-demodulated and de-interleaved into coded bit streams. Turbo decoders then decode the bit streams iteratively by exchanging LLRs of signals between two MAP decoders. After some iterations, the extrinsic LLRs of coded bit streams are interleaved and inputted into virtual channel detectors as *a priori* LLRs. Using this information, the virtual channel detectors estimate data signal vectors and output soft QPSK signals. The Turbo decoders then again decode the inputted bit streams and output extrinsic LLRs into the virtual channel detectors. The transferring detected signals and LLRs are performed iteratively between the virtual channel detector and the Turbo decoder.

With the virtual channel detector, signal vectors $\mathbf{D}_i$ in (3.6) are decomposed into real signal and phase elements. The receiver index i is omitted for simplicity in the rest of this section. The lth entry of $\mathbf{D}$, d_l, is decomposed into a real signal s_l and a phase θ_l as $d_l = s_l \mathrm{e}^{\mathrm{j}\theta_l}$, where $s_l = \pm\sqrt{2}$ and $\theta_l = \pm\pi/4$. When the decomposition of a scalar is extended to a vector, $\mathbf{D}$ is rewritten as follows [43].

$$\mathbf{D} = \mathbf{\Omega}(\varphi)\mathbf{S}(\varphi), \tag{3.7}$$

$$\mathbf{\Omega}(\varphi) := \begin{bmatrix} \operatorname{diag}\left[\cos\theta_1, \cdots, \cos\theta_{n_\mathrm{S}}\right] \\ \operatorname{diag}\left[\sin\theta_1, \cdots, \sin\theta_{n_\mathrm{S}}\right] \end{bmatrix}, \tag{3.8}$$

$$\mathbf{S}(\varphi) := \begin{bmatrix} s_1(\varphi) & \cdots & s_{n_\mathrm{S}}(\varphi) \end{bmatrix}^\mathrm{T}, \tag{3.9}$$

where $\operatorname{diag}[\cdots]$ represents a diagonal matrix. $\mathbf{\Omega}(\varphi) \in \mathbb{C}^{2n_\mathrm{S} \times n_\mathrm{S}}$ and $\mathbf{S}(\varphi) \in \mathbb{C}^{n_\mathrm{S}}$ are called a rotation matrix and a real signal vector, respectively. φ is a "phase pattern," which is defined as follows:

$$\varphi := \sum_{l=1}^{n_\mathrm{S}} \left(\frac{\theta_l}{\pi/2} + \frac{1}{2} \right) 2^{l-1}. \tag{3.10}$$

The phase pattern φ ranges from 0 to $2^{n_\mathrm{S}} - 1$. From (3.7), (3.6) is rewritten as follows:

$$\mathbf{Y} = \mathbf{\Phi}(\varphi)\mathbf{S}(\varphi) + \mathbf{N}, \tag{3.11}$$

$$\mathbf{\Phi}(\varphi) := \mathbf{H}\mathbf{\Omega}(\varphi). \tag{3.12}$$

As is expressed in (3.11), the channel model can be regarded that the real signal vector $\mathbf{S}(\varphi)$ is transmitted in the channel $\mathbf{\Phi}(\varphi) \in \mathbb{C}^{2n_\mathrm{R} \times n_\mathrm{S}}$, which is called "a virtual channel". While the size of the channel matrix $\mathbf{H}$ is $2n_\mathrm{R} \times 2n_\mathrm{S}$, that of the virtual channel $\mathbf{\Phi}(\varphi)$ is $2n_\mathrm{R} \times n_\mathrm{S}$. In a word, the number of the columns of the virtual channel $\mathbf{\Phi}(\varphi)$ is half of that of the channel matrix $\mathbf{H}$, which means that the number of the spatially multiplexed streams in the virtual channel looks half of that in the channel $\mathbf{H}$. If the number of the streams is reduced, the streams can be detected with higher performance by linear detectors, such as the OSD.

The OSD detects the real signal vector in all the virtual channels, $\mathbf{\Phi}(\bar{\varphi})$ for $\bar{\varphi} = 0, \cdots, 2^{n_\mathrm{S}} - 1$, where $\bar{\varphi}$ is a tentative phase pattern. In the OSD, basically, the transmission signal is detected with an MMSE filter, and the interference associated with the previously detected signals is canceled from the received signal vector.

This step is iterated by n_S times in the OSD. The lth-step MMSE filter $\mathbf{W}^{(l)}(\bar{\varphi})$ is defined as

$$\mathbf{W}^{(l)}(\bar{\varphi}) := \left(\mathbf{\Phi}^{(l)}(\bar{\varphi})\left[\mathbf{\Phi}^{(l)}(\bar{\varphi})\right]^{\mathrm{T}} + \frac{\sigma_{\mathrm{n}}^2}{\sigma_{\mathrm{s}}^2}\mathbf{I}\right)^{-1}\mathbf{\Phi}^{(l)}(\bar{\varphi}), \tag{3.13}$$

where σ_{n}^2, σ_{s}^2, and $\mathbf{I}$ represent the noise power, the signal power, and the unit matrix. $\mathbf{\Phi}^{(l)}(\bar{\varphi})$ denotes the virtual channel in the lth step. It is assumed that the signals are detected in the order of the antenna number for simplifying the notation. The lth-stream signal is detected as

$$s_{\mathrm{det},l}(\bar{\varphi}) = [\boldsymbol{w}_l(\bar{\varphi})]^{\mathrm{T}}\,\mathbf{Y}, \tag{3.14}$$

where $\boldsymbol{w}_l(\bar{\varphi})$ represents the lth column of $\mathbf{W}^{(l)}(\bar{\varphi})$. The hard decision signal $\bar{s}_{\mathrm{det},l}(\bar{\varphi})$ is defined as follows:

$$\bar{s}_{\mathrm{det},l}(\bar{\varphi}) := \sqrt{2}\,\mathrm{sgn}\left[s_{\mathrm{det},l}(\bar{\varphi})\right], \tag{3.15}$$

where $\mathrm{sgn}\,[x]$ represent a sign function. Using these hard decision signals, the interference cancellation is carried out as

$$\mathbf{Y}^{(l+1)} = \mathbf{Y}^{(l)} - \boldsymbol{\phi}_l^{(l)}(\bar{\varphi})\bar{s}_{\mathrm{det},l}(\bar{\varphi}), \tag{3.16}$$

where $\mathbf{Y}^{(1)}$ is set to $\mathbf{Y}$. The soft real signal vector $\mathbf{S}_{\mathrm{det}}(\bar{\varphi})$ and hard decision real signal vector $\bar{\mathbf{S}}_{\mathrm{det}}(\bar{\varphi})$ are defined as

$$\mathbf{S}_{\mathrm{det}}(\bar{\varphi}) := \begin{bmatrix} s_{\mathrm{det},1}(\bar{\varphi}) & \cdots & s_{\mathrm{det},n_S}(\bar{\varphi}) \end{bmatrix}^{\mathrm{T}}, \tag{3.17}$$

$$\bar{\mathbf{S}}_{\mathrm{det}}(\bar{\varphi}) := \begin{bmatrix} \bar{s}_{\mathrm{det},1}(\bar{\varphi}) & \cdots & \bar{s}_{\mathrm{det},n_S}(\bar{\varphi}) \end{bmatrix}^{\mathrm{T}}. \tag{3.18}$$

The virtual channel detector selects the most likely phase pattern based on the proposed technique described in the following section, and outputs the information associated with the signals to the Turbo decoder via the interleaver. The Turbo decoder estimates the LLR with the signal from the interleaver, and feeds back only the extrinsic information of the LLR to the MIMO detector.

3.4.2 LLR Calculation of SISO Iterative Receiver

The iterative detector with virtual channels calculates the LLRs of both the real signal and the phase in order to feed estimated signals to the Turbo decoder. This section explains LLR calculation of SISO iterative receiver with virtual channels at first. This calculation technique is a simple conversion from LLRs of complex signals d_l to real signal s_l and phase θ_l. The performance of SISO and SHISO receivers is compared with in Section 3.5 to show that SHISO receivers explained in Section 3.4.3 achieves better BER performance. First, the detector in the SISO receiver obtains the LLR of the phase element $\Lambda_l^{(\theta)}$, using the Max-Log-MAP approximation as follows:

$$\begin{aligned}\Lambda_l^{(\theta)} &:= \log \frac{\mathbb{P}\left(\theta_l = +\frac{\pi}{4} \,\middle|\, \mathbf{Y}\right)}{\mathbb{P}\left(\theta_l = -\frac{\pi}{4} \,\middle|\, \mathbf{Y}\right)} \\ &= \Lambda_{\mathrm{a},l}^{(\theta)} + \max_{\bar{\varphi} \,|\, \theta_l = +\frac{\pi}{4}} \left\{ \sum_{m \neq l}^{n_\mathrm{S}} \Lambda_{\mathrm{a},m}^{(\theta)} + J(\bar{\varphi}) \right\} - \max_{\bar{\varphi} \,|\, \theta_l = -\frac{\pi}{4}} \left\{ \sum_{m \neq l}^{n_\mathrm{S}} \Lambda_{\mathrm{a},m}^{(\theta)} + J(\bar{\varphi}) \right\},\end{aligned} \tag{3.19}$$

$$J(\bar{\varphi}) := -\frac{1}{2\sigma_\mathrm{n}^2} \left| \mathbf{Y} - \mathbf{\Phi}(\bar{\varphi}) \tilde{\mathbf{S}}(\bar{\varphi}) \right|^2, \tag{3.20}$$

where $\Lambda_{\mathrm{a},l}^{(\theta)}$ represents the *a priori* information of the phase θ_l fed back from the Turbo decoder via the converter, which is described in Section 3.4.3. In addition, $\max\limits_{\text{constraint}} \{\cdot\}$ denotes the maximum value under the indicated constraint. The LLR of the phase is provided to an slicer to extract only the sign from the LLR. When the sign is positive, $\theta_l = \pi/4$ is estimated as a transmitted phase. Otherwise, $\theta_l = -\pi/4$ is estimated. This processing is regarded as a hard decision. After the processing is applied for all phase elements θ_l, the most likely phase pattern $\bar{\varphi}_{\mathrm{est}}$ is decided from (3.10) and the virtual channel $\mathbf{\Phi}(\bar{\varphi}_{\mathrm{est}})$ is calculated from (3.8) and (3.12).

Next, the LLR of the real signal $\Lambda_l^{(s)}(\bar{\varphi}_{\mathrm{est}})$ in the most likely virtual channel $\bar{\varphi}_{\mathrm{est}}$ is calculated as follows:

$$\begin{aligned}\Lambda_l^{(s)}(\bar{\varphi}_{\mathrm{est}}) &:= \log \frac{\mathbb{P}\left(s_l = +\sqrt{2} \,\middle|\, \mathbf{Y}\right)}{\mathbb{P}\left(s_l = -\sqrt{2} \,\middle|\, \mathbf{Y}\right)} \\ &= \Lambda_{\mathrm{a},l}^{(s)} + \max_{\mathbf{S} \,|\, s_l = +\sqrt{2}} \left\{ \sum_{m \neq l}^{n_\mathrm{S}} \Lambda_{\mathrm{a},m}^{(s)} + J_s(\mathbf{S}) \right\} - \max_{\mathbf{S} \,|\, s_l = -\sqrt{2}} \left\{ \sum_{m \neq l}^{n_\mathrm{S}} \Lambda_{\mathrm{a},m}^{(s)} + J_s(\mathbf{S}) \right\},\end{aligned} \tag{3.21}$$

$$J_s(\mathbf{S}) := -\frac{1}{2\sigma_\mathrm{n}^2} \left| \mathbf{Y} - \mathbf{\Phi}(\bar{\varphi}_{\mathrm{est}}) \mathbf{S} \right|^2. \tag{3.22}$$

The MIMO detector outputs the extrinsic bit LLR to the Turbo decoder. The extrinsic bit LLR is defined as

$$\Lambda_{\mathrm{ex},l}^{(s)} \coloneqq \Lambda_l^{(s)}(\bar{\varphi}_{\mathrm{est}}) - \Lambda_{\mathrm{a},l}^{(s)}, \tag{3.23}$$

$$\Lambda_{\mathrm{ex},l}^{(\theta)} \coloneqq \Lambda_l^{(\theta)} - \Lambda_{\mathrm{a},l}^{(\theta)}. \tag{3.24}$$

This LLR is converted to the bit LLR and then inputted into the Turbo decoder.

3.4.3 LLR Calculation of Proposed SHISO Iterative Receiver

LLR of Real Signals

In order to improve signal estimation performance, a SHISO iterative receiver is designed. The SHISO iterative receiver calculates the LLR of phase patterns φ and outputs a signal vector $\mathbf{D}$ over the estimated virtual channel $\mathbf{\Phi}(\bar{\varphi}_{\mathrm{est}})$, while SISO iterative receiver calculates and outputs the LLR of each real signal s_l and phase θ_l. The LLR of the real signal $\lambda_l^{(s)}(\bar{\varphi})$ in the virtual channel $\mathbf{\Phi}(\bar{\varphi})$ can be defined as

$$\lambda_l^{(s)}(\bar{\varphi}) \coloneqq \log \frac{\mathbb{P}\left(s_l(\bar{\varphi}) = +\sqrt{2} \,\middle|\, \mathbf{Y}\right)}{\mathbb{P}\left(s_l(\bar{\varphi}) = -\sqrt{2} \,\middle|\, \mathbf{Y}\right)}, \tag{3.25}$$

where $\mathbb{P}\left(s_l(\bar{\varphi}) = \pm\sqrt{2} \,\middle|\, \mathbf{Y}\right)$ represents an *a posteriori* probability of the real signal in the lth-stream, $s_l(\bar{\varphi})$, when $\mathbf{Y}$ is received. The numerator of (3.25) can be approximately calculated with the Max-Log-MAP approximation as,

$$\begin{aligned} &\log \mathbb{P}\left(s_l(\bar{\varphi}) = +\sqrt{2} \,\middle|\, \mathbf{Y}\right) \\ &\simeq \log \mathbb{P}\left(s_l(\bar{\varphi}) = +\sqrt{2}\right) - \log \mathbb{P}\left(\mathbf{Y}\right) \\ &\quad + \max_{s_l(\bar{\varphi}) = +\sqrt{2}} \left\{ \sum_{m \neq l}^{n_{\mathrm{S}}} \log \mathbb{P}\left(s_m(\bar{\varphi})\right) - \frac{1}{2\sigma_{\mathrm{n}}^2} \left|\mathbf{Y} - \mathbf{\Phi}(\bar{\varphi})\mathbf{S}(\bar{\varphi})\right|^2 \right\}. \end{aligned} \tag{3.26}$$

Because the exact calculation of (3.26) needs lots of complex calculations, the LLR of the real signal $\lambda_l^{(s)}(\bar{\varphi})$ is calculated more simply using the following hypothesis [40]. In order to simplify the maximization in (3.26), the second term is transformed into L2-norm of real signal vectors using (3.14) as follows:

$$\left|\mathbf{Y} - \mathbf{\Phi}(\bar{\varphi})\mathbf{S}(\bar{\varphi})\right|^2 \simeq \sum_{l}^{n_{\mathrm{S}}} \frac{\left(s_{\mathrm{det},l}(\bar{\varphi}) - s_l(\bar{\varphi})\right)^2}{\left|\boldsymbol{w}_l(\bar{\varphi})\right|^2}, \tag{3.27}$$

where $|\boldsymbol{w}_l(\bar{\varphi})|^2$ is a scale factor. When the term in the left hand side of (3.27) is substituted for (3.26), the maximization with respect to $s_m(\bar{\varphi})$ can be performed independently. In a word, $s_m(\bar{\varphi})$ can be selected that satisfies $s_m(\bar{\varphi}) = \arg\max\left\{\log\mathbb{P}\left(s_m(\bar{\varphi})\right) - \left(s_{\mathrm{det},m}(\bar{\varphi}) - s_m(\bar{\varphi})\right)^2\right\}$. Therefore, the terms $s_m(\bar{\varphi})$ become common except $m = l$ between the numerator and the denominator in (3.25). Hence, the LLR of the real signals $\lambda_l^{(\mathrm{s})}(\bar{\varphi})$ can be approximately obtained as

$$\begin{aligned}\lambda_l^{(s)}(\bar{\varphi}) &\simeq \Lambda_{\mathrm{a},l}^{(s)}(\bar{\varphi}) - \frac{1}{2\sigma_{\mathrm{n}}^2\,|\boldsymbol{w}_l(\bar{\varphi})|^2}\left\{\left|s_{\mathrm{det},l}(\bar{\varphi}) - \sqrt{2}\right|^2 - \left|s_{\mathrm{det},l}(\bar{\varphi}) + \sqrt{2}\right|^2\right\}\\ &= \Lambda_{\mathrm{a},l}^{(s)}(\bar{\varphi}) + \frac{2\sqrt{2}s_{\mathrm{det},l}(\bar{\varphi})}{\sigma_{\mathrm{n}}^2\,|\boldsymbol{w}_l(\bar{\varphi})|^2}.\end{aligned} \tag{3.28}$$

where $\Lambda_{\mathrm{a},l}^{(s)}(\bar{\varphi})$ represents *a priori* information of the real signal $s_l(\bar{\varphi})$, which is defined as

$$\Lambda_{\mathrm{a},l}^{(s)}(\bar{\varphi}) := \log\frac{\mathbb{P}\left(s_l(\bar{\varphi}) = +\sqrt{2}\right)}{\mathbb{P}\left(s_l(\bar{\varphi}) = -\sqrt{2}\right)}. \tag{3.29}$$

This *a priori* information is provided by the Turbo decoder.

By making a hard decision of $\lambda_l^{(s)}(\bar{\varphi})$, real signal vector $\tilde{\mathbf{S}}(\bar{\varphi})$ can be obtained in all the virtual channels.

$$\tilde{\mathbf{S}}(\bar{\varphi}) := \begin{bmatrix}\tilde{s}_1(\bar{\varphi}) & \cdots & \tilde{s}_{n_{\mathrm{S}}}(\bar{\varphi})\end{bmatrix}, \tag{3.30}$$

$$\tilde{s}_l(\bar{\varphi}) := \sqrt{2}\ \mathrm{sgn}\left[\lambda_l^{(s)}(\bar{\varphi})\right]. \tag{3.31}$$

The transmitted virtual channel is estimated with the estimated real signals by a technique explained in the following part.

LLR of Phase Pattern

The proposed detector calculates the LLR of the phase pattern $\Lambda_{\bar{\varphi}}(\bar{\varphi} : \bar{\varphi}')$ in order to select the optimum phase pattern that maximizes an *a posteriori* probability. Here, $\bar{\varphi}'$ is a phase pattern that differs from $\bar{\varphi}$. The LLR of the phase patterns is defined as

$$\Lambda_{\bar{\varphi}}(\bar{\varphi} : \bar{\varphi}') := \log\frac{\mathbb{P}\left(\bar{\varphi}\,|\,\mathbf{Y}\right)}{\mathbb{P}\left(\bar{\varphi}'\,|\,\mathbf{Y}\right)} = \log\frac{\mathbb{P}\left(\mathbf{Y}\,|\,\bar{\varphi}\right)\mathbb{P}\left(\bar{\varphi}\right)}{\mathbb{P}\left(\mathbf{Y}\,|\,\bar{\varphi}'\right)\mathbb{P}\left(\bar{\varphi}'\right)}, \tag{3.32}$$

where $\mathbb{P}(\bar{\varphi} \mid \mathbf{Y})$, $\mathbb{P}(\mathbf{Y} \mid \bar{\varphi})$, and $\mathbb{P}(\bar{\varphi})$ represent an *a posteriori* probability of the phase pattern, a conditional probability when a signal vector with a phase pattern $\bar{\varphi}$ is transmitted, an *a priori* probability of the virtual channel with the phase pattern $\bar{\varphi}$. $\mathbb{P}(\bar{\varphi})$ can be expressed as follows:

$$\mathbb{P}(\bar{\varphi}) = \prod_{l=1}^{n_{\mathrm{S}}} \mathbb{P}(\theta_l), \tag{3.33}$$

where $\mathbb{P}(\theta_l)$ represents *a priori* probability of the phase θ_l. Using (3.33), (3.32) can be rewritten as

$$\begin{aligned} \Lambda_{\bar{\varphi}}(\bar{\varphi} : \bar{\varphi}') &= \sum_{l=1}^{n_{\mathrm{S}}} \log \frac{\mathbb{P}(\theta_l)}{\mathbb{P}(\theta_l')} + \log \mathbb{P}(\mathbf{Y} \mid \bar{\varphi}) - \log \mathbb{P}(\mathbf{Y} \mid \bar{\varphi}') \\ &= \sum_{l=1}^{n_{\mathrm{S}}} \Lambda_\theta(\theta_l : \theta_l') - \frac{1}{2\sigma_{\mathrm{n}}^2} \left|\mathbf{Y} - \mathbf{\Phi}(\bar{\varphi})\tilde{\mathbf{S}}(\bar{\varphi})\right|^2 \\ &\quad + \frac{1}{2\sigma_{\mathrm{n}}^2} \left|\mathbf{Y} - \mathbf{\Phi}(\bar{\varphi}')\tilde{\mathbf{S}}(\bar{\varphi}')\right|^2, \end{aligned} \tag{3.34}$$

where *a priori* information $\Lambda_\theta(\theta_l : \theta_l')$ is defined as

$$\Lambda_\theta(\theta_l : \theta_l') \coloneqq \begin{cases} +\Lambda_{\mathrm{a},l}^{(\theta)} & \left(\theta_l = +\frac{\pi}{4},\ \theta_l' = -\frac{\pi}{4}\right) \\ -\Lambda_{\mathrm{a},l}^{(\theta)} & \left(\theta_l = -\frac{\pi}{4},\ \theta_l' = +\frac{\pi}{4}\right) \\ 0 & \left(\theta_l = \theta_l'\right) \end{cases}, \tag{3.35}$$

$$\Lambda_{\mathrm{a},l}^{(\theta)} \coloneqq \log \frac{\mathbb{P}\left(\theta_l = +\frac{\pi}{4}\right)}{\mathbb{P}\left(\theta_l = -\frac{\pi}{4}\right)}, \tag{3.36}$$

where $\Lambda_{\mathrm{a},l}^{(\theta)}$ represents *a priori* information of the lth phase θ_l that is fed back from the decoder. Although the definition of the phase is regarded as an application of the principle of the bit LLR, the definition is not equal to that of the bit LLR, which is explained later. The optimum phase pattern $\bar{\varphi}_{\mathrm{est}}$ is selected to satisfy the following equation.

$$\Lambda_{\bar{\varphi}}(\bar{\varphi}_{\mathrm{est}} : \bar{\varphi}') \geq 0 \quad \text{for } \forall \bar{\varphi}' \neq \bar{\varphi}_{\mathrm{est}}. \tag{3.37}$$

For the selected phase pattern $\bar{\varphi}_{\mathrm{est}}$, the estimated data signal vector $\mathbf{D}_{\mathrm{det}}(\bar{\varphi}_{\mathrm{est}})$ can be calculated according to the definition of $\mathbf{D}$ in (3.7).

$$\mathbf{D}_{\mathrm{det}}(\bar{\varphi}_{\mathrm{est}}) \coloneqq \mathbf{\Omega}(\bar{\varphi}_{\mathrm{est}})\mathbf{S}_{\mathrm{det}}(\bar{\varphi}_{\mathrm{est}}). \tag{3.38}$$

The estimated data vector $\mathbf{D}_{\mathrm{det}}(\bar{\varphi}_{\mathrm{est}})$ is output to the Turbo decoder through the de-interleaver. In other words, the proposed receiver provides the Turbo decoder with those output signals via the interleaver. This means that the detector does not output extrinsic information, which is a big difference from Turbo equalizers: a representative of iterative receivers.

a priori Information Fed Back to the MIMO Detector for Iterative Decoding

The Turbo decoder calculates the bit LLR $L^{(d)}_{\mathrm{d},v}$ in the same way as usual Turbo decoders. The bit LLR is defined as

$$L^{(d)}_{\mathrm{d},v} := \log \frac{\mathbb{P}\left(c_{\mathrm{d},v} = 1 \,\middle|\, \mathbf{D}\right)}{\mathbb{P}\left(c_{\mathrm{d},v} = 0 \,\middle|\, \mathbf{D}\right)}, \tag{3.39}$$

where $c_{\mathrm{d},v}$ represents the vth bit. After some iterations of the decoding, the Turbo decoder feeds back the extrinsic bit LLR $L_{\mathrm{ex},v}$ to the MIMO detector as *a priori* information $L_{\mathrm{a},u}$ via the interleaver.

$$L_{\mathrm{a},u} = \pi\left[L_{\mathrm{ex},v}\right], \tag{3.40}$$

where $\pi[\cdot]$ represents a function of the interleaver. Whereas the extrinsic bit LLRs are fed back from the Turbo decoder, the MIMO detector requires the *a priori* information of the real signal and the phase. Therefore, the extrinsic bit LLRs are converted into the *a priori* information of the real signals $s_l(\bar{\varphi})$ and the phase θ_l. The proposed conversion can be obtained by the following derivation:

$$\begin{aligned}\Lambda^{(s)}_{\mathrm{a},l}(\bar{\varphi}) &= \log \frac{\mathbb{P}\left(s_l(\bar{\varphi}) = +\sqrt{2}\right)}{\mathbb{P}\left(s_l(\bar{\varphi}) = -\sqrt{2}\right)} = \log \frac{\mathbb{P}\left(\mathrm{Re}[d_l] = +1\right)}{\mathbb{P}\left(\mathrm{Re}[d_l] = -1\right)} \\ &= L_{\mathrm{a},2u}, \end{aligned} \tag{3.41}$$

$$\begin{aligned}\Lambda^{(\theta)}_{\mathrm{a},l} &= \log \frac{\mathbb{P}\left(\theta_l = +\frac{\pi}{4}\right)}{\mathbb{P}\left(\theta_l = -\frac{\pi}{4}\right)} = \log \frac{\mathbb{P}\left(d_l = +1 + \mathrm{j}\right) + \mathbb{P}\left(d_l = -1 - \mathrm{j}\right)}{\mathbb{P}\left(d_l = -1 + \mathrm{j}\right) + \mathbb{P}\left(d_l = +1 - \mathrm{j}\right)} \\ &= \log \frac{\dfrac{\mathbb{P}\left(\mathrm{Re}[d_l] = +1\right)\mathbb{P}\left(\mathrm{Im}[d_l] = +1\right)}{\mathbb{P}\left(\mathrm{Re}[d_l] = -1\right)\mathbb{P}\left(\mathrm{Im}[d_l] = -1\right)} + 1}{\dfrac{\mathbb{P}\left(\mathrm{Im}[d_l] = +1\right)}{\mathbb{P}\left(\mathrm{Im}[d_l] = -1\right)} + \dfrac{\mathbb{P}\left(\mathrm{Re}[d_l] = +1\right)}{\mathbb{P}\left(\mathrm{Re}[d_l] = -1\right)}} \\ &= \max\left[L_{\mathrm{a},2u} + L_{\mathrm{a},2u+1}, 0\right] - \max\left[L_{\mathrm{a},2u}, L_{\mathrm{a},2u+1}\right], \end{aligned} \tag{3.42}$$

where Re $[\cdot]$ and Im $[\cdot]$ represent a real part and an imaginary part of a complex number, respectively. Note that the $2u$th and $(2u+1)$th bits correspond to the real part and the imaginary part of the lth QPSK signal, respectively.

3.4.4 Extended MAP Estimation for Virtual Channel Detection

The virtual channel is detected based on the MAP in (3.32), assuming that the real signals in the virtual channel $\mathbf{\Phi}(\bar{\varphi})$ are almost the same to those in $\mathbf{\Phi}(\bar{\varphi}')$. This assumption is also applied in [40, 43], but the assumption does not always hold true. In order to achieve better detecting performance, a novel estimation criterion for the virtual channel detection is designed where it is taken into account that the real signals in a virtual channel might be different from those in the others. The proposed estimation criterion applies an LLR $\Lambda_{\mathbf{D}}(\bar{\varphi} : \bar{\varphi}')$ of the phase pattern $\bar{\varphi}$, which is defined as

$$\Lambda_{\mathbf{D}}(\bar{\varphi} : \bar{\varphi}') \coloneqq \log \frac{\mathbb{P}\left(\mathbf{Y} \mid \mathbf{D}(\bar{\varphi})\right) \mathbb{P}\left(\mathbf{D}(\bar{\varphi})\right)}{\mathbb{P}\left(\mathbf{Y} \mid \mathbf{D}'(\bar{\varphi})\right) \mathbb{P}\left(\mathbf{D}'(\bar{\varphi})\right)}. \tag{3.43}$$

Because the rotation matrices $\mathbf{\Omega}(\bar{\varphi})$ and the real signal vectors $\mathbf{S}(\bar{\varphi})$ can be assumed to be independent from each other, the LLR of the phase pattern $\Lambda_{\mathbf{D}}(\bar{\varphi} : \bar{\varphi}')$ can be rewritten using (3.7) as follows:

$$\begin{aligned}
\Lambda_{\mathbf{D}}(\bar{\varphi} : \bar{\varphi}') = {} & \log \frac{\mathbb{P}\left(\mathbf{Y} \,\middle|\, \mathbf{\Omega}(\bar{\varphi})\tilde{\mathbf{S}}(\bar{\varphi})\right) \mathbb{P}\left(\mathbf{\Omega}(\bar{\varphi})\right) \mathbb{P}\left(\tilde{\mathbf{S}}(\bar{\varphi})\right)}{\mathbb{P}\left(\mathbf{Y} \mid \mathbf{\Omega}(\bar{\varphi}')\mathbf{S}'(\bar{\varphi})\right) \mathbb{P}\left(\mathbf{\Omega}(\bar{\varphi}')\right) \mathbb{P}\left(\mathbf{S}'(\bar{\varphi})\right)} \\
= {} & \sum_{l}^{n_{\mathrm{S}}} \log \frac{\mathbb{P}(\theta_l)}{\mathbb{P}(\theta_l')} + \sum_{l}^{n_{\mathrm{S}}} \log \frac{\mathbb{P}(s_l(\bar{\varphi}))}{\mathbb{P}(s_l'(\bar{\varphi}))} \\
& + \log \mathbb{P}\left(\mathbf{Y} \,\middle|\, \mathbf{\Omega}(\bar{\varphi})\tilde{\mathbf{S}}(\bar{\varphi})\right) - \log \mathbb{P}\left(\mathbf{Y} \mid \mathbf{\Omega}(\bar{\varphi}')\mathbf{S}'(\bar{\varphi})\right) \\
= {} & \sum_{l}^{n_{\mathrm{S}}} \Lambda_{\theta}(\theta_l : \theta_l') + \sum_{l}^{n_{\mathrm{S}}} \Lambda_{s}(s_l : s_l') \\
& - \frac{1}{2\sigma_{\mathrm{n}}^2} \left|\mathbf{Y} - \mathbf{\Phi}(\bar{\varphi})\tilde{\mathbf{S}}(\bar{\varphi})\right|^2 + \frac{1}{2\sigma_{\mathrm{n}}^2} \left|\mathbf{Y} - \mathbf{\Phi}(\bar{\varphi}')\mathbf{S}'(\bar{\varphi})\right|^2,
\end{aligned} \tag{3.44}$$

$$\Lambda_s(s_l : s_l') \coloneqq \begin{cases} +\Lambda_{\mathrm{a},l}^{(s)} & \left(s_l = +\sqrt{2},\ s_l' = -\sqrt{2}\right) \\ -\Lambda_{\mathrm{a},l}^{(s)} & \left(s_l = -\sqrt{2},\ s_l' = +\sqrt{2}\right) \\ 0 & \left(s_l = s_l'\right) \end{cases}, \tag{3.45}$$

where $\Lambda_{\mathrm{a},l}^{(s)}$ represents *a priori* information of the real signal defined in (3.29). As is similar to (3.37), the optimum phase pattern $\bar{\varphi}_{\mathrm{est}}$ that satisfies the following equation is selected:

$$\Lambda_{\mathbf{D}}(\bar{\varphi}_{\mathrm{est}} : \bar{\varphi}') \geq 0 \quad \text{for } \forall\bar{\varphi}' \neq \bar{\varphi}_{\mathrm{est}}. \tag{3.46}$$

Then, the optimum signal vector $\mathbf{D}_{\mathrm{det}}(\bar{\varphi}_{\mathrm{est}})$ is calculated as

$$\mathbf{D}_{\mathrm{det}}(\bar{\varphi}_{\mathrm{est}}) \coloneqq \mathbf{\Omega}(\bar{\varphi}_{\mathrm{est}})\mathbf{S}_{\mathrm{det}}(\bar{\varphi}_{\mathrm{est}}). \tag{3.47}$$

This optimum signal vector is output to the Turbo decoder through the de-interleaver. Because not only $\Lambda_{\theta}(\theta_l : \theta_l')$ but also $\Lambda_s(s_l : s_l')$ are taken into account in the virtual channel detection, the proposed detection is expected to achieve better performance than the detection using (3.34) and (3.37).

3.4.5 Procedure of Proposed SHISO Receiver

The MIMO detector estimates the signal vector $\mathbf{D}_{\mathrm{det}}(\bar{\varphi}_{\mathrm{est}})$ based on the proposed scheme described in Sections 3.4.3 and 3.4.4. The vector $\mathbf{D}_{\mathrm{det}}(\bar{\varphi}_{\mathrm{est}})$ is output to the Turbo decoder, which feeds back the extrinsic bit LLR to the MIMO detector. This operation is iterated N_{out} times in the proposed receiver. Because the vector $\mathbf{D}_{\mathrm{det}}(\bar{\varphi}_{\mathrm{est}})$ is the product of the hard decision rotation matrix $\mathbf{\Omega}(\bar{\varphi}_{\mathrm{est}})$ and the soft real signal vector $\mathbf{S}_{\mathrm{det}}(\bar{\varphi}_{\mathrm{est}})$ as is defined in (3.38), the vector is called as a semi-hard decision signal vector. This is the reason why the proposed receiver is named as a SHISO iterative receiver. The proposed receiver has the iterative signal processing between the MIMO detector and the Turbo decoder and the iterative processing of the Turbo decoding. To distinguish the two iteration processing, the iterative exchange of the signals between the MIMO detector and the Turbo decoder is called as "outer iteration," and the iterative exchange of extrinsic bit LLR between the two component decoder in the Turbo decoder is called as "inner iteration." N_{out} and N_{in} denote the number of the outer and inner iterations, respectively. Here, the Turbo decoders decode signals a total of $N_{\mathrm{out}} \times N_{\mathrm{in}}$ times.

3.5 Analysis of Proposed Receiver in SU-MIMO Environments

In this section, the BER performances of the proposed receiver were evaluated by computer simulation. Because (3.6) can be regarded as an overloaded SU-MIMO system, the performance was evaluated in overloaded SU-MIMO environments and then, it is applied to cooperative MIMO systems in Section 3.6. Simulation parameters are listed in Table 3.1. The channel impulse responses were independently and identically distributed (i.i.d) and were quasi-static. The receiver was assumed to have the perfect CSI for simplicity. Although Doppler shift occurs when vehicles are moving at high speed, many channel estimation methods are proposed [50, 51] that can be applied to vehicular environments and thus, performance degradation is assumed to be negligible. The Turbo code [45] was utilized as error correction code. The Max-log MAP algorithm was applied to all the MAP estimations.

3.5.1 SHISO Iterative Receiver

The BER performance of the proposed receiver is shown in Figure 3.3. Simulations were performed with some combinations of the outer iterations and the inner iterations, i.e., N_{out} and N_{in}, but $N_{\mathrm{out}} \times N_{\mathrm{in}}$ was kept to 48 in all the combinations. The performance of the SISO iterative receiver introduced in Section 3.4.2 is also shown. The setting of $(N_{\mathrm{out}}, N_{\mathrm{in}})$ is $(6, 8)$ in the SISO iterative receiver. Obviously, the performance of the SISO iterative receiver is much worse than that of the proposed receiver. It is also shown that the BER performance with $(N_{\mathrm{out}}, N_{\mathrm{in}}) = (48, 1)$ is better than the performance with $(24, 2)$ by about 0.8 dB at BER $= 10^{-4}$. The Turbo decoder increases the LLR (3.39) assuming the input signals $\mathbf{D}_{\mathrm{det}}(\bar{\varphi}_{\mathrm{est}})$ are well estimated, and effects of $\mathbf{D}_{\mathrm{det}}(\bar{\varphi}_{\mathrm{est}})$ misestimation increases with the number of Turbo iterations. It is difficult for the MIMO detector to correct misestimated signals with the fed back LLRs if fed back LLRs have strong correlation with $\mathbf{D}_{\mathrm{det}}(\bar{\varphi}_{\mathrm{est}})$ obtained at the previous detection. Therefore, the BER performance with $N_{\mathrm{in}} = 1$ is better than those with $N_{\mathrm{in}} > 1$.

In order to analyze the BER performance of the proposed receiver, LLRs of misestimated bits were evaluated. Figure 3.4 shows the empirical cumulative

Table 3.1: Simulation parameters for receiver evaluation in SU-MIMO systems.

Parameters	Values
Number of antennas	6×2
Modulation scheme	OFDM-QPSK
Channel model	10-path Rayleigh fading
Forward error correction	Turbo code, rate $1/3$
Number of sub carriers	512
Data packet length	16384 bits

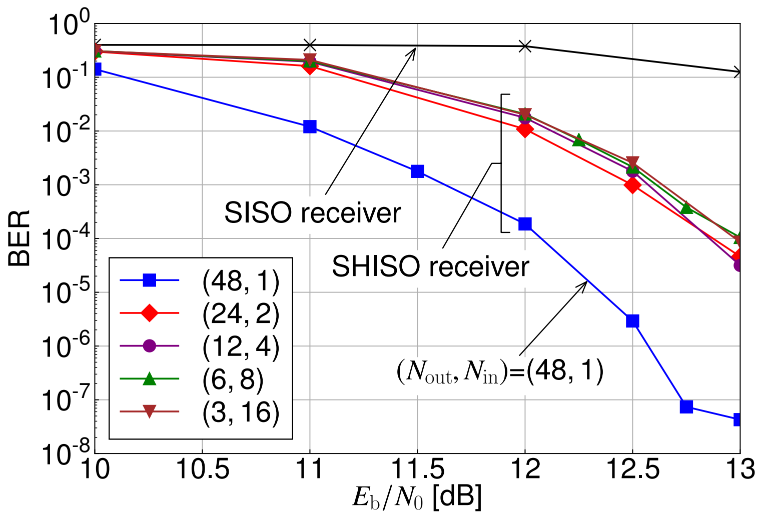

Figure 3.3: BER performance of the proposed receiver with the different number of iterations. ©2015 IEICE

distribution function (CDF) of misestimated extrinsic bit LLRs which were fed back from the Turbo decoder to the MIMO detector. The misestimated extrinsic bit LLR is defined as the extrinsic bit LLR whose sign is different from that of the transmitted bit. Because the values shown in the figure are the extrinsic bit LLRs multiplied by the corresponding transmitted bits, the signs of the misestimated extrinsic bit LLRs are only minus. In the figure, the plot with "$(N_{\rm out}, N_{\rm in})$, last" shows the empirical CDF of the misestimated extrinsic bit LLRs at the last iterations, while the plot with "$(N_{\rm out}, N_{\rm in})$, first" shows the CDFs of misestimated extrinsic bit LLRs at the first iterations. Because an extrinsic bit LLR is dealt as

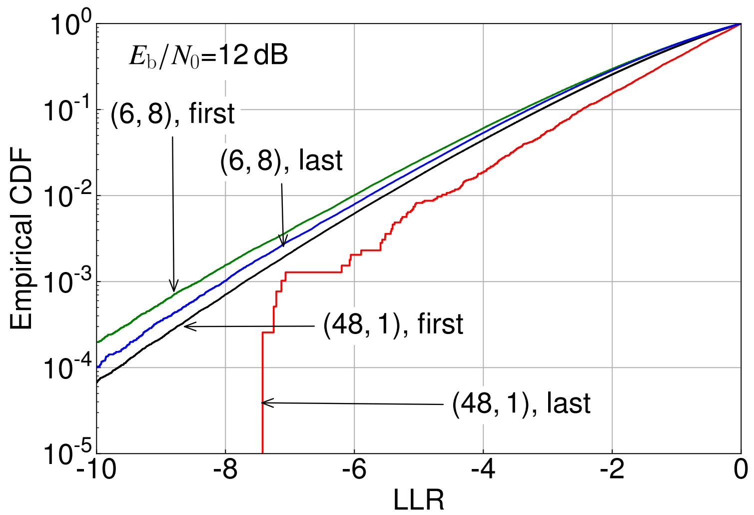

Figure 3.4: Empirical CDF of misestimated extrinsic bit LLR. ©2015 IEICE

reliability in the MAP estimation in principle, a misestimated extrinsic bit LLR, which is not reliable, should be close to zero, e.g., $L_{\mathrm{ex},v} = \log \frac{\mathbb{P}(\mathrm{Re}[d_l]=+1)}{\mathbb{P}(\mathrm{Re}[d_l]=-1)} \approx 0$ in the proposed receiver. If a misestimated extrinsic bit LLR with a big absolute value is provided to the MIMO detector, performance of the proposed detector is not improved enough. As is shown in Figure 3.4, the distribution of the misestimated bit LLR has a bigger absolute value with relatively higher probability. Because the SHISO iterative receiver circulates the misestimated extrinsic bit LLRs between the MIMO detector and the Turbo decoder, the misestimated extrinsic bit LLR with a big absolute value not only deteriorates the signal detection at the MIMO detector, but also degrades the Turbo decoding. Although the performance shown in Figure 3.4 is not that of the SISO receiver, the similar performance is expected to appear at the decoder output signals, because only the extrinsic LLRs only replace the semi-hard decision signals in the SISO receiver. Therefore, the performance of the SISO receiver can be explained with the performance in Figure 3.4, and the misestimated extrinsic bit LLRs degrades the SISO iterative receiver.

As is described above, the MIMO detector outputs the hard decision signals associated with the phase to the Turbo decoder in the proposed SHISO receiver. When the misestimated extrinsic bit LLRs are fed back to the MIMO detector, the misestimated bits are included in the hard decision signals with a certain probability due to the wrong feedback information. However, because the amplitude of the hard decision signals is rounded to one that is much smaller than that from misestimated extrinsic bit LLR, the damage from the misestimated bits is limited in the proposed SHISO receiver, especially, in the Turbo decoder. As is shown in Figure 3.4, for instance, the absolute values of the misestimated bit LLR happened to reach to 10, which were much bigger than one. Therefore, the proposed SHISO iterative receiver achieved better performance than the SISO iterative receiver, which was confirmed by Figure 3.3. Generally speaking, SISO iterative receivers are well-known to achieve the best performance when the distribution of the input signal is Gaussian. However, when the misestimated extrinsic bit LLRs have distribution that the big values appear at high probability, SISO iterative receivers are not always optimum and might have worse performance than SHISO iterative receivers.

The misestimated extrinsic bit LLRs with $(N_{\text{out}}, N_{\text{in}}) = (48, 1)$ were smaller than those with the others at the last iteration. This means that no inner iteration (i.e., $N_{\text{in}} = 1$) reduces the possibility to feed back the misestimated extrinsic bit LLRs with big absolute values to the decoder. This is the reason why the proposed receiver with $N_{\text{in}} = 1$ achieved better performance than that with $N_{\text{in}} \geq 2$ as shown in Figure 3.3.

3.5.2 Receiver with Proposed Extended MAP Estimation

The BER performance with the extended MAP estimation explained in Section 3.4.4 is shown in Figure 3.5. The BER performance with $(N_{\text{out}}, N_{\text{in}}) = (48, 1)$ was better than that with $(24, 2)$ by about 2.5 dB at BER $= 10^{-5}$. The proposed receiver with $N_{\text{in}} = 1$ achieved the best performance among the various iteration combinations, while Turbo decoders usually improve decoding performance by increasing the number of Turbo iterations, which corresponds to that of the inner iterations.

Figure 3.6 shows the empirical CDF of the misestimated extrinsic bit LLRs which are fed back from the Turbo decoder to the MIMO detector. Similar to Figure 3.4, the misestimated extrinsic bit LLRs with $(N_{\text{out}}, N_{\text{in}}) = (48, 1)$ were much smaller than the others at the last iterations. Hence, the performance shown in Figure 3.6 strongly supports that the proposed receiver with $(N_{\text{out}}, N_{\text{in}}) = (48, 1)$ achieves better performance than that with $N_{\text{in}} \geq 2$. While the absolute values of the misestimated bit LLRs at the last iterations were bigger than those at the

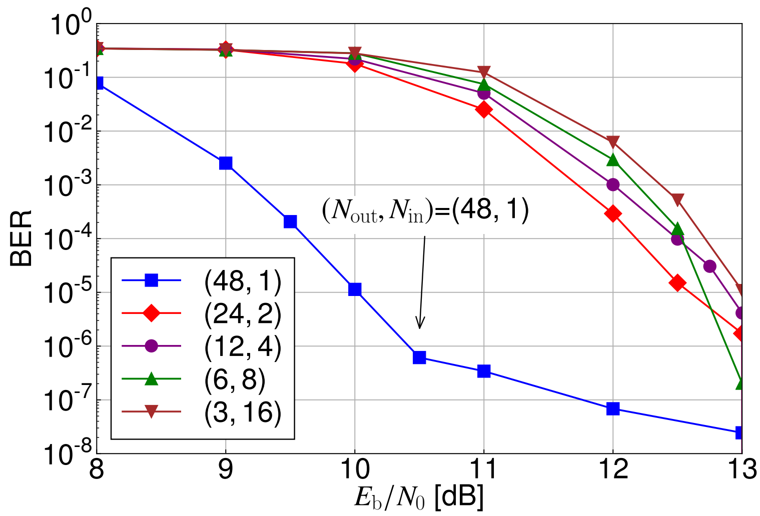

Figure 3.5: BER performance of the extended MAP estimation with the different numbers of iterations. ©2015 IEICE

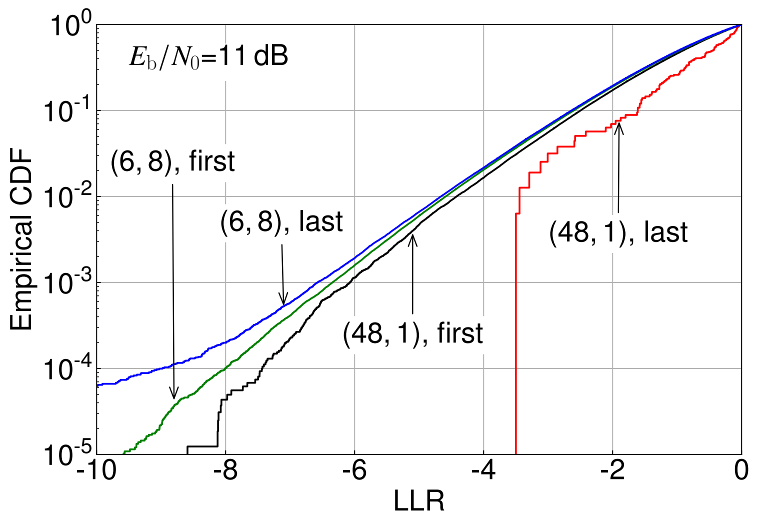

Figure 3.6: Empirical CDF of misestimated extrinsic bit LLR with the extended MAP estimation. ©2015 IEICE

first iterations in Figure 3.4, only the LLRs with $(N_{\mathrm{out}}, N_{\mathrm{in}}) = (48, 1)$ at the last iterations were smaller than those at the first iterations in Figure 3.6. The reason could be considered as follows.

Because the estimation criterion with the LLR in (3.32) can not calculate the

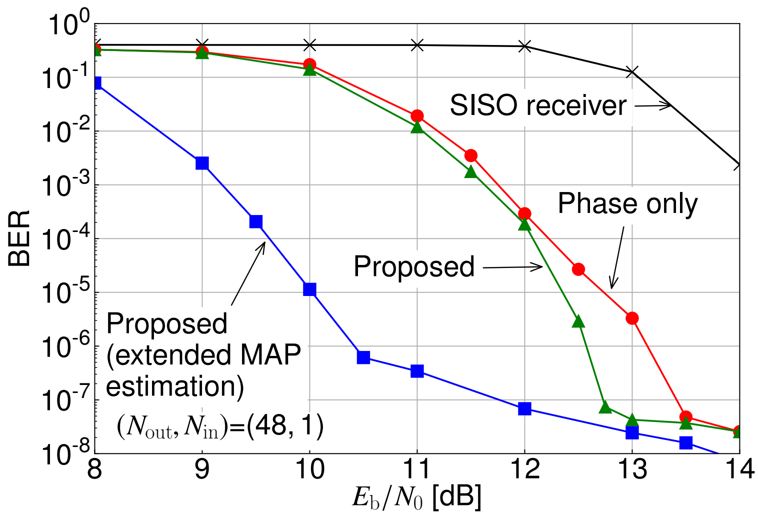

Figure 3.7: Performance comparison with Turbo coded detectors. ©2015 IEICE

marginal distribution with high precision, the SHISO iterative detector outputs the data vector $\mathbf{D}_{det}(\bar{\varphi}_{est})$ that has error symbols associated with the misestimated extrinsic bit LLRs. When the data vector is provided to the Turbo decoder, the probability that the Turbo decoder enhances the absolute values of the misestimated extrinsic bit LLRs is increased. On the other hand, because the extended MAP estimation in (3.43) estimates the marginal distribution with higher accuracy, the MIMO detector based on the extended MAP estimation generates the data vector $\mathbf{D}_{det}(\bar{\varphi}_{est})$ in which the error symbols are less correlated with the misestimated extrinsic bit LLRs as the *a priori* information. As is shown in Figure 3.6, the absolute values of the misestimated bit LLRs tend to raise as the number of the inner iteration is increased. When the extended MAP criterion is applied to the SHISO receiver with $(N_{out}, N_{in}) = (48, 1)$, the absolute values of the misestimated extrinsic bit LLRs is probably made to reduce as the number of the outer iterations increases.

Hence, the extended MAP estimation with $(N_{out}, N_{in}) = (48, 1)$ is expected to enable the MIMO receiver to achieve much better performance than the other receiver configurations. When the LLR in (3.43) is applied, the extended MAP estimation with $(N_{out}, N_{in}) = (48, 1)$ selects the estimated data vector $\mathbf{D}_{det}(\bar{\varphi}_{est})$ that limits the increase of the misestimated bit LLR, because the proposed estimation calculates the marginal distribution more exactly.

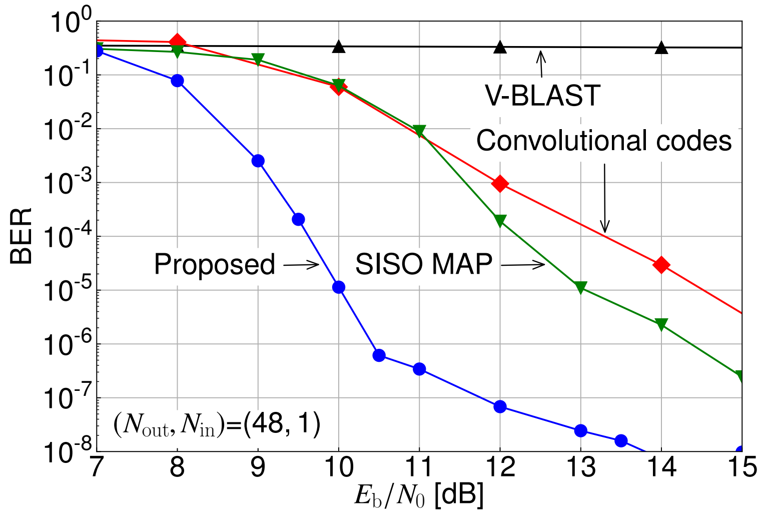

Figure 3.8: Performance comparison with conventional detectors. ©2015 IEICE

The performance of the proposed receiver with extended MAP estimation is compared with that of the other configurations in Figure 3.7. The receiver labeled as “Phase only” in the figure fed back only the extrinsic bit LLRs associated with the virtual channels to the MIMO detector from the Turbo decoder. The proposed receiver achieved better performance than the receiver with only the phase information by approximately 0.5 dB at BER = 10^{-6}. Moreover, the proposed receiver with the extended MAP estimation achieved a gain of 2.5 dB at BER = 10^{-5} compared with that without the extended MAP estimation.

The BER performance of the proposed receiver with the extended MAP estimation was compared with that of the SISO MAP iterative receiver with the Turbo code, the vertical Bell laboratories layered space-time (V-BLAST) [52] with the Turbo code, and the SISO iterative receiver with the convolutional code [40] in Figure 3.8. In the figure, the SISO MAP iterative receiver with the Turbo code and the SISO iterative virtual channel receiver with convolutional code are labelled as “SISO MAP” and “Convolutional code”, respectively. In the SISO MAP iterative receiver, the MAP detection with brute force search was performed. For fair comparison, the extrinsic bit LLRs were circulated between the MAP detector and the Turbo decoder in the SISO MAP iterative receiver. As is well-known, when the number of the receive antennas is less than that of the streams, linear MIMO detectors such as the V-BLAST, do not have capability to detect the signal

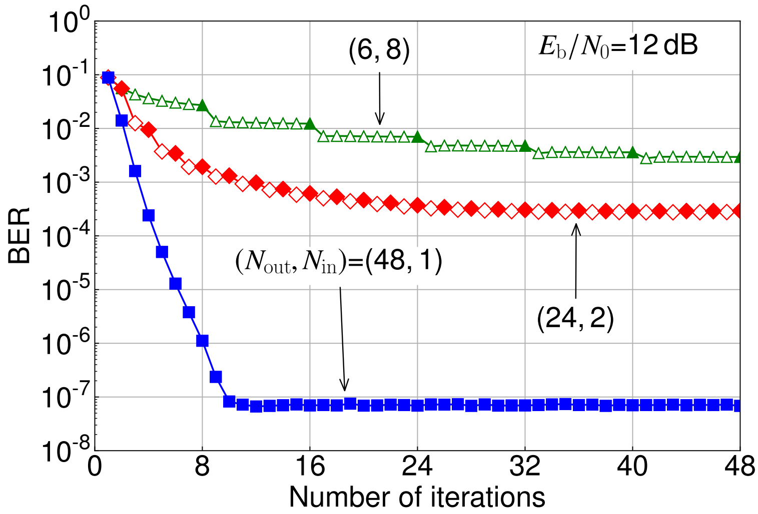

Figure 3.9: BER convergence performance of the proposed receiver with the extended MAP estimation when $E_b/N_0 = 12$ dB. The BER performance is improved by the outer iteration rather than the inner iteration. ©2015 IEICE

streams due to lack of the number of degrees of freedom. Even though the Turbo decoder follows the V-BLAST detector, the performance was much worse than the others. The performance of the V-BLAST had an irreducible error at BER of 0.5. The SISO iterative receiver with the convolutional code [40] achieved much better performance than the V-BLAST, because the non-linear signal detection was performed in addition to the linear detection in the the receiver. However, the performance of the iterative receiver was inferior to the SISO MAP iterative receiver. The proposed receiver with the extended MAP estimation achieved furthermore better performance than the SISO MAP iterative receiver by 3.0 dB at BER = 10^{-5}. In principle, the MAP achieves the best performance when the misestimated bit LLR comes close by zero owing to low reliability of the bit. However, some misestimated bit LLRs grow high when the Turbo decoder is applied as is shown above. This degrades the SISO MAP iterative receiver.

As is shown in Figure 3.8, the BER performance of the proposed receiver was steeper than that of the conventional receiver. The steep BER performance was typical to iterative decoding such as Turbo decoding, even though $(N_{out}, N_{in}) = (48, 1)$; the Turbo iteration as the inner iteration was not performed. In principle, such a performance can not be obtained without a Turbo decoder, which corresponds to

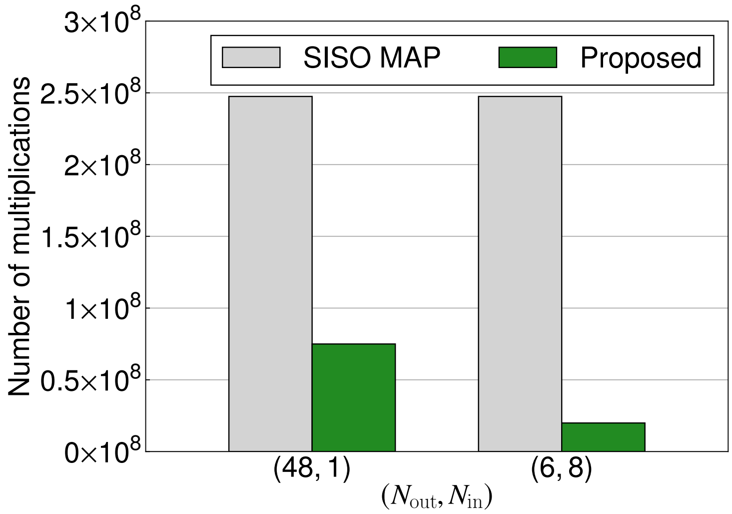

Figure 3.10: Complexity in terms of the number of multiplications. ©2015 IEICE

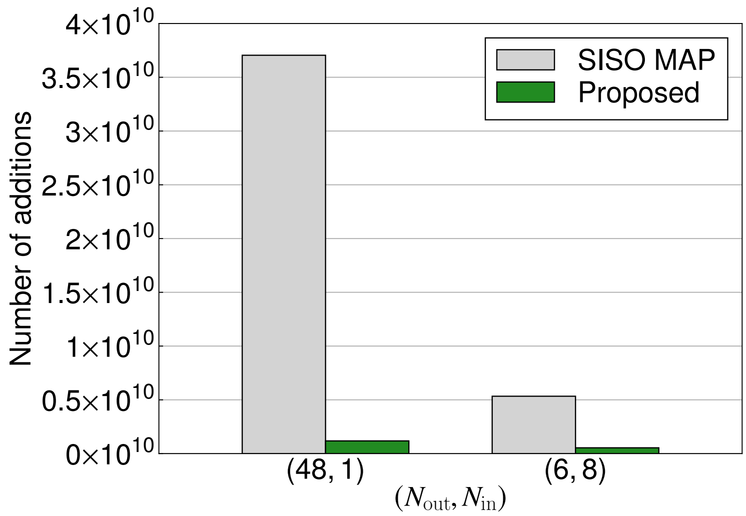

Figure 3.11: Complexity in terms of the number of additions. ©2015 IEICE

the inner decoder in the proposed receiver. Hence, the Turbo decoder as the inner decoder plays a crucial role to improve the performance.

The BER convergence performances are shown in Figure 3.9 at $E_{\mathrm{b}}/N_0 = 12$ dB. Unfilled markers in the figure indicate the BER performance of the Turbo decoder outputs when the inner iteration is once finished. Filled markers indicate the BER performance at the last inner iterations of each outer iterations. It is shown that the estimation performance was improved by the outer iteration rather than the inner iteration. Therefore, increasing the number of the outer iterations improved the BER performance. In addition, the BER convergence with $N_{\mathrm{in}} = 1$ was faster than that with $N_{\mathrm{in}} \geq 2$.

The number of multiplications and additions performed in the MIMO detectors are compared with those in the SISO MAP iterative receiver in Figure 3.10, and Figure 3.11, respectively. When $(N_{\mathrm{out}}, N_{\mathrm{in}}) = (48, 1)$, the number of multiplications in the proposed receiver is 30.3% of that required in the SISO MAP iterative receiver and the number of additions required in the proposed receiver is 3.2% of that in the other. Therefore, it can be said that the proposed receiver is less complex than the SISO MAP iterative receiver.

3.6 Simulation Evaluations of Proposed Precoding with Limited CSI

In this section, the BER performances of the proposed precoding method were evaluated by computer simulations. The simulation parameters are listed in Table 3.2. The simulated system had two transmitters with four antennas each and two receivers with two antennas each. The channel impulse responses were i.i.d and quasistatic. The receivers estimated CSI perfectly and fed them back to the transmitters with no error. The SHISO iterative receiver without extended MAP estimation was applied to detect signals.

The BER performances obtained with different precoding methods are shown in Figure 3.12. Labels in the figure indicate which transmitters are selected by the receivers as CSI-feedback targets. In different-transmitters-selected cases, two types of precoding matrices were used: a right singular vector matrix $\mathbf{V}_{ij}$ and $\mathbf{P} = \frac{1}{\sqrt{2}} [\mathbf{I}\ \mathbf{I}]^{\mathrm{T}}$. When the receivers fed CSI back to all transmitters, the best performance was achieved because the receivers only needed to detect four-stream signals using two antennas, while the receivers needed to detect six-stream signals when the other cases. However, the amount of feedback CSI is larger when the receivers select all transmitters than when they select one of the transmitters. In case where the receivers selected different transmitters, the precoding with the right singular matrix $\mathbf{V}_{ij}$ achieved better BER performance by about 2.8 dB in

Table 3.2: Simulation parameters for the precoding method evaluation in MU-MIMO systems.

Parameters	Values
Number of antennas	$\{4,4\} \times \{2,2\}$
Modulation scheme	OFDM-QPSK
Channel model	10-path Rayleigh fading
Forward error correction	Turbo code, rate $1/3$
Number of sub carriers	512
Data packet length	16384 bits

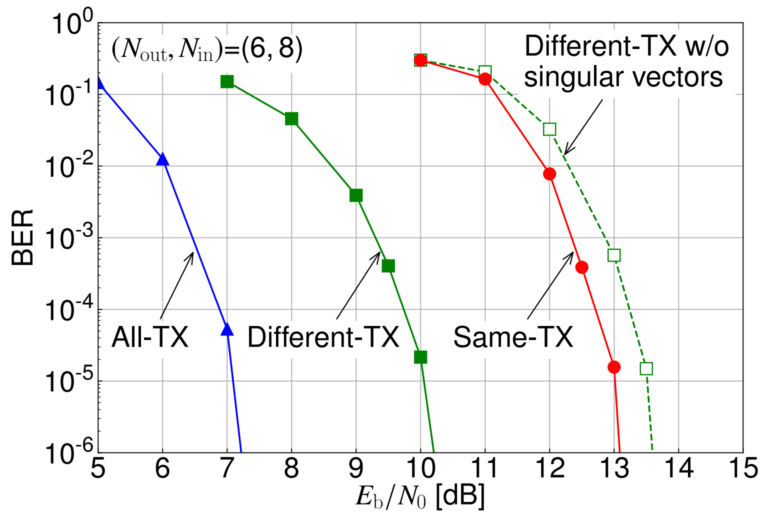

Figure 3.12: BER Performance of the proposed precoding method where $(N_{\rm out}, N_{\rm in}) = (6, 8)$. SHISO iterative receiver without extend MAP estimation is applied. The BER performance is improved when receivers select different transmitters compared with that of when they select the same transmitter.

$E_{\rm b}/N_0$ than that with the simple matrix $\mathbf{P}$. This is because the proposed method is equivalent to water-filling power allocation over $\mathbf{H}_{ii}$ in (3.5), while equal power allocation is performed with $\mathbf{P}$. Moreover, the performance when using the right singular matrix $\mathbf{V}_{ij}$ was better than the performance when the receivers select the same transmitter.

The performance with different number of iterations is shown in Figure 3.13. It

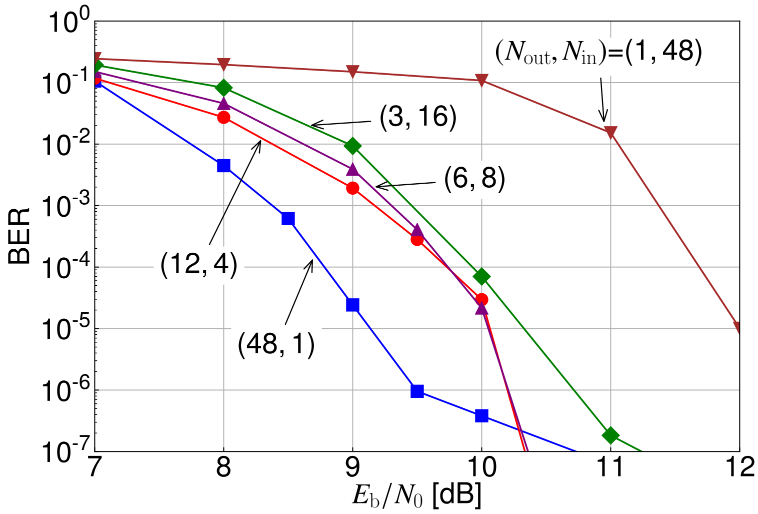

Figure 3.13: BER performance with various numbers of iterations when receivers select different transmitters to feed CSI back to.

is assumed that receivers select different transmitters to feed CSI back to. $N_{\rm out} = 1$ implies that the Turbo decoders do not feed back the LLRs to the virtual channel detectors. On the other hand, when $N_{\rm in} = 1$, two MAP decoders decode signals only once and feed the LLRs back to the virtual channel detectors. Similar to SU-MIMO environments, the system with $(N_{\rm out}, N_{\rm in}) = (48, 1)$ shows the best performance.

3.7 Conclusions

This chapter proposed a novel receiver referred to as a SHISO iterative receiver employing virtual channels with a Turbo decoder for for cooperative MIMO systems with limited feedback CSI. The proposed receivers can detect signals even when interfered signals are received and the number of signal streams exceeds the number of receive antennas. In the proposed SHISO iterative receiver, the extrinsic bit LLR is fed back from the decoder to the MIMO detector as an *a priori* information, and the real signal and the hard decision signal of the phase are provided to the Turbo decoder. Moreover, this chapter proposed a new estimation criterion, named as "extended MAP estimation" for the MIMO detector to select the most likely virtual channel. The proposed receiver was evaluated in a 6×2

SU-MIMO system. If the product of the number of the outer iterations and that of the inner iterations was set to 48, the proposed receiver with the inner iteration $N_{\mathrm{in}} = 1$ achieved better performance than that with $N_{\mathrm{in}} \geq 2$. Even when the extended MAP estimation was applied to the proposed receiver, the combination of $(N_{\mathrm{out}}, N_{\mathrm{in}}) = (48, 1)$ made the receiver achieve the best performance in that with the other combinations.

The proposed receiver with the extended MAP estimation achieved better performance than the original SHISO MIMO receiver by 2.5 dB at BER = 10^{-5}. The proposed receiver with the extended MAP estimation attained by 3.0 dB better performance than the SISO MAP iterative receiver at BER = 10^{-5}, because the misestimated extrinsic bit LLR provided by the detector deteriorated the Turbo decoding in the SISO MAP iterative receiver. Besides, the proposed receiver had lower computational complexity than the SISO MAP iterative receiver. In summary, the proposed receiver achieved better transmission performance with relatively low computational complexity compared with the SISO MAP iterative receiver.

The performance of the precoding method with the proposed SHISO iterative receiver was evaluated. The results showed that feeding back CSI to the different transmitters and using right singular matrices for precoding improved BER performances when the receivers feed CSI back to only one of the transmitters. If receivers feed CSI back to all transmitters, the BER performance was improved. However, this scheme required larger amount of feedback CSI, which means that there is a tradeoff between the amount of feedback CSI and the BER performance.

Chapter 4

Cooperative mmWave Relay Expansion

4.1 Background

This chapter studies a vehicle position control method to solve the relay disconnection problem and extend the coverage of RSUs. The proposed method enables position-controllable vehicles, such as autonomous vehicles, to change their relative positions, where LOS paths are available and V2V relays can be connected by lane change or overtaking. A simple example is shown in in Figure 4.1. Let vehicles #1, #2, and #4 have mmWave communication devices, while vehicle #3 does not have one. Vehicles #1 and #2 are initially connected with each other on mmWave channels, but vehicles #2 and #4 are not connected because of the blockage by vehicle #3. In this case, by moving vehicle #2 to a position where a LOS path between vehicle #2 and #4 becomes available, the relay length can be extended and thus, the RSU coverage is extended to include vehicle #4.

Cooperative position controls of vehicles have been studied in [8, 9, 53, 54]. While they focus on improving the stability and robustness of formation and platooning control, they do not consider improving communication quality. In the fields of robots and wireless sensors, movement or position control methods to improve the connectivity of multi-hop communications have been discussed [55, 56]. However, these prior works do not focus on the relay length, and they consider conventional microwave communications where no harmful blockage

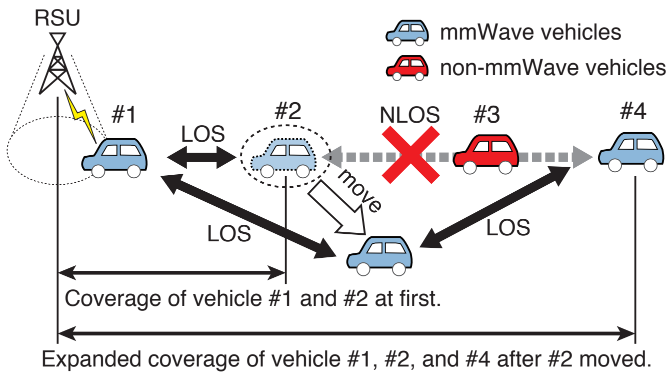

Figure 4.1: Concept of mmWave relaying with vehicle position controls. Vehicle #3 initially blocks the path between vehicles #2 and #4. When vehicle #2 changes its position, vehicles #2 and #4 communicate with each other via a LOS path; thus, the multi-hop relay becomes long. ©2019 IEICE

occurs.

[57] proposed a vehicle position control method for coverage expansion in mmWave vehicular networks and revealed the maximum gain of coverage improvement by optimizing vehicle positions. However, this work uses a centralized algorithm, which is not sufficiently scalable, and does not consider the movement of each vehicle to its optimal position. To maximize the relay length, both positions of vehicles and their movement paths should be optimized. However, the optimization problem of collision-free path planning of multiple vehicles is an NP-hard problem [58]. Therefore, the optimal solution cannot be obtained even if centralized manners are applied. Moreover, centralized algorithm is not practical for vehicle controls because it cannot be applied when lots of vehicles exist in wide areas, thus a distributed mechanism is required that enables vehicles to expand relay length by moving to good positions without collision.

In this chapter, a DeepRL-based vehicle position control method is developed, where each vehicle distributedly decides its movement without knowledge of the optimal position or global information other than that of the surrounding vehicles. RL is introduced to obtain a movement strategy via which vehicles decide their movement in order to increase coverage based on their own information, such as locations of the surrounding vehicles. Because such a strategy is high-dimensional and non-linear function, DeepRL, which combines RL algorithms and deep learning methods, is employed. To increase the learning speed by updating the strategy cooperatively, the proposed method utilizes one of the distributed DeepRL algorithms, A3C [39], which was originally developed for parallel processing. In A3C, multiple agents update the shared strategy cooperatively, while acting in multiple environments independently. By applying the cooperative-strategy-updating scheme to the coverage-improvement problem, multiple vehicles can cooperatively and efficiently learn the strategies; this allows them to make decisions without communicating with each other. Because DeepRL algorithms achieve high performance in problems where the environment state is represented as a pictorial image, this chapter designs a three-dimensional state representation like color images for the coverage expansion problem.

The simulation results show that vehicles can learn the coverage-increasing strategy using the DeepRL algorithm. It is demonstrated that the learned strategies achieve high performance even when the traffic conditions and the penetration ratio of mmWave-available vehicles are changed from that in the learning phases.

The contributions of this chapter are summarized as follows:

(1) This chapter presents a solution for blockage problems in mmWave vehicular networks. The proposed method is based on position control of vehicles, whereas conventional works [23–25] have assumed that vehicle positions are specified and not controllable.

(2) This chapter presents a distributed DeepRL-based vehicle movement-control algorithm. By leveraging a DeepRL algorithm, A3C, the proposed algorithm enables vehicles to learn a movement strategy, which involves complex mapping from surrounding vehicle positions to movement action.

(3) The simulation results justify that the proposed algorithm achieves high performance even when the environment conditions (e.g., the penetration ratio of mmWave-communicable vehicles and vehicle density) of learning and test phases are not the same.

The rest of this chapter is organized as follows: Related works are discussed in Section 4.2. Then, a system model is described in Section 4.3, and the DeepRL-based approach to improve coverage is presented in Section 4.4. Finally, simulation results are presented in Section 4.5 and conclusions are drawn in Section 4.6.

4.2 Related Works

Since the currently available vehicular communication protocols, DSRC and C-V2X, cannot meet the increasing demand of high-data-rate vehicular communications for sharing enormous sensor data and providing infotainment because of their limited bandwidth, mmWave communication is an essential technique for vehicular communications. It offers huge bandwidth (e.g., 9 GHz in 60 GHz band) and realizes beyond-Gbit/s throughput. In addition, offloading data transmission of non-safety applications from the microwave bands to the mmWave bands can reduce the pressure on the microwave band, and should be used for critical applications such as vehicle collision warning systems and self-driving systems. The authors of [13] provide a survey of mmWave vehicular communications, including detailed analysis of mmWave spectrum, PHY, and MAC designs for mmWave communications that can be applied to vehicular communications. MAC protocols for mmWave multi-hop relaying for vehicular networks have been studied in [59, 60]. In [59], an ALOHA-based protocol is evaluated for a one-lane highway scenario, and it is demonstrated that multi-hop achieves better performance than single-hop in disseminating information to a certain number of vehicles. The authors of [60] study content delivery using heterogeneous networks consisting of the licensed Sub-6 GHz band, DSRC, and mmWave communications. They introduce fuzzy logic to select efficient cluster heads considering the vehicle velocity, vehicle distribution, and antenna height. Whereas these studies assume that vehicle movements are given, this chapter proposes a control method of vehicle movements in order to avoid blockage.

Multi-hop relaying for increasing the coverages of RSUs has been studied for the microwave vehicular adhoc network (VANET). The authors of [23] propose multi-hop V2V relaying to compensate for the sparsity of RSUs. [24] minimizes the number of vehicles that communicate with RSUs by constructing clusters where messages are transmitted via V2V relays. The authors of [25] propose a forwarding algorithm to extend the coverage of RSUs for urban areas. The algorithm realizes multi-directional dissemination in intersections by considering the geographic positions of vehicles. Although these prior studies show high performance when the vehicle density is high, relay disconnections by obstacles are not considered because these studies assume microwave VANETs. The proposed method leverages the mobility controllability of autonomous vehicles to connect vehicles via LOS paths. Such a topology-modifying scheme is one of the differences between the proposed method and conventional methods.

Position control of vehicles has been studied in the literature of cooperative vehicle platoon and formation controls [8, 9, 53, 54]. The authors of [9] develop a platoon-management protocol based on VANET. In the protocol, the platoon leader sends beacons that contain platoon parameters to followers in a multi-hop manner, and each follower maintains an appropriate inter-vehicle space. [8] proposes an intra-platoon management strategy that ensures platoon stability under the presence of communication delays. The authors of [53, 54] study formation controls for cooperative vehicles. They utilize graph theory and demonstrate the robustness of their methods. In [61], a formation-control method based on potential fields is proposed for unmanned aerial vehicles. Although these methods, which rely on vehicular communication techniques, improve the stability or robustness of vehicle formations, they are not intended to improve communication quality. Moreover, they assume that the desired patterns or inter-vehicle distances are given, whereas this work focuses on finding the relative positions that increase the coverage of wireless networks.

Some researchers of robot control systems, not vehicles, have proposed movement control or positioning schemes to improve the connectivity of multi-hop networks. The authors of [55] propose a block-movement algorithm to construct fault-tolerant adhoc networks for autonomous multi-robot systems. However, coverage expansion is not discussed in [55]. As a decentralized deployment method, virtual force algorithms (VFAs) are introduced in [62, 63]. These algorithms focus on increasing the sensor coverage of wireless sensor networks (WSNs) under the constraints of the desired connectivity. VFAs are also used in [56] for vehicle self-deployment in order to form fault-tolerant adhoc networks. The authors of [56] utilize an evolutionary algorithm (EA) to determine the velocity and virtual forces for fitness values of the EA. VFAs perform well in these studies because they assume microwave communications, in which connection quality between two nodes increases as they become closer. In mmWave communications, however, blockage

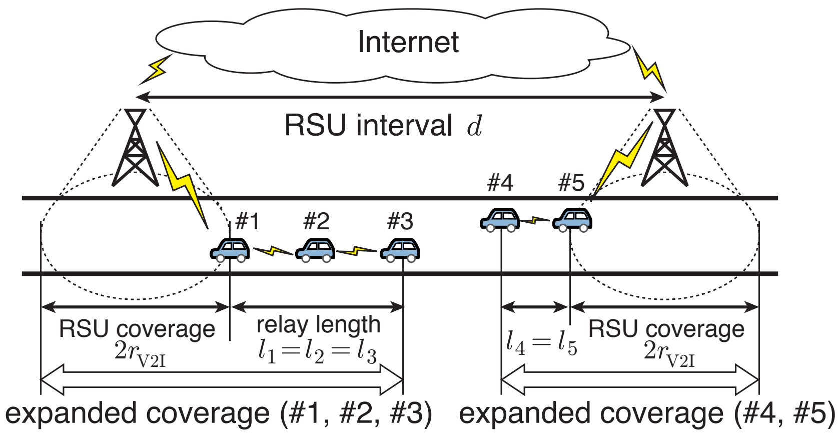

Figure 4.2: System model of coverage expansion by mmWave relays. Coverage is expanded through multi-hop relaying. l_i denotes the length along the road of the relay chains to which vehicle i belongs. The expanded mmWave V2I communication range of vehicle i can be expressed as $2r_{\mathrm{V2I}} + l_i$. ©2019 IEICE.

effects decrease the connectivity of non-line-of-sight (NLOS) communications; thus, mmWave connectivity, as a function of positions, has local maxima. Therefore, VFAs, which are based on gradients, are not expected to improve mmWave connectivity because vehicles are trapped at the local maxima.

Note that other approaches to solve the blockage problem are discussed, and beamforming is a promising technique that controls the directionality of array antennas to leverage a strong reflected signal [64–66]. This work does not conflict with beamforming and can be used simultaneously. For example, when a LOS path is not available but a NLOS path with a strong signal is available, beamforming solves the blockage problem. However, if there are no LOS and strong NLOS paths, the proposed method moves vehicles to leverage a strong path and extend the relay length.

4.3 System Model

Figure 4.2 illustrates a system model of this work. This work considers a straight N_{l}-lane highway with mmWave RSUs deployed at intervals of d. A single direction is considered because aim of this work is to create relay chains that remain unchanged for a long time. For simplicity, it is assumed that vehicles are located at grid points. it is also assumed that the average velocities of all the vehicles are nearly the same, which is confirmed in [67], where the authors demonstrate that velocity variance decreases as the ratio of vehicles with adaptive cruise control increases, which is one of the key technologies in autonomous vehicles. Two cases are considered in the simulation evaluations: one where the velocity is constant and the other where it fluctuate. When the vehicles move at a constant and equal velocity, the relative positions of the vehicles do not change. When the velocity fluctuates, the movements on the relative positions can be modeled as random walks. A region of interest (RoI) also moves with the vehicles at the same velocity as them.

A simplified mmWave communication model is assumed in which vehicles can be connected if and only if the distance between the vehicles is less than a certain distance and a LOS path is available. It is also assumed that link qualities of the mmWave channels are ideally predictable. This assumption is not unrealistic considering state-of-the-art prediction methods. For example, the authors of [22, 68] present a mmWave propagation loss model for V2V communications. Another approach is proposed in [69, 70], where the authors predict the throughput of mmWave communications and received signal strength of mmWave radios using image sensor data.

There are non-mmWave vehicles and mmWave vehicles, which are subdivided into controllable mmWave vehicles and uncontrollable mmWave vehicles. Whereas the non-mmWave vehicles only use microwave communication systems, mmWave vehicles use both microwave and mmWave communication systems and constitute the multi-hop relay chains for increasing coverage. Microwave communication systems, such as DSRC and C-V2X, enable all the vehicles to share information on vehicle positions and their control signals, whose packet sizes are very small. It is assumed that the effect of transmission loss and delay is negligible because the duration for a transmission is less than 100 ms which is much less than the decision-making interval of vehicles. For example, in DSRC, the vehicles broadcast their position every 100 ms [29]. Therefore, the vehicles can retransmit dropped packets several times and the probability that the vehicles fail to receive all the retransmitted packets is very low. The mmWave vehicles can access RSUs over mmWave channels within a distance of r_{V2I} and communicate with each other only when they are within a distance of r_{V2V} and there are no vehicles blocking their LOS paths. The controllable vehicles can change their relative positions on the road in order to expand coverage, while uncontrollable vehicles do not change their relative positions or move randomly because they have other driving strategies or are driven by humans.

Let n, n_{m}, and n_{c} denote the total number of vehicles, all mmWave vehicles, and the number of controllable mmWave vehicles in the RoI, respectively. $R_{\mathrm{mm}} := n_{\mathrm{m}}/n$ and $R_{\mathrm{c}} := n_{\mathrm{c}}/n_{\mathrm{m}}$ denote the ratio of the number of the mmWave vehicles to the total number of vehicles and the ratio of the number of the controllable vehicles to the total number of mmWave vehicles, respectively. Let P_{a}, P_{n}, P_{c}, and P_{u} denote the sets of all grid positions in the RoI, the non-mmWave vehicle positions, the controllable mmWave vehicle positions, and the uncontrollable mmWave vehicle positions, respectively. $P_{\mathrm{c}} \in \mathcal{P}$ is a variable that the proposed method controls, where $\mathcal{P} := 2^{P_{\mathrm{a}} \setminus (P_{\mathrm{n}} \cup P_{\mathrm{u}})}$ represents a power set of $P_{\mathrm{a}} \setminus (P_{\mathrm{n}} \cup P_{\mathrm{u}})$.

A quality metric is defined for the proposed method as the proportion of areas where vehicles can connect to RSUs through multi-hop relay chains based on the coverage of each vehicle. When using mmWave vehicles as relay nodes, the mmWave V2I communication range of vehicle i is expressed as $r_i = 2r_{\mathrm{V2I}} + l_i(P_{\mathrm{c}})$, as shown in Figure 4.2. Here, $l_i(P_{\mathrm{c}})$ denotes the length along the road of the relay chains to which vehicle i belongs. Because RSUs are deployed at intervals of d, it is sufficient to consider d-long sections of road. The coverage for vehicle i is expressed as follows:

$$C_i(P_{\mathrm{c}}) = \min\left\{\frac{r_i}{d}, 1\right\}. \tag{4.1}$$

Note that the coverage $C_i(P_{\mathrm{c}})$ increases linearly with the length of the multi-hop relay chain. The average of the vehicles' coverage is defined as a quality metric, as follows:

$$C_{\mathrm{avg}}(P_{\mathrm{c}}) := \frac{1}{n_{\mathrm{m}}} \sum_{i=1}^{n_{\mathrm{m}}} C_i(P_{\mathrm{c}}). \tag{4.2}$$

An example of expanding coverage by changing vehicle positions is shown in Figure 4.3. Non-mmWave, controllable mmWave, and uncontrollable mmWave vehicles are depicted as red, dark blue, and light blue vehicles in Figure 4.3, respectively. Vehicles #1–#5 are all mmWave vehicles, but only vehicles #1 and

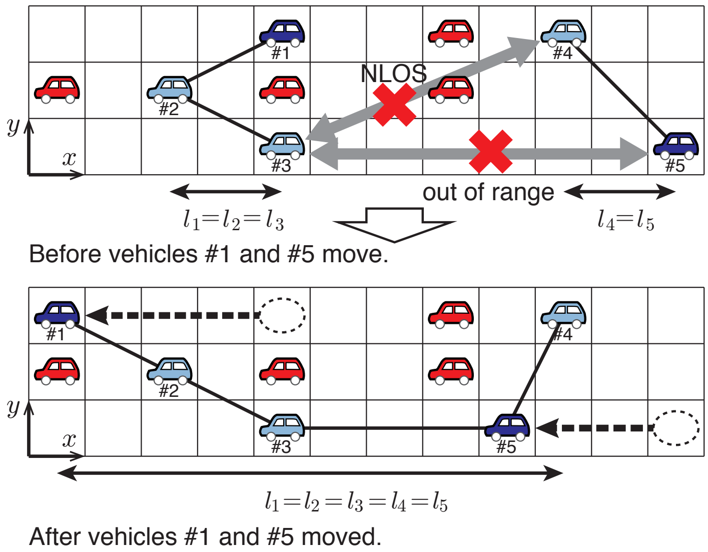

Figure 4.3: Example of coverage expansion by vehicle movements. Non-mmWave, controllable mmWave, and uncontrollable mmWave vehicles are depicted as red, dark blue, and light blue vehicles, respectively. The mmWave relay length is extended by changing the positions of vehicles #1 and #5. ©2019 IEICE

#5 are controllable. Before vehicles #1 and #5 move, the relay chains on the left and right sides cannot be connected using the mmWave bands because they are out of communication range or non-mmWave vehicles are blocking the LOS. However, after vehicles #1 and #5 move, vehicles #3 and #5 become connected. At this point, all mmWave vehicles can be connected, and the length of the relay chain is extended. $C_{\mathrm{avg}}(P_{\mathrm{c}})$ increases as a result.

4.4 Distributed Vehicle Movement Controls

4.4.1 Motivation for Using Reinforcement Learning

Although [57] revealed the capability of coverage improvement using vehicle position control, solving the vehicle-movement problem is still a big challenge. Because vehicle-moving strategies should be scalable and decentralized for practical usage, each vehicle should be able to decide its movement for increasing coverage by itself. Because of conventional microwave communication systems, information on the surrounding vehicles' positions are available for each controllable vehicle to decide its movement. This section formulates the decision-making problem as an MDP such that it can be solved by RL. Using the RL scheme, vehicles can learn the optimal positions to increase coverage and go there without being instructed to. Because the observed states have large dimensions, traditional RL methods cannot be applied to the problem; thus, a DeepRL algorithm is required for function approximation. The proposed method utilizes the DeepRL algorithm, A3C, because it is advantageous in terms of convergence efficiency and learning speed [39].

While vehicles are learning strategies using the A3C algorithm, they share DNN models with other vehicles. To this end, a model management server that stores a global model is required. The model management server updates the global model using gradients collected from the vehicles and distributes the up-to-date model to the vehicles. These data are transmitted via microwave channels or mmWave relays if they are available. In this system, vehicles do not always have to be connected to the model management server. They opportunistically upload their gradient, and then, the model management server updates the global model. Once the well-trained model is obtained, there is no need for vehicles to share DNN models during the operation phase. Therefore, controllable vehicles decide their movements by using the model in a decentralized way. Following portion of this section explains how vehicles learn movement strategies of coverage expansion using the RL algorithm. State designs is also described that improve the performance of increasing coverage.

4.4.2 Deep-Reinforcement-Learning-Based Algorithm

Controllable vehicles, called agents, interact with an environment over a number of discrete time steps. The relationship between an agent and the environment is shown in Figure 4.4. At each time step t, agent i observes the surrounding states $s_{i,t}$ representing other vehicles' positions and types. The detailed definitions of the states are given by (7), (8), and (9) in Section 4.4.3. The surrounding vehicle information is shared via microwave channels, and the observation range is limited

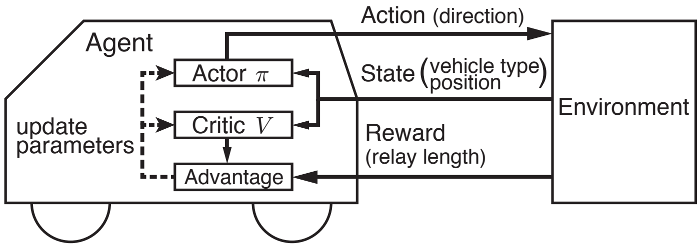

Figure 4.4: Actor-critic reinforcement learning model. ©2019 IEICE

by the microwave communication range, which determines the dimension of the states. The observation area is limited by the range of DSRC communications, where positions and types of vehicles are broadcasted and shared with each other. According to an action-selection policy $\pi(a_{i,t}|s_{i,t})$, agents select an action $a_{i,t}$ from a set of actions $\mathcal{A}$ consisting of *forward*, *back*, *right*, *left*, and *stay*. Note that these actions represent changing relative positions with respect to the other vehicles. After moving to the next position, agent i receives a reward $r_{i,t}$. A reward from each step is defined as:

$$r_{i,t} := \begin{cases} \alpha l_i + r_{\mathrm{p}} & \text{if an agent selects a prohibited direction} \\ \alpha l_i & \text{otherwise,} \end{cases} \tag{4.3}$$

where l_i and $\alpha(> 0)$ denote a relay length and parameter balancing the reward and penalty, respectively. $r_{\mathrm{p}}(< 0)$ denotes a penalty that is added when an agent selects a direction, where the vehicle should not move. In order to avoid car accidents, the prohibited direction is defined as the direction where other vehicles exist or are moving to and where the agent gets off the road. Relay length information is calculated by the following procedure. Agents broadcast their position information via the relay over the mmWave channel. Then, the agents calculate the relay length l_i as the length along the road direction between the head and tail vehicles using shared position information. Such information sharing can be completed within a short period compared to the decision-making interval of the RL scheme.

The goal of RL is to optimize the action-selection policy $\pi(a_{i,t}|s_{i,t})$ to maximize the future accumulated reward $R_{i,t} := \sum_{\tau=0}^{\infty} \gamma^{\tau} r_{i,t+\tau}$, where $\gamma \in [0, 1)$ is a discount factor. The expectation of $R_{i,t}$ from step t underlying π is called the value function, which is defined as $V^{\pi}(s_{i,t}) := \mathbb{E}\left[R_{i,t}|s_{i,t}\right]$. Each agent acts to maximize its own accumulated reward $R_{i,t}$, which can be calculated from information obtained by the agent; thus, the proposed method works in a distributed manner.

A3C [39] is employed as the implementation of DeepRL. A3C learns the optimal policy with sharing models and experiences by multiple agents; thus, it suits the considered problem in which multiple vehicles are required to learn a similar strategy. Algorithm 4.1 shows the detailed procedure of the A3C learning phase in each episode, which consists of $T_{\max}$ time steps. For more detail, please refer to [39]. A3C parameterizes the policy function $\pi(a_{i,t}|s_{i,t};\theta)$ and the value function $V(s_{i,t};\theta_{\mathrm{v}})$, where θ and θ_{v} denote globally shared parameters of π and V, respectively. The globally shared parameters are stored in the model management server. Agents first downloads the globally shared parameters and copy them to agent-specific parameters θ_i and $\theta_{\mathrm{v},i}$ when they have started learning (Line 3 in Algorithm 4.1). The agents act $t_{\max}$ times in accordance with their agent-specific policies independently and store rewards from each step (Lines 4–9 in Algorithm 4.1). The agents calculate the gradients of updating parameters $\varDelta\theta_i$ and $\varDelta\theta_{\mathrm{v},i}$ at interval $t_{\max}$ (Lines 10–17 in Algorithm 4.1). The calculated gradients are uploaded to the model management server, and then, the server updates the globally shared parameters θ and θ_{v} by gradient ascent and gradient descent, respectively (Lines 18–19 in Algorithm 4.1). After sufficient time steps, the shared policy and value functions each converge to the corresponding optimal functions. The gradients $\varDelta\theta_i$ and $\varDelta\theta_{\mathrm{v},i}$ are calculated as follows:

$$\begin{aligned}\theta\colon \varDelta\theta_i = &\sum_{\tau=t}^{t+t_{\max}} \nabla_{\theta_i} \log\pi(a_{i,\tau}|s_{i,\tau};\theta_i)A(a_{i,\tau},s_{i,\tau};\theta_{\mathrm{v},i})\\ &+\beta\nabla_{\theta_i}H(\pi(s_{i,\tau};\theta_i)),\end{aligned} \tag{4.4}$$

$$\theta_{\mathrm{v}}\colon \varDelta\theta_{\mathrm{v},i} = c_{\mathrm{v}}\sum_{\tau=t}^{t+t_{\max}} \partial\left(A(a_{i,\tau},s_{i,\tau};\theta_{\mathrm{v},i})\right)^2/\partial\theta_{\mathrm{v},i}, \tag{4.5}$$

where β, $H(\pi(s_{i,\tau};\theta_i))$, and c_{v} denote a regularization parameter, the entropy of $\pi(s_{i,\tau};\theta_i)$, and a coefficient that balances θ and θ_{v}, respectively. $A(a_{i,\tau},s_{i,\tau};\theta_{\mathrm{v},i})$ is an estimation of the advantage of action $a_{i,\tau}$ in state $s_{i,\tau}$ [39], defined as:

$$A(a_{i,\tau},s_{i,\tau};\theta_{\mathrm{v},i}) \coloneqq \sum_{u=0}^{\tau'-1}\gamma^u r_{i,\tau+u} + \gamma^{\tau'}V(s_{i,\tau+\tau'};\theta_{\mathrm{v},i}) - V(s_{i,\tau};\theta_{\mathrm{v},i}), \tag{4.6}$$

Algorithm 4.1 Algorithm for updating policy and value model parameters.

1: Initialize $t \leftarrow 0$.
2: **while** $t < T_{\max}$ **do**
3: Download the globally shared parameters and copy them to agent-specific parameters: $\theta_i \leftarrow \theta$, $\theta_{\mathrm{v},i} \leftarrow \theta_{\mathrm{v}}$.
4: $t_{\mathrm{start}} \leftarrow t$
5: **for** $t \in \{t_{\mathrm{start}}, \ldots, t_{\mathrm{start}} + t_{\max}\}$ **do**
6: perform action $a_{i,t}$ according to policy $\pi(a_{i,t}|s_{i,t};\theta_i)$
7: receive reward $r_{i,t}$
8: $t \leftarrow t + 1$
9: **end for**
10: Reset gradients $\Delta\theta_i$ and $\Delta\theta_{\mathrm{v},i}$ to 0.
11: $R_{i,t} \leftarrow V(s_{i,t};\theta_{\mathrm{v},i})$
12: **for** $\tau \in \{t_{\mathrm{start}} + t_{\max} - 1, \ldots, t_{\mathrm{start}}\}$ **do**
13: $R_{i,\tau} \leftarrow r_{i,\tau} + \gamma R_{i,\tau+1}$
14: $A(a_{i,\tau}, s_{i,\tau};\theta_{\mathrm{v},i}) \leftarrow R_{i,\tau} - V(s_{i,\tau};\theta_{\mathrm{v},i})$
15: $\Delta\theta_i \leftarrow \Delta\theta_i + \nabla_{\theta_i} \log \pi(a_{i,\tau}|s_{i,\tau};\theta_i) A(a_{i,\tau}, s_{i,\tau};\theta_{\mathrm{v},i}) + \beta \nabla_{\theta_i} H(\pi(s_{i,\tau};\theta_i))$
16: $\Delta\theta_{\mathrm{v},i} \leftarrow \Delta\theta_{\mathrm{v},i} + c_{\mathrm{v}} \partial \left(A(a_{i,\tau}, s_{i,\tau};\theta_{\mathrm{v},i}) \right)^2 / \partial\theta_{\mathrm{v},i}$
17: **end for**
18: Upload gradients $\Delta\theta_i$ and $\Delta\theta_{\mathrm{v},i}$ to the server
19: [SERVER] Update parameters θ and θ_{v}
20: **end while**

where τ' is a counter that is incremented at each step in the loop (Lines 12–17 in Algorithm 4.1).

In a common A3C learning phase, multiple agents in multiple independent environments share the parameters θ and θ_{v} of the learning models. This model sharing enables efficient convergence due to the independence between training data sets. Although there is a single environment in the considered problem, the observed states of multiple agents are different and have little correlation if their distances are great enough. DNN models therefore converge due to model sharing.

4.4.3 State Designs and Network Models

This section designs three state definitions: (1) vehicle positions and types (PT); (2) vehicle positions, types, and continuous relay lengths (PTCL); and (3) vehicle positions, types, and discrete relay lengths (PTDL). The performance of these state definitions are compared in Section 4.5 and showed that PTCL and PTDL, which include relay length information, achieve greater coverage than PT.

States $s_{i,t}$ are defined as three-dimensional $K \times X \times Y$ feature planes, where K, X, and Y denote the number of features and the observation ranges of the x and y axes, respectively. A feature plane design is introduced in AlphaGo [37]. Feature planes represent different features in different planes and convolutional neural networks (CNN) are expected to adaptively optimize their parameters to each feature. Let $s_{i,t}^{(k,x,y)}$ denote each state element, where k and (x, y) represent a feature index and a relative position observed from the vehicle i, respectively. The center of each feature plane represents the position of vehicle i. While X is limited by the microwave communication range, Y is defined as $Y := 2N_\mathrm{l} - 1$ to cover all lanes. The state elements $s_{i,t}^{(k,x,y)}$ in PT are defined as follows:

$$s_{i,t}^{(1,x,y)} := \begin{cases} 1 & \text{if a mmWave vehicle positions at } (x, y), \\ 0 & \text{otherwise}, \end{cases} \tag{4.7}$$

$$s_{i,t}^{(2,x,y)} := \begin{cases} 1 & \text{if a non-mmWave vehicle positions at } (x, y), \\ 0 & \text{otherwise}, \end{cases} \tag{4.8}$$

$$s_{i,t}^{(3,x,y)} := \begin{cases} 1 & \text{if } (x, y) \text{ is empty}, \\ 0 & \text{otherwise}. \end{cases} \tag{4.9}$$

In order to improve the coverage performance of RL-based methods, states with additional information is designed regarding the achievable relay length $\hat{l}_i(x, y)$ when vehicle i would move to position (x, y). $\hat{l}_i(x, y)$ is calculated by each agent using vehicle positions and type information. Each agent is required to estimate whether a stable mmWave communication link could be established to calculate $\hat{l}_i(x, y)$. Link stability can be estimated using path-loss prediction models [22,68], which enable vehicles to predict path loss considering blockage effects caused by other vehicles. Margins can be considered for the received power required to establish links in order to avoid misprediction. Additional PTCL features are

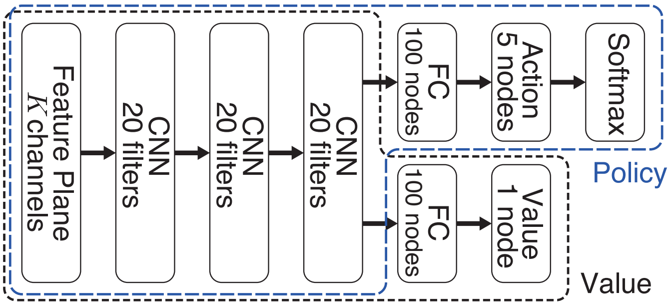

Figure 4.5: DNN models of policy and value functions. ©2019 IEICE

defined as follows:

$$s_{i,t}^{(4,x,y)} := \rho \hat{l}_i(x,y), \tag{4.10}$$

where ρ denotes a normalization factor. The features for $k = 1, 2, 3$ are defined to be the same as PT.

In contrast to PTCL, relay length $\hat{l}_i(x,y)$ of PTDL is encoded to one-hot vectors, which are employed in AlphaGo [37]. State elements for $k \in \{4, \ldots, K\}$ are defined as follows:

$$s_{i,t}^{(k,x,y)} := \begin{cases} 1 & \text{if } \hat{l}_i(x,y) \in \mathcal{R}_k, \\ 0 & \text{otherwise}, \end{cases} \tag{4.11}$$

$$\begin{aligned} \mathcal{R}_4 &:= \{0\}, \\ \mathcal{R}_k &:= (L_k, L_{k+1}] \quad \text{for } k = 5, \ldots, K-1, \\ \mathcal{R}_K &:= (L_K, \infty), \end{aligned} \tag{4.12}$$

where L_k denotes a border series used to encode relay lengths $\hat{l}_i(x,y)$ into one-hot vectors.

After pre-processing, states $s_{i,t}$ are input into a policy function π and a value function V. Their DNN models are shown in Figure 4.5. The lower CNN layers are shared by two functions, and the higher fully connected (FC) layers are separated. Such a shared model is used in [39]. The number of layers is restricted to three in order to achieve high convergence speeds. Although DeepRL performance increases with the number of layers, convergence rates decrease because the number of parameters increases. This is a trade off between the performance and computation time.

4.5 Simulation Evaluations

4.5.1 Simulation Setup

In the simulations, the vehicles were located at randomly selected grid points. Let λ denote the density of vehicles in each lane. Vehicle types were determined randomly according to the ratio R_{mm} and R_{c}. The controllable vehicles had their actions controlled by the proposed RL algorithm. On the other hand, the non-mmWave vehicles and uncontrollable vehicles did not change their relative positions or selected action among *forward*, *stay*, and *back* in order to simulate two scenarios where they drive at equal and constant velocities and where they change their velocities randomly. If more than one vehicle selected the same grid, the vehicle that had the highest priority moved to the selected grid, while the others did not change their positions. Penalties were given to vehicles that could not move to the selected grid. The priority was defined as follows:

- Non-mmWave vehicles and uncontrollable vehicles have greater priority than controllable vehicles.
- Forward vehicles have greater priority if their types are the same.
- Vehicles with small y position values have greater priority if their types and x position values are the same.

The first rule is applied to prevent the proposed method from interrupting the other vehicles' movement. The second one simulates the realistic driving manners. The third one is also applied to simplify the simulation. The mmWave vehicles could communicate with each other over the mmWave band if the distance between them was less than 50 m. Blocking by other vehicles is detected as follows: A line from the sender to the receiver is drawn and the grid sections that cross the line are listed. If there is no vehicle on the listed grid sections, the sender and the receiver can communicate with each other via LOS path. Link qualities of the mmWave channels are ideally predictable.

Table 4.1: Parameters of DeepRL-based vehicle position control simulations.

Parameters	Values
Length of RoI	1 km
Number of lane N_l	4
Number of grids	200×4
Lane width	3.5 m
RSU interval d	1 km
mmWave V2V communication range r_{V2V}	50 m
mmWave V2I communication range r_{V2I}	100 m
Size of the observation area $X \times Y$	41×7
Normalization factor for PTCL ρ	$0.005\,\mathrm{m}^{-1}$
The number of features of PTDL K	9
Boarder series of PTDL L_k $(k = 5, \ldots, 9)$	$0, 25, 50, 100, 150$
Reward balancing parameter α	$0.5\,\mathrm{m}^{-1}$
Penalty r_p	-2
Discount factor γ	0.1
Maximum time steps per episode T_{max}	100
Number of episodes (learning phase)	300
Number of episodes (test phase)	100
Update intervals t_{max}	2
Regularization parameter β	0.01
Optimizer	Shared RMSProp [39]
Coefficient of balancing gradients c_v	0.5

Python-based simulations are performed to determine the performance of the movement strategy based on DeepRL. The RL simulations consist of two phases, the learning and test phases. In the learning phase, the controllable vehicles move around and update their RL models according to Algorithm 4.1. 300 episodes are performed to learn strategy. At the beginning of each episode, non-mmWave vehicles and uncontrollable vehicles are relocated randomly in order to obtain a general strategy. Some models are obtained under different conditions: the vehicle density, ratio of mmWave vehicles, and ratio of controllable vehicles. It is assumed

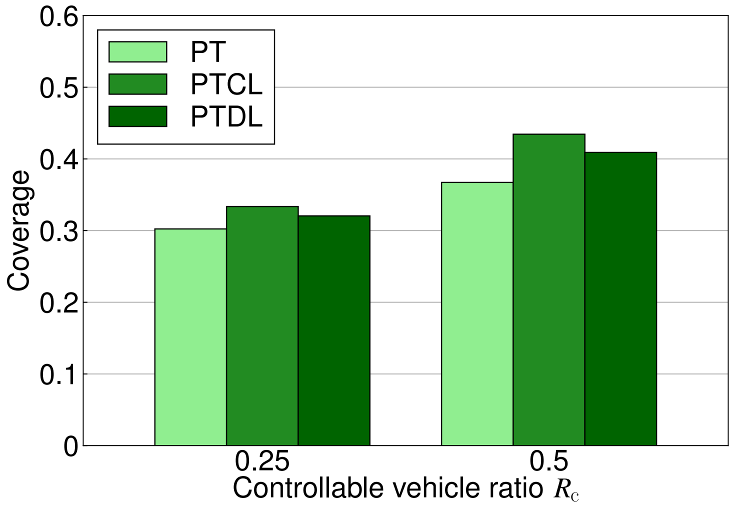

Figure 4.6: Coverage of different state designs when λ = 0.02 veh/m/lane and R_{mm} = 0.4. Uncontrollable vehicles move at constant velocities. The results of PTCL and PTDL are greater coverage than that of PT. ©2019 IEICE

that the conditions are stable while learning each model. The performance of the globally shared policy models obtained from the learning phases is evaluated in the test phase. At the beginning of the evaluations, the shared policy models are copied to agent-specific models and they are not updated while being evaluated. The conditions in the learning and test phases can be different, and the performance of the different models is compared under the same evaluation conditions. The RL simulation parameters and their values are listed in Table 4.1. Parameters are decided to simulate low density environments because the relay disconnection occurs often when the vehicle density is low. When the vehicle density is high, the proposed method may not work because movable spaces are restricted and relay length does not increase. However, in such cases, the relay disconnection is not a severe problem if there are enough mmWave vehicles and mmWave relays can be formed.

4.5.2 Performance of Reinforcement-Learning-Based Method

The coverage performance with three types of states PT, PTCL, and PTDL when λ = 0.02 veh/m/lane and R_{mm} = 0.4 is shown in Figure 4.6. It can be seen that

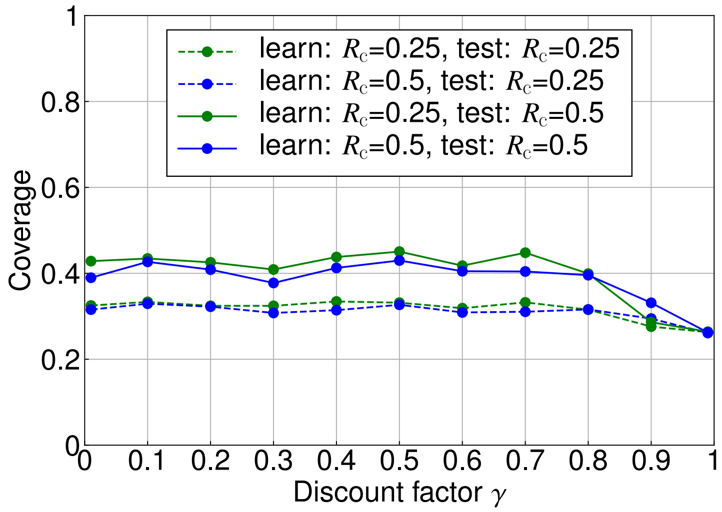

Figure 4.7: Coverage for different discount factors γ when λ = 0.02 veh/m/lane, R_{mm} = 0.4, and PTCL is used as the state type. Uncontrollable vehicles move at constant velocities. Policies learned when $\gamma \leq 0.8$ show higher performance. ©2019 IEICE

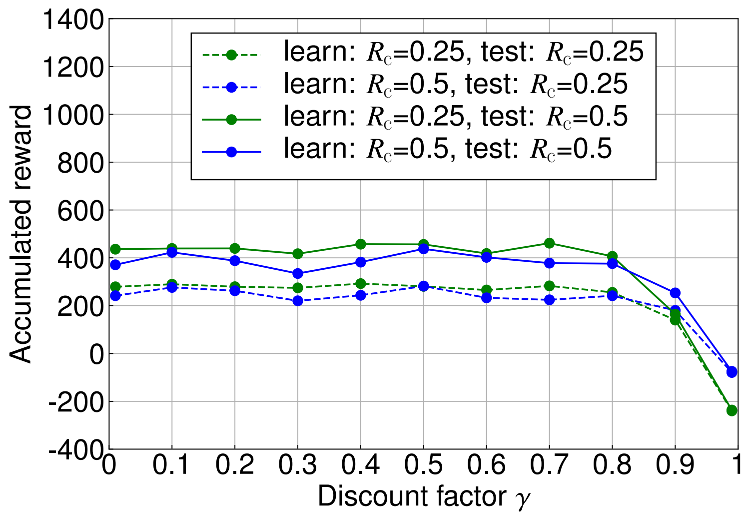

Figure 4.8: Accumulated reward for different discount factors γ when λ = 0.02 veh/m/lane, R_{mm} = 0.4, and PTCL is used as the state type. Uncontrollable vehicles move at constant velocities. ©2019 IEICE

PTCL and PTDL achieve higher performance than PT, which means that additional

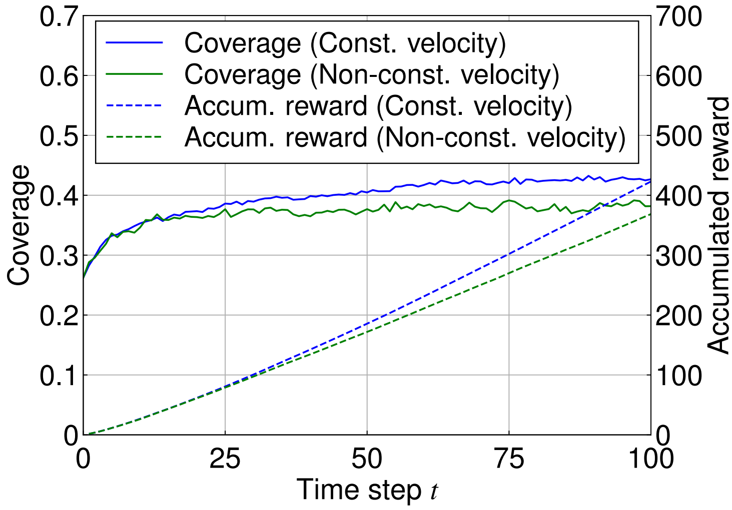

Figure 4.9: Coverage and accumulated reward as functions of time steps when λ = 0.02 veh/m/lane, R_{mm} = 0.4, R_{c} = 0.5, and PTCL is used as the state type. Accumulated rewards increase linearly even after coverage becomes constant. ©2019 IEICE

relay length information improves the performance of RL-based methods.

Figures 4.7 and 4.8 show the coverage performance and accumulated reward with different discount factors when λ = 0.02 veh/m/lane, R_{mm} = 0.4, and the state type is PTCL. When the discount factor γ is greater than 0.8, the coverage decreases. In particular, when $\gamma = 0.99$, the accumulated rewards are less than zero, which means that agents failed to learn a reasonable policy under the hyper parameter settings and the simulation scenarios.

The coverage and accumulated reward as functions of time step t are shown in Figure 4.9. Simulations are performed under two conditions where non-mmWave vehicles and uncontrollable vehicles run at equal and constant velocities and where they change their velocities randomly. In both conditions, the coverage increases as the agents change their positions. Coverage is greater when uncontrollable vehicles move at the same velocity, than when uncontrollable vehicles move at different velocities. Accumulated reward increases linearly even when $t > 75$ because nearly constant rewards are given to agents after the coverage converges.

Coverage and accumulated reward as functions of the number of episodes in learning phases are shown in Figure 4.10. 50-episode moving averages are shown

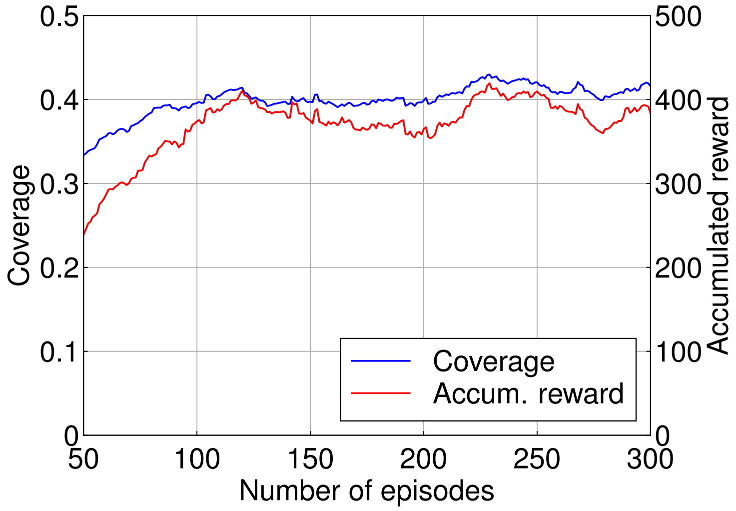

Figure 4.10: Moving average of coverage and accumulated reward as functions of the number of training episodes when $\lambda = 0.02$ veh/m/lane, $R_{\mathrm{mm}} = 0.4$, $R_{\mathrm{c}} = 0.5$, and PTCL is used as the state type. Uncontrollable vehicles move at constant velocities. ©2019 IEICE

because the achievable coverage in each episode varies due to the random variables such as the number of vehicles and initial vehicle positions. It is shown that coverage and accumulated reward increase at first, and then do not increase when the number of episodes is greater than 120. This is because various experiences improve agents' strategies at first, whereas additional experiences do not contribute to improving the strategies as much after the agents have learned from many experiences.

The coverage performance with different models obtained in different learning conditions is shown in Figure 4.11. 20 models are trained in learning environments with varying R_{c} and R_{mm}, transferred them to test environments with $R_{\mathrm{mm}} = 0.4, 0.7, 1.0$ and $R_{\mathrm{c}} = 0.5$, and evaluated coverage of the position controls using the models. The models learned when $0.3 \leq R_{\mathrm{mm}} \leq 0.7$ show approximately the same performance, which means these models can be applied when the penetration ratio is changed from that in the learning phases. On the other hand, the models learned when $R_{\mathrm{mm}} \geq 0.9$ show lower performance. When there are many mmWave vehicles in the learning phases, large coverage can be achieved without movement of agents. Therefore, the agents cannot learn aggressive moving policies. This

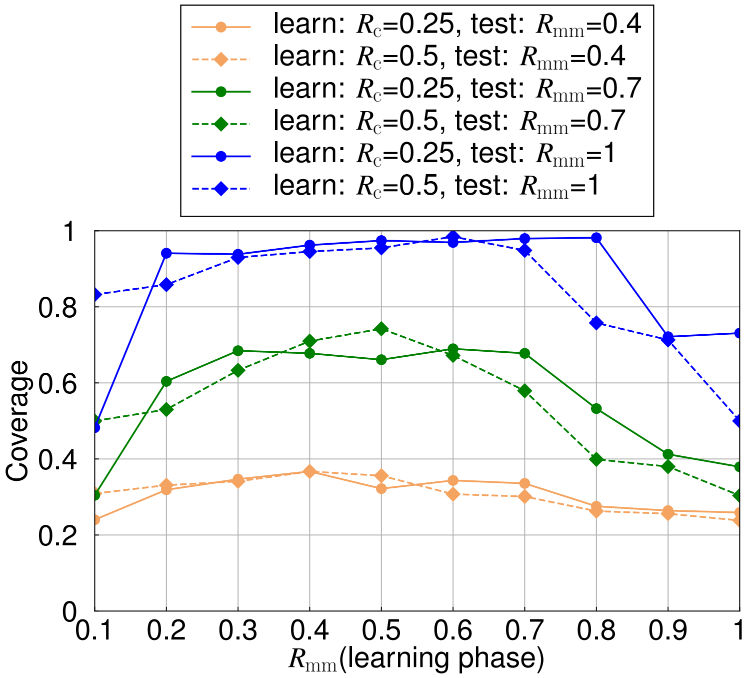

Figure 4.11: Coverage performance of models learned in different learning conditions R_{mm} and R_{c} when $\lambda = 0.02$ veh/m/lane. PT is used as the state type, and uncontrollable vehicles move at constant velocities. R_{c} is set to 0.5 in test environments. The models learned when $0.3 \leq R_{\mathrm{mm}} \leq 0.7$ show relatively higher performance. ©2019 IEICE

is why the models learned with large R_{mm} show lower performance. The models learned when $R_{\mathrm{c}} = 0.25$ and $R_{\mathrm{mm}} = 0.1$ also show lower performance. This is because the number of agents is too small to learn policies that increase coverage.

The coverage performance of the RL-based method with PTCL is compared with that of random positions and VFA under conditions when $\lambda = 0.02$ veh/m/lane, $R_{\mathrm{mm}} = 0.4$, and uncontrollable vehicles move at constant and equal velocities in Figure 4.12. As a comparative method, exponential VFA [63] is applied with parameters $W_a = 1$, $W_r = 10000$, $\beta_1 = \beta_2 = 2$, and $D_{\mathrm{th}} = 50$ m. Details of these parameters are described in [63]. The coverage achieved with the RL-based method is higher than the coverage of random positions and VFAs. For example, the coverage obtained from the RL-based method is about 1.7 times the coverage obtained with random positions when $R_{\mathrm{c}} = 0.5$. Although vehicles with VFA ad-

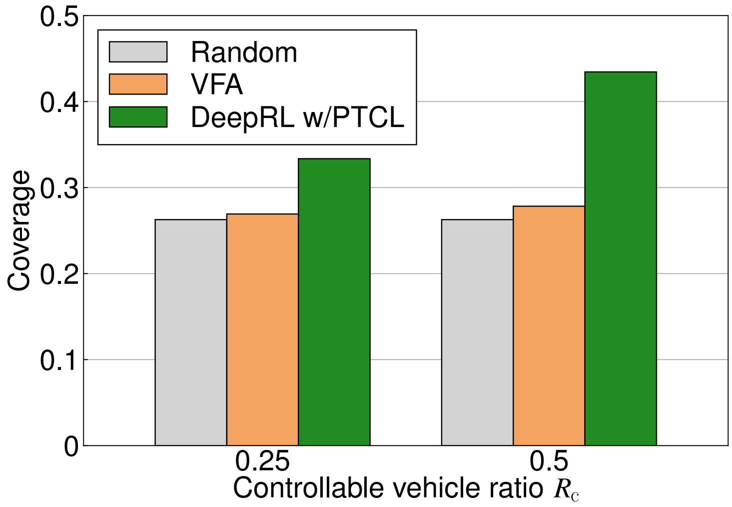

Figure 4.12: Coverage of different movable methods when λ = 0.02 veh/m/lane, R_{mm} = 0.4 and uncontrollable vehicles move at constant velocities. RL shows higher performance than random and VFA. ©2019 IEICE

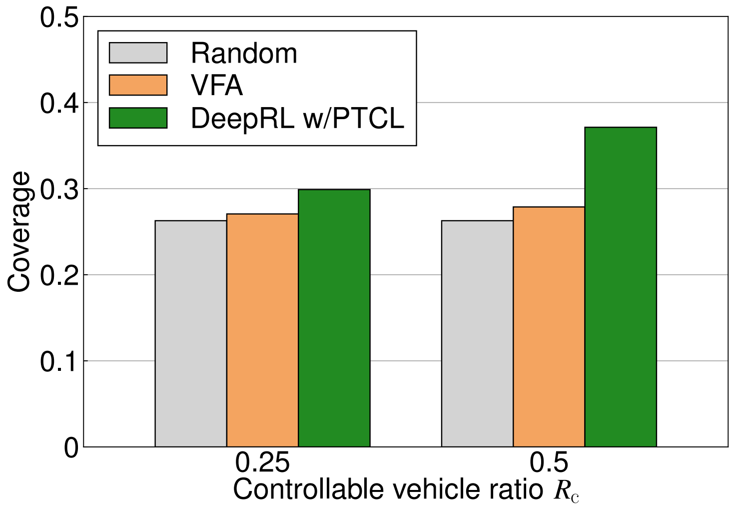

Figure 4.13: Coverage of different movable methods when λ = 0.02 veh/m/lane, R_{mm} = 0.4 and uncontrollable vehicles move at random velocities. RL shows higher performance than random and VFA. ©2019 IEICE

just distances between themselves in order to connect with each other, they do not consider blockage of mmWave communications. On the other hand, vehicles with

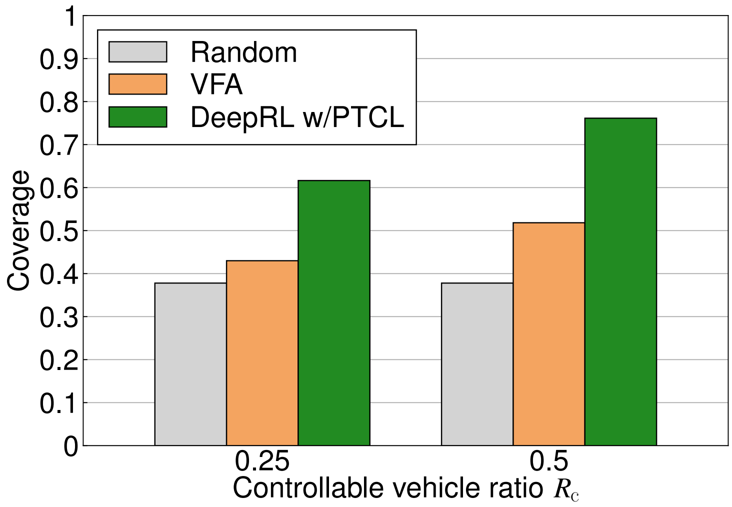

Figure 4.14: Coverage of different movable methods when λ = 0.01 veh/m/lane, R_{mm} = 1 and uncontrollable vehicles move at constant velocities. ©2019 IEICE

RL agents optimize their actions to expand their coverage following the learned policy models. Consequently, the performance of DeepRL exceeds that of VFA.

The coverage performance with different method is compared with that of random positions and VFA under conditions when λ = 0.02 veh/m/lane, R_{mm} = 0.4, and uncontrollable vehicles move at different velocities in Figure 4.13. It is notable that the performance of the proposed method exceeds that of VFA even when the vehicles move at different velocities.

Coverage performance when λ = 0.01 veh/m/lane, R_{mm} = 1, and uncontrollable vehicles move at constant and equal velocities is shown in Figure 4.14. The training of the RL-based methods were conducted under the conditions with λ = 0.02 and R_{mm} = 0.4, and the model transferred to this evaluation environment. The RL performance shows larger coverages than the results with R_{mm} = 0.4 in Figure 4.12 because there are fewer obstacles that disrupt the movement of the controllable vehicles (i.e., RL agents) and thus, they easily move to positions where long relays can be achieved. Furthermore, VFAs show lower performance than the RL-based methods because they rely on the assumption that all vehicles are controllable while they are not in the environment.

4.5.3 Comparisons with Other RL Algorithm

The following part of this section discusses other RL algorithms compared with one used in the proposed method for the position control problem. As introduced in [35], there are many RL algorithms. The table-based Q-learning is one of most widely used algorithm for various problems. However, the algorithm is not suitable for the considered problem because it requires large memory capacity, whereas it is difficult for vehicles to have large memory. In the table-based Q-learning, an action-value function is represented as a table, called Q table, and the memory capacity required to store the table is proportional to the number of values that the state $s_{i,t}$ can take. It increases exponentially with the observation range $X \times Y$; thus, the table-based Q-learning is difficult to apply for the considered problem when the observation range becomes large.

DQN [36] can be a candidate algorithm. DQN utilizes DNN to approximate an action-value function instead of using the Q table; thus, the required memory capacity can be small when the state is large. However, DQN cannot leverage experiences obtained by multiple vehicles while the vehicles try to learn similar strategies, because the algorithm is designed for single-agent problems.

There are several multi-process DeepRL algorithms, which can be applied to multi-agent environments. The DeepRL algorithms can leverage experiences of multiple agent to update a model; thus, it can learn a strategy faster and the strategy can be achieved higher performance than single-agent RL algorithm [38, 39]. The proposed method applied A3C [39] to the relay expansion problems as a state-of-the-art multi-process DeepRL algorithm and it was shown that the proposed method can increase coverage. The detailed performance comparison between A3C and other multi-agent RL algorithms is not evaluated, because the focus of this chapter is not on designing or determining the best RL algorithm.

4.6 Conclusions and Future Works

This chapter proposed a vehicle position control method for mmWave vehicular networks that increases coverage through multi-hop V2V relaying. A3C, which is one of the state-of-the-art of RL methods, is adopted to obtain practical movement strategies and designed states with relay length information that improved system performance in terms of increasing coverage. The simulation results showed that the RL-based strategy achieved 1.7 times the coverage of random positions when the penetration ratio of mmWave vehicles was 40% and half of the mmWave vehicles employed the proposed RL algorithm. Moreover, the RL-based strategy increased coverage, even when the vehicle density and penetration ratio of mmWave vehicles differed from those of the learning phase.

Future direction of this work includes evaluating the performance of the proposed method with metrics other than relay length. One of the advantages of RL is applicability for tasks with other objectives by redesigning the reward. For example, the reliability and connectivity of the multi-hop network is more important than relay length when the vehicular network is used for safety applications or vehicular cloud computing. The proposed method has potential to achieve such objectives.

A method to share and aggregate models learned by the vehicles to improve their performance is also included in the future work. Current work assumed that the model sharing is conducted ideally, i.e., the sharing is done without delay, loss, and bandwidth consumption. The model-sharing method should be designed in consideration of scalability, delay, loss, and bandwidth consumption of wireless communications.

Chapter 5

Cooperative Perception with mmWave Concurrent Transmission

5.1 Background

As vehicles become increasingly automated, the number of sensors equipped on vehicles increases and an increasingly massive amount of data are generated while driving. Cooperative perceptions, with which vehicles share sensor data, such as camera and LiDAR data, extend a vehicle's perceptual range to cover its blind spots or locate hidden objects. Because cooperative perceptions require high-throughput communication systems, mmWave communications, which can leverage huge bandwidth and efficient spatial reuse, have been attracting much attention. This chapter proposes a data-sharing algorithm using mmWave concurrent transmission in order to increases the spatial reuse efficiency.

There have been a few studies on concurrent transmissions in mmWave vehicular networks. For example, [71] proposed a beam-width-controlling scheme to reduce beam-alignment delay by considering signal-to-interference plus noise power ratio (SINR). Most concurrent transmission protocols for mmWave communications are found not in vehicular networks, but in WSNs [72–74]. However, such protocols do not adopt data caching because their objectives are not data sharing. In data sharing, the same data are sent from the source vehicles to different vehicles and thus, the same data might be transmitted redundantly without data caching. Additionally, their algorithms do not consider the geographical information in transmitted data. There have been many studies on data dissemination methods for DSRC-based VANETs, some of which utilize the geographical information in disseminated data. [75, 76] proposed the data aggregation of the geographical information to suppress redundant data broadcasts. [77] proposed controlling the frequency of broadcasting. However, these studies did not discuss concurrent transmission or multihop routing with directional antennas.

Concurrent dissemination with data caching was proposed in [78], where the authors presented a system to realize a RSU-controlled concurrent dissemination by two communication mode: V2I and V2V communications. [78] proposed a graph-based algorithm, where potential transmissions (from which, to which, and which data should be transmitted) and their conflicts (e.g. half duplex and interference constraints) are represented as a graph, i.e., two transmissions are connected when they cannot be operated at the same time. Each vertex has weight that represents the priority of receiver vehicles. Then, the optimal concurrent transmission schedule for multihop dissemination can be obtained by solving the maximum weighted independent set (MWIS) problem on the graph. Although the MWIS problem is one of the NP-hard problems, a greedy algorithm with a performance guarantee to maximize the total vertex weights can be utilized. However, [78] does not assume mmWave communications and thus, it cannot be used directly for mmWave communications. There is also room to utilize the geographical information in the transmitted data for cooperative perceptions.

The algorithm for sharing perceptual data proposed in this chapter is based on [78] to realize concurrent transmission with data caching. Because the algorithm in [78] optimizes concurrent transmissions considering not only pair selection of the transmitter and receiver but also which data to transmit among the currently cached data, it effectively reduces redundant transmission in data sharing, where the same data are transmitted to different vehicles. However, the original algorithm is based on microwave communications, meaning it must be modified for mmWave communications. [78] designed a conflict rule, which is utilized to decide which pair of transmission vertices of the graph should be connected, considering radio interference among omnidirectional antennas. A new rule is designed for mmWave communications by estimating interference among narrow-beam directional antennas, which are utilized for mmWave communications to obtain high gain. Because the conflict rule should be defined between two transmissions, this chapter develops an interference approximation scheme that can calculate the interference between two transmissions without summing all possible interferences. By using the newly designed rule, near-optimal concurrent transmission in mmWave networks can be realized.

A prioritization method is also designed in order to enlarge the perceivable region for situations where data-sharing time is limited. Although [78] gave high priority to receiver vehicles that soon run out of the service area of the RSU, such a prioritization does not fit for cooperative perceptions at an intersection. On the other hand, giving high priority to data corresponding to regions far from an intersection enlarges the perceivable area based on shared data because regions near the center of the intersection are covered by many vehicles, meaning it is desirable to transmit data far from the intersection. Such a prioritization scheme can be realized by customizing the weight function of the MWIS problem.

The main contributions of this chapter are summarized as follows:

(1) A data-sharing algorithm for cooperative perception is proposed, which improves spatial reuse by considering interference among narrow-beam directional antennas and increases the perceivable region by prioritizing the data to be forwarded based on geographical information, even if not all data can be collected. In order to realize concurrent transmission, the algorithm presented in [78] is employed.

(2) It is proven that if the data-sharing time is sufficiently long and the vehicular network is represented as a connected graph, the proposed data-sharing algorithm guarantees that all data are shared with all vehicles.

5.2 Related Works

Data sharing for cooperative perceptions should achieve a large perceivable area within a short period, in particular 100 ms for safety applications. Key techniques to meet this requirement are concurrent transmission with directional antennas for improving system throughput, efficient routing with cached data for reducing redundant transmission, and leveraging geographical information in transmitted data.

Dissemination algorithms with directional antennas for VANETs have been studied by many researchers. [79] presented theoretical analysis of content dissemination time in vehicular networks with directional antennas and demonstrated that directional antennas accelerate content propagation. [80] proposed a broadcast protocol for directional antennas in VANETs. In this protocol, the furthest receiver forwards data packets along road segments and a directional repeater forwards the data in multiple directions at intersections. In contrast to the protocol in [80], which considers the positions of transmitters, the proposed algorithm considers the positions where data are obtained to achieve a large perceivable region.

Dissemination algorithms for local information were proposed in [75–77]. In [75], a scalable dissemination protocol, called segment-oriented data abstraction and dissemination (SODAD), and its application, self-organizing traffic-information system (SOTIS), were proposed. SOTIS is a mechanism for gathering traffic information sensed by vehicles. It aggregates the received traffic information from road segments and sends only up-to-date information to vehicles. In [76], Zone Flooding and Zone Diffusion were proposed to suppress redundant data broadcasting. In Zone Flooding, only vehicles in a flooding zone forward received packets. Zone Diffusion is a data aggregation method considering geographical information, where vehicles merge road environment data as it is received and broadcast only merged data. [77] proposed controlling the frequency of information broadcasting and selecting the data to send to reduce communication traffic. Although these studies considered the geographical information in each datum, they did not focus on concurrent transmission.

The authors of [71] proposed vehicle pairing and beam-width controlling for mmWave VANETs. In the protocol in [71], pairs of transmitters and receivers are selected based on matching theory and beam widths are determined via particle swarm optimization. This protocol successfully improves throughput and reduces delay by considering SINR. Other concurrent transmission methods for mmWave communications have been proposed for WSN, rather than VANETs [72–74]. The authors of [72] formulated the concurrent transmission scheduling problem as an optimization problem to maximize the number of flows to satisfy the quality-of-service requirements of each flow. In [73], relay selection and spatial reuse were jointly optimized to improve network throughput and a blockage robust algorithm was proposed. The authors of [74] minimized transmission time by solving an optimization problem. Although these algorithms for concurrent transmissions presented in [71–74] achieved efficient spatial reuse, redundant data were transmitted because their primary objective was not data sharing and thus, they did not consider situations where the same data are sent to different receivers. Additionally, they did not consider geographical information.

The authors of [78] proposed an RSU-controlled scheduling that maximizes system throughput in hybrid V2I/V2V communications. This algorithm realizes concurrent dissemination based on the graph theory. It also adopts a data caching mechanism. The algorithm proposed in [78] generates graphs for dissemination scheduling, where the set of vertices represents potential transmissions consisting of a transmitter, receiver, and data, and the set of edges represents pairs of transmissions that cannot be performed at the same time. The authors of [78] proved that optimal scheduling can be obtained by solving the MWIS problem for a generated graph. However, because the algorithm in [78] assumes omnidirectional antennas, interference calculations must be extended for mmWave communications, where narrow-beam directional antennas are utilized. Additionally, there is still room to improve the efficiency of data transmissions for cooperative perception by leveraging the geographical information in perceptual data. Thus, a data-sharing algorithm in mmWave vehicular networks that increases perceivable regions should be developed for traffic safety, especially when data-sharing time is limited.

5.3 System Model

The system model of data sharing with mmWave concurrent transmissions is shown in Figure 5.1. At an intersection, there are vehicles equipped with mmWave communication devices for data transmission via V2V channels and microwave communication devices for control signal transmission via V2I channels. Vehicles participating in cooperative perception are selected among vehicles within tens of meters from the center of the intersection considering stopping distance. The number of participants is also limited to N_{v} vehicles because it is difficult to complete data sharing owing to the time limit when the number of participants is large. The vehicles perceive the surrounding environment utilizing their sensors, such as LiDARs or cameras. It is assumed that the vehicle sensors cover a

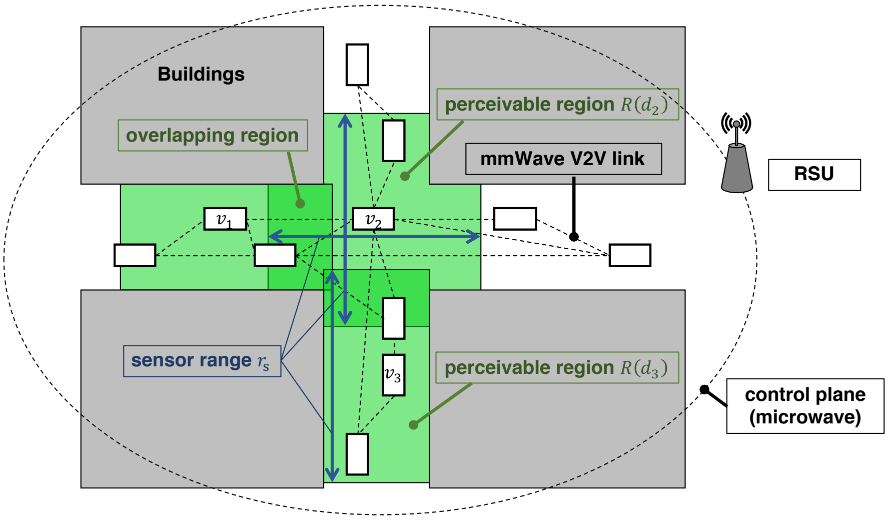

Figure 5.1: System model of data sharing with mmWave concurrent transmissions (Top view). ©2019 IEICE

surrounding rectangular region (on road segments) or cross-shaped region (at the intersection), bounded by the buildings along the roads and their sensor range r_s. The data generated by vehicle v_i is denoted as d_i. The sizes of d_i are assumed to be approximately the same among vehicles for simplicity. The vehicles share the data with each other to obtain information regarding the intersection and then perform cooperative perception.

Data are transmitted through mmWave V2V channels to reduce the pressure on V2I channels. However, control signals, which must be broadcasted to all vehicles, are transmitted through microwave V2I channels. There is an RSU (or an eNodeB) that covers all vehicles near the intersection on the microwave channel and performs scheduling based on vehicle positions and mmWave V2V link topology. While a large amount of sensor data are transmitted over the mmWave V2V channels, control signals and position information, which are relatively small, can be broadcasted by the RSU utilizing DSRC or C-V2X.

The time frame for data sharing is shown in Figure 5.2. The vehicles perform sensing at an interval of T and generate d_i. The data update interval consists of the scheduling period and data-sharing period. In the scheduling period, data-sharing scheduling is determined by the RSU. Vehicle position information obtained from global positioning system (GPS) is sent to the RSU, which then estimates the

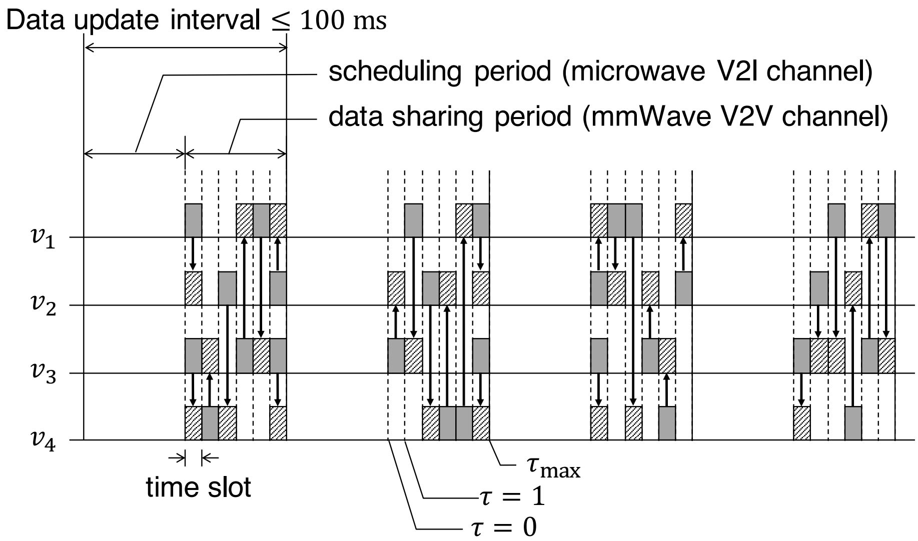

Figure 5.2: Time frame for data sharing. All vehicles generate their perceptual data at the beginning of each data update interval. They transmit their data during the data-sharing period. ©2019 IEICE

mmWave connectivity between vehicles and determines the preferred data to be shared.

In the data-sharing period, vehicles share their data through mmWave V2V channels. The data-sharing period consists of $\tau_{\max}$ time slots, each of which is sufficiently long to transmit one datum. Let $\tau \in \{0, 1, \ldots, \tau_{\max}\}$ denote the index of a time slot. $\tau_{\max}$ is limited by the transmitted data volume and data rate.

By sharing data d_i, the perceivable region is enlarged. Let $\boldsymbol{d}_{i,\tau}$ and $R_{i,\tau}$ denote the dataset possessed by vehicle v_i and the perceivable region of the dataset $\boldsymbol{d}_{i,\tau}$, respectively. $R_{i,\tau}$ is defined as $R_{i,\tau} := \bigcup_{d \in \boldsymbol{d}_{i,\tau}} R(d)$, where $R(d)$ denotes the perceivable region of d (i.e., the region covered by the sensor of a single vehicle). At the beginning of the data-sharing period, the datasets are initialized as $\boldsymbol{d}_{i,0} \leftarrow \{d_i\}$. When vehicle v_i transmits $d_k \in \boldsymbol{d}_{i,\tau}$ to vehicle v_j, v_j updates its dataset $\boldsymbol{d}_{j,\tau}$ as follows:

$$\boldsymbol{d}_{j,\tau+1} \leftarrow \boldsymbol{d}_{j,\tau} \cup \{d_k\}. \tag{5.1}$$

Subsequently, the area of region $R_{j,\tau}$ is enlarged. System performance is evaluated based on the normalized perceivable area, which is defined as follows:

$$\hat{S}_\tau := S(R_{i,\tau})/S(R_{\text{all}}), \tag{5.2}$$

where $S(R)$ and R_{all} denote the area of region R and the area covered by all data, defined as $R_{\text{all}} := \bigcup_{i=1}^{N_\text{v}} R(d_i)$, respectively.

At the end of the data-sharing period, the vehicles regenerate d_i by sensing. Then, the RSU collects vehicle position information and determines scheduling for sharing new perceptual data in the following scheduling period.

5.4 Data-Sharing Algorithm

In the scheduling period, the RSU selects transmitters, receivers, and data to be transmitted during each time slot. First, the RSU constructs a vehicular network graph that represents the network topology of the mmWave vehicular network by estimating the connectivity between vehicles based on their positions and a propagation loss model. Second, a graph that is utilized to determine concurrent transmission behavior is constructed from the vehicular network graph for each time slot. Because the vertices of the graph represent transmissions, each of which consists of a transmitter, receiver, and data to be transmitted, and the edges of the graph represent conflicts between two transmissions, independent sets in the graph represent sets of transmissions that do not conflict with each other. Therefore, by solving the MWIS problem for the graph, referred to as a scheduling graph, the optimal concurrent transmission can be found for each time slot.

Although the proposed algorithm is based on that in [78], considered system model in this chapter is quite different from that in [78]. First, quite a short period (i.e., 100 ms) is considered, while long-span dissemination was discussed in [78]. Because [78] designed a prioritization based on vehicle mobility over a long period, the prioritization design is modified to enlarge perceivable regions within a short period. Second, objective of the proposed algorithm is to share data generated by vehicles with each other, while [78] assumed that each vehicle requests data that is stored in the RSU. This chapter proves that data sharing can be completed by the proposed algorithm if the vehicular network graph is connected and there are enough time slots. Third, a scheduling graph construction scheme is redesigned in order to apply mmWave communications for data transmission. Especially, conflict rules between two potential transmissions are modified to reflect the mmWave propagation characteristics. Finally, data are transmitted through V2V channels to reduce the pressure on V2I channels, while [78] utilized both V2I and V2V channels for data transmission. The following subsections describe the details of constructing a vehicular network graph and scheduling graph.

5.4.1 Vehicular Network Graphs

The RSU estimates the connectivity between each pair of vehicles and defines the vehicular network graph $\boldsymbol{G}_{\mathrm{v}}$ as follows:

$$\boldsymbol{G}_{\mathrm{v}} := (\mathcal{V}, \mathcal{L}), \tag{5.3}$$

$$\mathcal{L} := \{\{v_i, v_j\} \mid v_i, v_j \in \mathcal{V}, LOSS(v_i, v_j) \leq \theta\}, \tag{5.4}$$

where $\mathcal{V}$, $\mathcal{L}$, $LOSS(v_i, v_j)$, and θ denote the set of vehicles, set of vehicle connections, mmWave propagation loss between v_i and v_j, and a threshold that indicates that mmWave communications are possible, respectively. The mmWave propagation loss can be obtained from the path loss models proposed in [22]. The authors of [22] measured the propagation loss of 60-GHz mmWave channels when there were one, two, or three vehicles between the transmitter and receiver. For scenarios with more than three blockers, [13] provided an extension to the path loss model. Another approach for predicting mmWave propagation loss was proposed in [70], where the authors predicted received signal power based on perceptual data. The threshold θ is calculated based on the Shannon capacity as follows:

$$B \log_2 \left(1 + \frac{P_{\mathrm{t}} G_{\mathrm{t}} G_{\mathrm{r}} / LOSS(v_i, v_j)}{BN}\right) \geq Rate, \tag{5.5}$$

$$\theta := \frac{P_{\mathrm{t}} G_{\mathrm{t}} G_{\mathrm{r}}}{BN \left(2^{Rate/B} - 1\right)}, \tag{5.6}$$

where B, P_{t}, G_{t}, G_{r}, N, and $Rate$ denote the bandwidth, transmission power, transmitter and receiver antenna gain, thermal noise power spectral density, and rate requirements, respectively. When calculating the vehicle connectivity, the antenna directions of the transmitter and receiver point at each other. It is also assumed that $\boldsymbol{G}_{\mathrm{v}}$ does not change within the data update interval because the interval is very short (less than 100 ms), meaning the mobility of the vehicles is negligible.

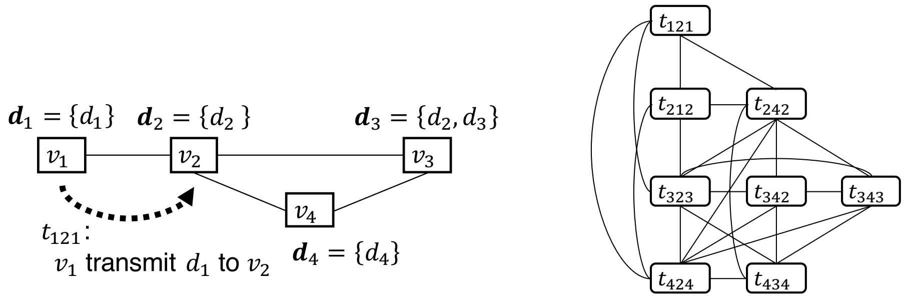

(a) Vehicular network graph $\boldsymbol{G}_{\mathrm{v}}$ (b) Scheduling graph $\boldsymbol{G}_{\mathrm{s}}$

Figure 5.3: Example of scheduling graph. t_{ijk} represents a transmission in which vehicle v_i sends d_k to vehicle v_j. ©2019 IEICE

5.4.2 Scheduling Graph and Data-Sharing Scheduling

For every time slot τ, the RSU selects transmitter and receiver vehicles from $\mathcal{V}$, as well as data $d_k \in \boldsymbol{d}_{i,\tau}$ to send for each transmitter vehicle v_i. This selection is calculated by solving the MWIS problem for the scheduling graphs, which are constructed as follows:

Algorithm 5.1 is utilized to construct scheduling graphs for each time slot $\boldsymbol{G}_{\mathrm{s},\tau} := (\mathcal{T}_\tau, C_\tau, W)$ from $\boldsymbol{G}_{\mathrm{v}}$, where $\mathcal{T}_\tau$, C_τ, and W denote the set of vertices, set of edges, and vertex weighting function such that $W\colon \mathcal{T}_\tau \to \mathbb{R}^+$, respectively. $\mathbb{R}^+$ is the set of positive real numbers. A transmission $t_{ijk} \in \mathcal{T}_\tau$ represents a set containing transmitter v_i, receiver v_j, and data d_k, meaning v_i transmits d_k to v_j. Each element in C_τ represents a conflict between two transmissions, meaning they cannot be performed concurrently. Further details are explained in Section 5.4.4. The weight of vertex $W(t_{ijk})$ represents the priority of each transmission, and its definition is described in Section 5.4.3. Figure 5.3b presents an example of a scheduling graph constructed from the vehicular network graph shown in Figure 5.3a. From Lines 2–10 in Algorithm 5.1, a set of transmissions $\mathcal{T}_\tau$ is obtained by listing all directly connected pairs of vehicles (i.e., neighbors in $\boldsymbol{G}_{\mathrm{v}}$) and data not possessed by receivers. Next, the conflict between each pair of transmissions is calculated in Lines 11–15.

A scheduling algorithm utilizing $\boldsymbol{G}_{\mathrm{s},\tau}$ is shown in Algorithm 5.2. In each time slot, a set of transmissions $\boldsymbol{t}_\tau \subset \mathcal{T}_\tau$ is selected. After the transmissions are performed, the datasets $\boldsymbol{d}_{i,\tau+1}$ are updated utilizing (5.1), and $\boldsymbol{G}_{\mathrm{s}}$ is recalculated

Algorithm 5.1 Constructing a scheduling graph

Input: $\boldsymbol{G}_{\mathrm{v}} = (\mathcal{V}, \mathcal{L}), \boldsymbol{d}_{i,\tau}$

Output: $\boldsymbol{G}_{\mathrm{s},\tau}$

Initialize $\mathcal{T}_\tau \leftarrow \emptyset, C_\tau \leftarrow \emptyset$
for all $v_i \in \mathcal{V}$ **do**
  for all v_j in neighbors of v_i **do**
    for all $d_k \in \boldsymbol{d}_{i,\tau}$ **do**
      if $d_k \notin \boldsymbol{d}_{j,\tau}$ **then**
        $\mathcal{T}_\tau \leftarrow \mathcal{T}_\tau \cup \{t_{ijk}\}$
      end if
    end for
  end for
end for
for all $t_{ijk}, t_{i'j'k'} \in \mathcal{T}_\tau$ **do**
  if t_{ijk} and $t_{i'j'k'}$ conflict with each other **then**
    $C_\tau \leftarrow C_\tau \cup \{\{t_{ijk}, t_{i'j'k'}\}\}$
  end if
end for
$\boldsymbol{G}_{\mathrm{s},\tau} \leftarrow (\mathcal{T}_\tau, C_\tau, W)$
return $\boldsymbol{G}_{\mathrm{s},\tau}$

Algorithm 5.2 Data-sharing scheduling

Input: $\boldsymbol{G}_{\mathrm{v}} = (\mathcal{V}, \mathcal{L})$.

Initialize $\boldsymbol{d}_i \leftarrow \{d_i\}$ for all i
Obtain $\boldsymbol{G}_{\mathrm{s},0}$ from Algorithm 5.1 with $\boldsymbol{G}_{\mathrm{v}}, \boldsymbol{d}_{i,0}$
$\tau \leftarrow 0$
while $\mathcal{T}_\tau \neq \emptyset \wedge \tau \leq \tau_{\max}$ **do**
  $\boldsymbol{t}_\tau \leftarrow$ MWIS of $\boldsymbol{G}_{\mathrm{s},\tau}$
  Perform $\boldsymbol{t}_\tau$ and update $\boldsymbol{d}_{i,\tau+1}$
  Obtain $\boldsymbol{G}_{\mathrm{s},\tau+1}$ from Algorithm 5.1 with $\boldsymbol{G}_{\mathrm{v}}, \boldsymbol{d}_{i,\tau+1}$
  $\tau \leftarrow \tau + 1$
end while

based on the updated $\boldsymbol{d}_{i,\tau+1}$. How to select transmissions in the proposed scheme is described in the following subsection. After the scheduling for all time slots in the data update interval is completed, each vehicle follows the determined schedule during the data-sharing period.

5.4.3 Priority of Transmissions

To perform scheduling, the controller calculates the MWIS of $\boldsymbol{G}_{\mathrm{s},\tau}$ to increase the number of transmissions performed in each time slot. Independent sets of $\boldsymbol{G}_{\mathrm{s},\tau}$ represent sets of non-conflicting transmissions and thus, maximum transmissions that can be performed concurrently can be obtained by solving the maximum independent set (MIS) problem. The MIS problem is a special case of MWIS, where the weight function W is a constant function (i.e., $W(t_{ijk}) = 1, \forall t_{ijk} \in \mathcal{T}_\tau$). The data-sharing algorithm with MIS is referred to as max transmission scheduling. Although max transmission scheduling maximizes the number of transmissions, it does not consider the perceivable region represented by the perceptual data. When $\tau_{\max}$ is small due to the limit of the data-sharing period, the algorithm stops before all data are shared with all vehicles. In such cases, vehicles perceive their environments based on limited information that covers only a limited area of the intersection.

To increase the perceivable area in such cases, prioritization for transmitted data can be implemented. Data from near the intersection tend to overlap with each other, because the vehicle density near intersections is higher than that far from intersections. Therefore, it is inefficient to forward data representing areas near intersections. In order to improve efficiency of data sharing another prioritization scheme is proposed, where a high priority is assigned to data that represent areas far from the intersection and lower priority is assigned to data that represent areas near the intersection. The algorithm with this prioritization is referred to as max distance scheduling. Distance priority can be represented as a weight function W of transmissions t_{ijk} as follows:

$$W(t_{ijk}) \coloneqq dist(p_k, p_\mathrm{c}), \tag{5.7}$$

where p_k, p_c, and $dist(a, b)$ denote the position of v_k, center of the intersection, and distance between positions a and b, respectively.

Although the MIS and MWIS problem are NP-hard problems, it has been proven that a simple greedy algorithm can approximately solve these problems with a guaranteed performance ratio of greater than or equal to $1/\Delta$, where Δ denotes the maximum degree of any vertex in the graph [81]. Thus, a greedy approach is applied to the proposed scheduling algorithm.

5.4.4 Conflict Rule of Interference

When constructing $\boldsymbol{G}_{\mathrm{s},\tau}$, conflicts between transmissions $t_{ijk} \in \mathcal{T}_\tau$ must be determined to obtain the set of edges C_τ. The rules used to determine the conflicts are referred to as conflict rules. The basic conflict rules are defined as follows:

(a) A transmitter cannot transmit different data at the same time or transmit data to different receivers because of the use of a narrow-beam directional antenna: t_{ijk} conflicts with $t_{i'j'k'}$ if $i = i'$.

(b) A receiver cannot receive data from multiple transmitters: t_{ijk} conflicts with $t_{i'j'k'}$ if $j = j'$.

(c) A vehicle cannot transmit and receive data simultaneously because of half-duplex communication: t_{ijk} conflicts with $t_{i'j'k'}$ if $i = j' \vee j = i'$.

Because the original algorithm proposed in [78] assumed a DSRC channel and omnidirectional antennas, the following conflict rule was added to the basic rules:

(d) A receiver near a transmitter cannot receive data from other transmitters: t_{ijk} conflicts with $t_{i'j'k'}$ if $v_j \in \mathcal{N}_{\boldsymbol{G}_\mathrm{v}}(v'_i) \vee v'_j \in \mathcal{N}_{\boldsymbol{G}_\mathrm{v}}(v_i)$, where $\mathcal{N}_{\boldsymbol{G}_\mathrm{v}}(v_i)$ denotes the neighborhood of v_i.

However, the conflict rule (d) does not match the considered problem because mmWave V2V communications are utilized.

Considering the narrow beam width and high attenuation of mmWave communications, it seems that the radio interference between two transmissions is negligible. In this case, the conflict set C_τ is defined only by the basic rules: (a), (b), and (c). However, interference sometimes occurs when an interferer is near a receiver or the transmission direction of the desired and interfering signal are nearly parallel.

In order to overcome interference, a conflict rule that reflects mmWave radio characteristics should be designed. However, it is difficult to estimate SINR during scheduling because interference cannot be calculated before all the transmitters and their antenna directions are determined. This section proposes an approximation method that can be adopted for the redesigned conflict rules, which are defined for only two transmissions and utilized when constructing the scheduling graphs.

Considering the narrow beam width and high attenuation of mmWave radio signals, it can be assumed that the largest interference signal is the main factor of SINR. Therefore, SINR can be approximated as follows:

$$SINR_{i,j} := \frac{P_{\mathrm{r}}^{(i,j)}}{BN + \sum_{k \neq i,j} I_k} \tag{5.8}$$

$$\approx \frac{P_{\mathrm{r}}^{(i,j)}}{BN + \max_{k \neq i,j}\{I_k\}}, \tag{5.9}$$

where $SINR_{i,j}$, $P_{\mathrm{r}}^{(i,j)}$, and I_k denote the SINR at vehicle v_i, whose desired signal comes from v_j, received signal strength of desired signals from v_j at vehicle v_i, and interference power from vehicle v_k, respectively. Although knowledge regarding all interference signals seems to be required when calculating $\max_{k \neq i,j}\{I_k\}$, a conflict rule can be designed between pairs of transmissions by assuming that the currently considered interferer is the largest one. The conflict rule reflecting interference is designed as follows:

(d') A receiver cannot receive data when interfering signals are large: t_{ijk} conflicts with $t_{i'j'k'}$ if $sinr(t_{ijk}, t_{i'j'k'}) \leq \Theta \vee sinr(t_{i'j'k'}, t_{ijk}) \leq \Theta$, where $sinr(t_{ijk}, t_{i'j'k'}) := P_{\mathrm{r}}^{(j,i)}/(BN + I_{i'})$ and $\Theta := 2^{Rate/B} - 1$.

Consider the interfering signals from $v_{j_{\mathrm{t}}}$ and $v_{k_{\mathrm{t}}}$ to $v_{i_{\mathrm{r}}}$, where $I_{j_{\mathrm{t}}} < I_{k_{\mathrm{t}}}$. $v_{j_{\mathrm{t}}}$ and $v_{k_{\mathrm{t}}}$ attempt to transmit signals to $v_{j_{\mathrm{r}}}$ and $v_{k_{\mathrm{r}}}$, respectively, and $v_{i_{\mathrm{r}}}$ receives signals from $v_{i_{\mathrm{t}}}$. If $sinr(t_{i_{\mathrm{t}}i_{\mathrm{r}}a}, t_{k_{\mathrm{t}}k_{\mathrm{r}}b}) \leq \Theta$, then the concurrent transmission of $t_{i_{\mathrm{t}}i_{\mathrm{r}}a}$ and $t_{k_{\mathrm{t}}k_{\mathrm{r}}b}$ cannot be scheduled by the proposed algorithm. Therefore, when calculating the interference from $v_{j_{\mathrm{t}}}$ to $v_{i_{\mathrm{r}}}$, there is no need to consider interference from $v_{k_{\mathrm{t}}}$, and the interference from $v_{j_{\mathrm{t}}}$ is assumed to be the largest. This assumption can be extended inductively for more than three transmitters.

5.4.5 Required Time Slot for Complete Data Sharing

In this subsection, the situation where sufficient time slots are available to complete data sharing is discussed. First, it is proven that the proposed scheduling algorithm terminates in finite time and that all data are shared with all vehicles if the data-sharing time is not limited and the vehicular network graph $\boldsymbol{G}_{\mathrm{v}}$ is connected. Then, the bounds for the required number of time slots are discussed.

Theorem 5.1. *If $\boldsymbol{G}_{\mathrm{v}}$ is connected, the proposed data-sharing algorithm terminates in finite time, and all the data initially possessed by vehicles are shared with all vehicles when the algorithm terminates, which can be expressed as follows:*

$$\forall i, \boldsymbol{d}_{i,\tau_{\mathrm{end}}} = \{d_1, \ldots, d_{N_{\mathrm{v}}}\}, \tag{5.10}$$

where τ_{end} denotes the step count at the end of Algorithm 5.2.

Proof. First, the proposed algorithm is proven to terminate in finite time and then, is is proven that all vehicles possess all data at the end of the algorithm.

Let n_τ denote the total size of the dataset $\boldsymbol{d}_{i,\tau}$, defined as $n_\tau := \sum_{i=1}^{N_{\mathrm{v}}} |\boldsymbol{d}_{i,\tau}|$, where $|\cdot|$ represents the cardinality of a set. When t_{ijk} is performed, meaning vehicle v_j receives data d_k, n_τ is updated as $n_{\tau+1} \leftarrow n_\tau + 1$ because $\mathcal{T}_\tau$ is constructed from all elements in t_{ijk} that satisfy $d_k \notin \boldsymbol{d}_{j,\tau}$ (Lines 5–7 in Algorithm 5.1). Let $m_\tau := |\boldsymbol{t}_\tau|$ denote the number of transmissions selected by the RSU. Then, n_τ is updated as $n_{\tau+1} \leftarrow n_\tau + m_\tau$ in each time slot. Meanwhile, the maximum value of n_τ is bounded by N_{v}^2. Therefore, the algorithm terminates in finite time if at least one transmission is selected in each time slot.

Next, it is proven that if there exists a vehicle that does not possess all data, at least one transmission can be performed. Assume v_i does not possess d_j, which means $d_j \notin \boldsymbol{d}_i$. Then, there exists a connected pair $\{v_\alpha, v_\beta\} \in \mathcal{L}$ on the paths between v_i and v_j that satisfies $d_j \in \boldsymbol{d}_\alpha \wedge d_j \notin \boldsymbol{d}_\beta$ because at least v_j possesses d_j. Note that the paths between v_i and v_j exist because $\boldsymbol{G}_{\mathrm{v}}$ is connected. Hence, $t_{\alpha\beta j} \in \mathcal{T}_\tau$ because v_α possesses d_j and v_β does not possess d_j, meaning $\mathcal{T}_\tau \neq \emptyset$. An independent set of a graph is not $\emptyset$ if a vertex set of the graph is not $\emptyset$. Therefore, $\boldsymbol{G}_{\mathrm{s},\tau}$ has an independent set whose size is greater than zero.

If not all vehicles possess all data, a transmission can be performed and thus, the algorithm does not terminate. When the algorithm terminates, all vehicles possess all data. Because it is guaranteed that the algorithm always terminates in finite time, all data can be shared with all vehicles in finite time. □

Now, the bounds of τ_{end} satisfies the following corollary:

Corollary 5.1. *If the vehicular network graph* $\boldsymbol{G}_{\text{v}}$ *is connected,* τ_{end} *is bounded as,*

$$\frac{N_{\text{v}}^2 - N_{\text{v}}}{\lfloor N_{\text{v}}/2 \rfloor} \leq \tau_{\text{end}} \leq N_{\text{v}}^2 - N_{\text{v}}, \tag{5.11}$$

where $\lfloor \cdot \rfloor$ *represents the floor function.*

Proof. At the beginning of the algorithm, it is clear that $n_0 = N_{\text{v}}$. From (5.10), $n_{\tau_{\text{end}}} = N_{\text{v}}^2$. Meanwhile, $n_{\tau_{\text{end}}}$ is also written as $n_{\tau_{\text{end}}} = n_0 + \sum_{\tau=0}^{\tau_{\text{end}}-1} m_\tau$. Because vehicles cannot transmit and receive data simultaneously, m_τ satisfies $m_\tau \leq \lfloor N_{\text{v}}/2 \rfloor$. Additionally, m_τ also satisfies $m_\tau \geq 1$ because at least one transmission is performed in each time slot. Therefore, τ_{end} satisfies (5.11). □

On one hand, τ_{end} is equal to the upper bound if only one vehicle transmits data in every time slot. On the other hand, τ_{end} achieves the lower bound if half of the vehicles send data in every time slot, which is the optimal case under the constraint that each vehicle cannot send and receive data simultaneously. In Section 5.5, simulation results demonstrate that τ_{end} is near the lower bound in many cases.

5.5 Simulation Evaluations

This section evaluates the proposed algorithm through simulations. The simulation parameters are summarized in Table 5.1. In the simulations, the distribution of inter-vehicle distance followed an exponential distribution. This assumption was confirmed in [82], where the authors demonstrated that the distribution of inter-vehicle distance follows an exponential distribution based on empirical data collected in a real environment. It was assumed the average distance between vehicles l_{avg} in each lane was approximately the same as the stopping distance for traffic safety. In the evaluated situations, $l_{\text{avg}} = 20$ m and 40 m, which are slightly larger than the stopping distances when the velocity is 40 km/h and 60 km/h,

Table 5.1: Parameters of mmWave concurrent transmission simulations.

Parameters	Values
Number of lanes	4
Lane width	3.5 m
Sidewalk width	4 m
Sensor range r_s	50 m
Bandwidth B	2.16 GHz
Thermal noise N	-174 dBm/Hz
Data rate *Rate*	1 Gbit/s
Transmission power P_t	10 dBm
Antenna beam width	15°, 30°

respectively [83]. An intersection with two roads and four buildings was evaluated assuming an urban area. Each road had four lanes and sidewalks on both sides. Each vehicle was modeled as a rectangle with a size of 1.7 m × 4.4 m. The N_v vehicles closest to the center of the intersection shared their data with each other. The number of participants N_v was fixed to 20 and 40 when l_{avg} was 20 m and N_v was fixed to 10 and 20 when l_{avg} was 40 m. If $(l_{avg}, N_v) = (20\,\mathrm{m}, 20)$ and $(40\,\mathrm{m}, 10)$, the perceivable region with shared data covers $(25\,\mathrm{m} + r_s/2)$ from the center of the intersection, because vehicles within approximately 25 m of the center of the intersection participate in data sharing. When the number of vehicles is doubled, perceivable region covers $(50\,\mathrm{m} + r_s/2)$ from the center of the intersection. The achievable coverage is sufficient for some applications, e.g., accident or congestion detection system with which a driver or self-driving system gets alerts and stops or slows down the vehicle when an accident or congestion is detected at the intersection. The number of blocking vehicles was decided by drawing lines from the transmitter to the receiver vehicles and counting the vehicles on the line as in [13]. The number of blockers was used to calculate the pass loss based on the model proposed in [22] and construct vehicular network graph $\boldsymbol{G}_v$ from (5.3) and (5.4). Threshold is calculated by (5.6) based on the Shannon capacity when deciding connectivity between two vehicles. Therefore, links that do not have enough capacity are never used to transmit data by the proposed algorithm. In

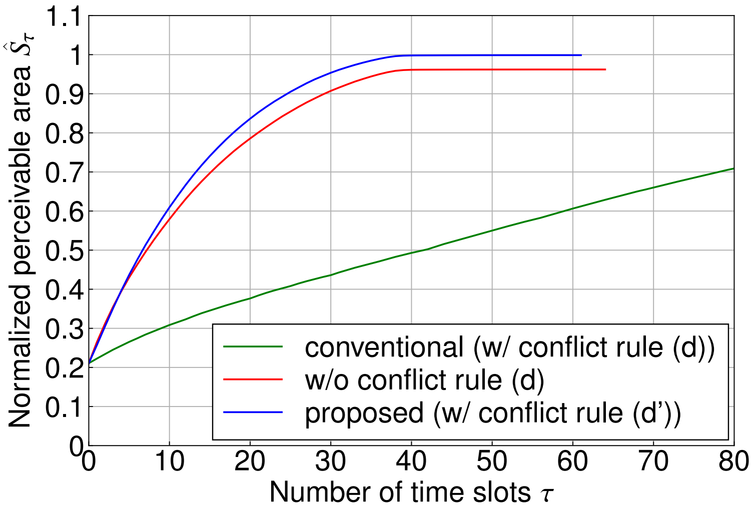

Figure 5.4: Normalized perceivable area as a function of the number of time slots when $(l_{\text{avg}}, N_{\text{v}}) = (40\,\text{m}, 20)$ and beam width is 15°. The normalized perceivable area is enlarged by utilizing the conflict rule (d'). ©2019 IEICE

the simulations, transmission succeeds when the data rate is less than the Shannon capacity calculated using SINR. It is also assumed that if the buildings blocked their LOS path, vehicles could not communicate with each other because of blockage effects. The antenna gain was calculated from the reference model in [84], which is originally developed for the IEEE 802.15.3c standard and adopted in the channel model measurements of the IEEE 802.11ad in [85]. Sensor range is decided to 50 m as typical value of spatial sensors, e.g., cameras and LiDARs.

In the simulations, the RSU first determined the scheduling. Next, vehicles transmitted data based on the scheduling. When interference occurred, a receiver failed to receive data. If a transmitter was scheduled to transmit data that it did not possess, it did not transmit any data during that time slot.

Figure 5.4 presents the normalized perceivable area $\hat{S}_\tau$ defined in Section 5.3 as a function of the number of time slots τ when $(l_{\text{avg}}, N_{\text{v}}) = (40\,\text{m}, 20)$. When the proposed data-sharing algorithm was used, the perceivable areas $\hat{S}_\tau$ were enlarged by data sharing at first. Then, $\hat{S}_\tau$ saturated when $\tau \geq 40$ because the entire region R_{all} was covered by the shared perceptual data. In other words, transmitted data after $\tau \geq 40$ did not contribute to enlarging the perceivable area because of overlap. Finally, the algorithm terminated at $\tau = 61$ when all scheduled

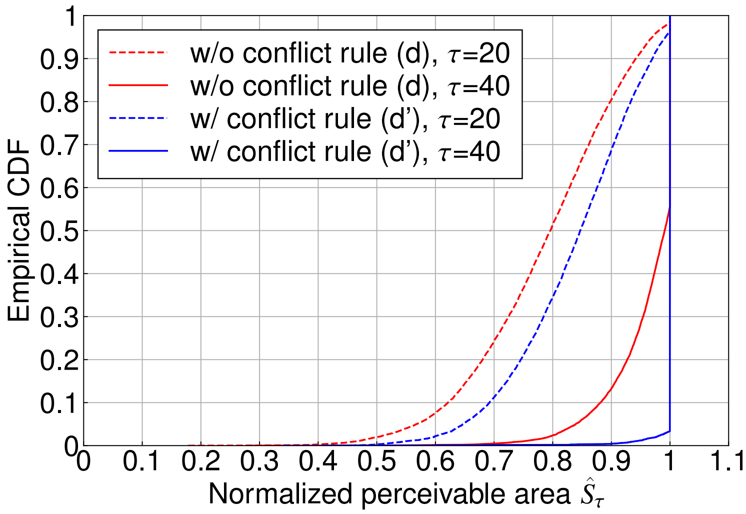

Figure 5.5: Empirical CDF of normalized perceivable area when $\left(l_{\text{avg}}, N_{\text{v}}\right) = (40\,\text{m}, 20)$. Nearly all vehicles achieve 90% of the perceivable area at $\tau = 40$ when the conflict rule (d') is utilized. ©2019 IEICE

transmissions were completed. The proposed algorithm achieved approximately twice the perceivable area compared with the conventional algorithm at $\tau = 40$. This is because the conventional algorithm assumed microwave communications and thus, few vehicles could transmit data concurrently because of the conflict rule (d), which was designed for microwave communications. In contrast, the proposed method achieved efficient concurrent transmission because its conflict rules reflect mmWave radio characteristics. Additionally, adopting the conflict rule (d') enlarged the perceivable area because when this rule is not adopted, certain interferences cannot be avoided and data sharing cannot be completed owing to transmission failure.

The empirical CDF of the normalized perceivable area $\hat{S}_\tau$ is shown in Figure 5.5. When utilizing the conflict rule (d'), nearly all vehicles achieved 90% of the normalized perceivable area at $\tau = 40$, whereas only 86% of the vehicles achieved 90% of the normalized perceivable area where interference was not considered when determining the scheduling.

The normalized perceivable areas with different inter-vehicle distances and number of vehicles are shown in Figure 5.6. The beam width was 15°. When the vehicle average inter-vehicle distance was the same, the smaller the number of

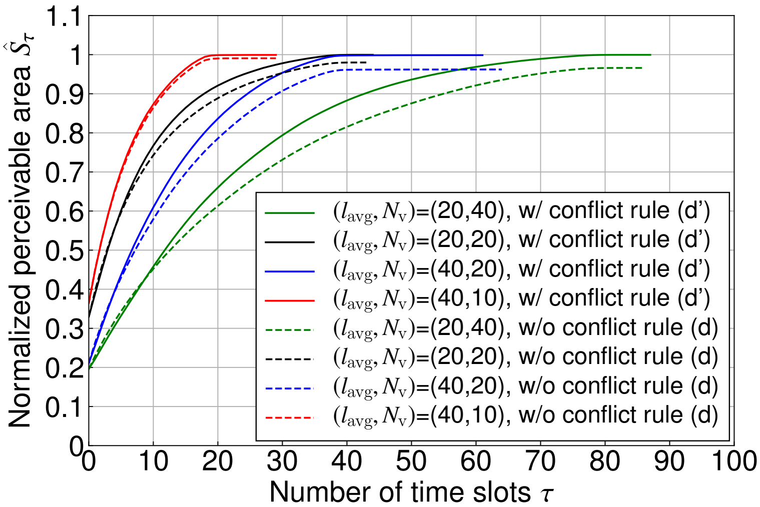

Figure 5.6: Normalized perceivable area when $(l_{\rm avg}, N_{\rm v}) = (20\,{\rm m}, 40), (20\,{\rm m}, 20), (40\,{\rm m}, 20), (40\,{\rm m}, 10)$ and the beam width is 15°. The differences between the performances with and without the mmWave interference conflict rule are smaller when the number of participants is small or inter-vehicle distance is large. Averages of normalizing factors $S(R_{\rm all})$ in (5.2) for $(l_{\rm avg}, N_{\rm v}) = (20\,{\rm m}, 40), (20\,{\rm m}, 20), (40\,{\rm m}, 20)$, and $(40\,{\rm m}, 10)$ are 6,161 m^2, 3,949 m^2, 5,793 m^2, and 3,616 m^2, respectively. ©2019 IEICE

vehicles, the faster the data sharing terminated. This is confirmed by (5.11). It is also shown that the superiority of adopting conflict rule (d') does not depend on $l_{\rm avg}$ and $N_{\rm v}$. The performance gain of adopting conflict rule (d') is larger when the number of participants is large or the inter-vehicle distance is small because interference is more likely to occur in these cases.

Figure 5.7 presents the normalized perceivable areas with beam widths of 15° and 30°, when $(l_{\rm avg}, N_{\rm v}) = (40\,{\rm m}, 20)$. The differences between the beam widths of 15° and 30° were larger when the conflict rule for mmWave interference was not adopted compared with when the rule (d') is adopted. This is because interferences occur more frequently with a wider beam width, but the proposed conflict rule (d') can successfully avoid interference.

Differences between the two priority designs when $(l_{\rm avg}, N_{\rm v}) = (40\,{\rm m}, 20)$ is shown in Figure 5.8. The max distance scheduling design achieved a larger perceivable area than the max transmission scheduling design when $\tau \leq 36$. $\hat{S}_\tau$ of

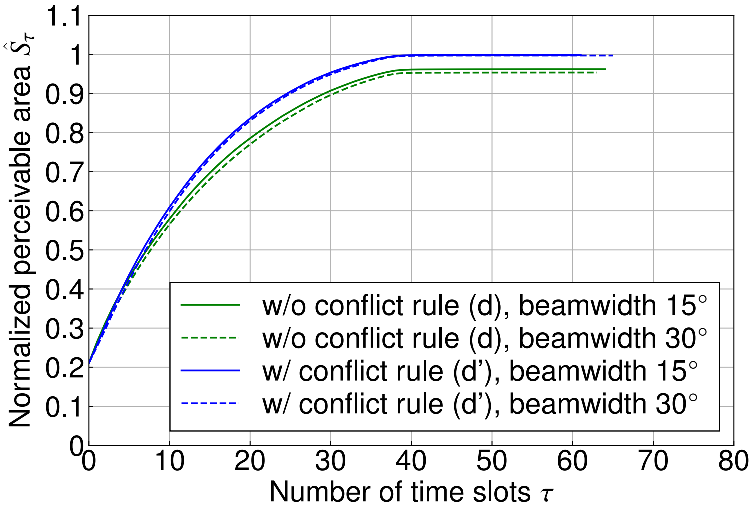

Figure 5.7: Normalized perceivable area when $(l_{\text{avg}}, N_{\text{v}}) = (40\,\text{m}, 20)$ and the beam width is 15° and 30°. The differences between the beam widths of 15° and 30° are larger when the mmWave interference conflict rule is not adopted compared with when the rule (d') is adopted. ©2019 IEICE

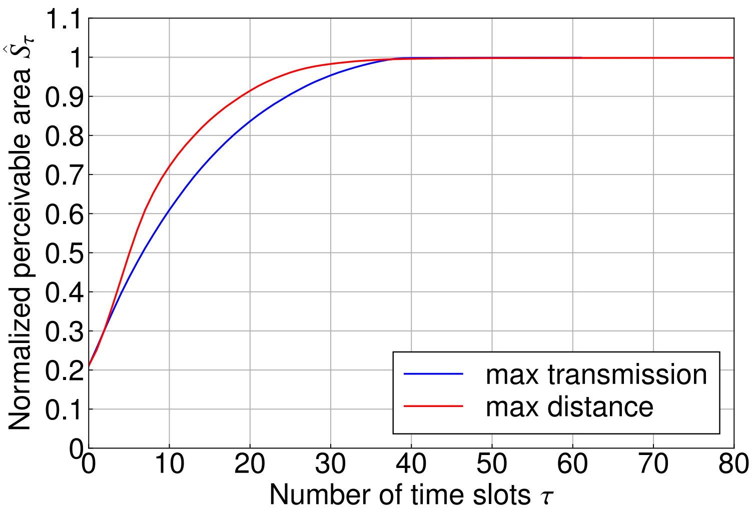

Figure 5.8: Normalized perceivable area with the different priority designs, when $(l_{\text{avg}}, N_{\text{v}}) = (40\,\text{m}, 20)$ and beam width is 15°. The conflict rule (d') is adopted. The perceivable area can be enlarged by prioritizing data far from the intersection when the number of time slot is limited. ©2019 IEICE

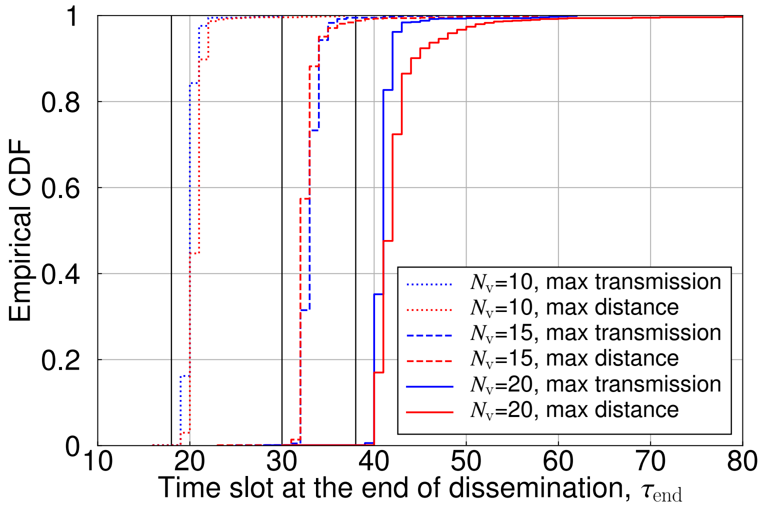

Figure 5.9: Empirical CDF of the number of time slots required to share all data. The conflict rule (d') is adopted. The beam width is 15° and inter-vehicle distance is 40 m. Black vertical lines represent lower bounds. The proposed algorithm achieves near-optimal scheduling. ©2019 IEICE

the max distance design was 20% larger than that of the max transmission design when $\tau = 8$. Based on the max distance scheduling, data far from the center of the intersection were transmitted at first and thus, the overlapping regions tended to be smaller than those in the algorithm without such priority control. Therefore, $\hat{S}_\tau$ became larger than that in the max transmission scheduling design. When the number of time slot was limited, such that $\tau_{\mathrm{max}} \leq 36$, the max distance scheduling design provided a larger perceivable area during every data update interval.

Figure 5.9 shows empirical CDF of the number of time slots required to share all data, denoted τ_{end}, when τ_{max} is much larger than τ_{end}. Inter-vehicle distance was assumed to be 40 m. From (5.11), the lower bounds of τ_{end} were calculated as 18, 30, and 38, for $N_{\mathrm{v}} = 10, 15, 20$. The lower bounds are depicted as black vertical lines in Figure 5.9. In most cases, τ_{end} were closer to the lower bounds than the upper bounds of 90, 210, and 380. In very few cases, as shown in Figure 5.9, the data-sharing algorithm terminated after fewer iterations than the lower bounds. This is because the vehicular network graphs $\boldsymbol{G}_{\mathrm{v}}$ were disconnected in such cases and thus, the data-sharing algorithm terminated before all data were shared. The differences between the protocols with and without prioritization can be observed when $N_{\text{v}} = 20$. The max transmission scheduling design achieved efficient data sharing because it maximized the number of transmitted data at each time slot, meaning the algorithm terminated faster than the max distance scheduling design when data-sharing time was not limited.

5.6 Conclusions and Future Works

This chapter proposed a data-sharing scheduling method with concurrent transmission for mmWave VANETs for cooperative perception. The algorithm in [78] was modified by designing a conflict rule that represents mmWave communication characteristics and a weight function that prioritizes data to be forwarded to enlarge the perceivable area. Simulation results demonstrated that the proposed conflict rule for scheduling graphs achieved a larger perceivable area compared with the original rules, which did not consider directional antennas. Priority control methods also enlarged the perceivable region by sharing data that covered areas far from an intersection at first. The priority control worked efficiently in situations where the number of time slots was limited. This chapter also proved that the proposed algorithms terminate in finite time and all data can be shared with all vehicles if a vehicular network is represented as a connected graph and there are sufficient time slots.

Future direction of this work is developing a data-aggregation and vehicle-selection method for reducing redundant data transmissions. The algorithm proposed in this chapter transmits data without considering overlapping regions covered by multiple data. To suppress the transmission of data representing overlapping regions can reduce data traffic without reducing the perceivable area. The data-aggregation method that aggregates some overlapping data to a single datum also reduces the amount of data to be transmitted. When the vehicles densely located, to select vehicles generating data considering their sensor coverage can reduce data transmissions including the same regions.

Another interest is to develop a scalable distributed scheduling method. In the proposed algorithm, an RSU, which act as a central controller, determines the schedule based on information from all vehicles participating in cooperative perception. When the number of vehicles is large, it is difficult for a central controller to obtain accurate information from all vehicles and to perfectly control whole schedules because mmWave channels vary rapidly. Therefore, distributed scheduling including hybrid schemes of centralized and distributed scheduling should be developed to reduce the amount of vehicle information transmitted to the RSU and to allow vehicles to decide scheduling autonomously using their own information.

Chapter 6

Conclusions

This thesis presented high-throughput vehicular communications with cooperative methods and applications in order to further improve traffic safety and efficiency and to realize diverse services by sharing the large amount of data obtained from vehicles. This thesis focused on cooperative MIMO, cooperative mmWave relay expansion, and concurrent transmission for cooperative perception.

The first topic was a vehicular cooperative MIMO scheme, which increases the channel capacity by coordinating multiple transmitters and multiple receivers and forming a large virtual MIMO system. This thesis proposed a precoding scheme with limited CSIT, which drastically reduced the amount of CSI feedback. An iterative MIMO detector was also proposed to overcome the inter-receiver interference caused by the lack of CSIT. The iteration scheme updating log likelihood ratio of transmitted signals and improves the BER performance.

The second topic was mmWave relay expansion for V2I. Although mmWave communications realize high-throughput data transmission, the RSU coverage tends to be small because of high attenuation by oxygen absorption and blockage effects. To solve this problem, multihop relaying can be utilized, and enlarging the relays increases the coverage. This thesis proposed a RL-based relay-expansion algorithm, where vehicles cooperatively change their relative positions to expand relays by avoiding blockages. The RL-based strategy achieved larger coverage than when the vehicles are distributed randomly, even when half of the mmWave vehicles employed the proposed RL algorithm. In addition, the RL-based strategy increased coverage, even when the vehicle density and penetration ratio of mmWave vehicles differed from those of the learning phase.

The third topic was cooperative perception with mmWave concurrent transmission. In order to expand the areas that vehicles perceive at intersections with poor visibility, vehicles share their perceptual sensor data with each other. A concurrent transmission scheduling was proposed to disseminate sensor data efficiently considering antenna directionality. A conflict rule was utilized to realize mmWave concurrent transmission and a weight function for prioritization was applied to enlarge the perceivable area. The proposed algorithms were proven to terminate in finite time, and all data can be shared with all vehicles participating in cooperative perception.

Bibliography

[1] N. Lu, N. Cheng, N. Zhang, X. Shen, and J. W. Mark, "Connected vehicles: Solutions and challenges," *IEEE Internet of Things Journal*, vol. 1, no. 4, pp. 289–299, Aug. 2014.

[2] M. Gerla, E. K. Lee, G. Pau, and U. Lee, "Internet of vehicles: From intelligent grid to autonomous cars and vehicular clouds," in *Proc. of 2014 IEEE World Forum on Internet of Things (WF-IoT)*, Seoul, Korea, Mar. 2014, pp. 241–246.

[3] M. Gerla, "Vehicular cloud computing," in *Proc. of 2012 The 11th Annual Mediterranean Ad Hoc Networking Workshop (Med-Hoc-Net)*, Ayia Napa, Cyprus, Jun. 2012, pp. 152–155.

[4] A. J. Ghandour, M. Di Felice, H. Artail, and L. Bononi, "Dissemination of safety messages in IEEE 802.11p/WAVE vehicular network: Analytical study and protocol enhancements," *Pervasive and mobile computing*, vol. 11, pp. 3–18, Apr. 2014.

[5] J. B. Kenney, "Dedicated short-range communications (DSRC) standards in the United States," *Proceedings of the IEEE*, vol. 99, no. 7, pp. 1162–1182, Jul. 2011.

[6] R. Molina-Masegosa and J. Gozalvez, "LTE-V for sidelink 5G V2X vehicular communications: A new 5G technology for short-range vehicle-to-everything communications," *IEEE Vehicular Technology Magazine*, vol. 12, no. 4, pp. 30–39, Dec. 2017.

[7] R. Chen, W. Jin, and A. Regan, "Broadcasting safety information in vehicular networks: issues and approaches," *IEEE Network*, vol. 24, no. 1, pp. 20–25, Jan. 2010.

[8] P. Fernandes and U. Nunes, "Platooning with IVC-enabled autonomous vehicles: Strategies to mitigate communication delays, improve safety and traffic flow," *IEEE Trans. Intell. Transp. Syst.*, vol. 13, no. 1, pp. 91–106, Mar. 2012.

[9] M. Amoozadeh, H. Deng, C.-N. Chuah, H. M. Zhang, and D. Ghosal, "Platoon management with cooperative adaptive cruise control enabled by vanet," *Vehicular communications*, vol. 2, no. 2, pp. 110–123, Apr. 2015.

[10] P. Lin, J. Liu, P. J. Jin, and B. Ran, "Autonomous vehicle-intersection coordination method in a connected vehicle environment," *IEEE Intell. Transp. Syst. Mag.*, vol. 9, no. 4, pp. 37–47, Oct. 2017.

[11] R. Hult, G. R. Campos, E. Steinmetz, L. Hammarstrand, P. Falcone, and H. Wymeersch, "Coordination of cooperative autonomous vehicles: Toward safer and more efficient road transportation," *IEEE Signal Process. Mag.*, vol. 33, no. 6, pp. 74–84, Nov. 2016.

[12] E. Ahmed and H. Gharavi, "Cooperative vehicular networking: A survey," *IEEE Trans. Intell. Transp. Syst.*, vol. 19, no. 3, pp. 996–1014, Mar. 2018.

[13] V. Va, T. Shimizu, G. Bansal, and R. W. Heath Jr., *Millimeter Wave Vehicular Communications: A Survey*. Now Publishers Inc., 2016.

[14] S.-W. Kim, B. Qin, Z. J. Chong, X. Shen, W. Liu, M. H. Ang, E. Frazzoli, and D. Rus, "Multivehicle cooperative driving using cooperative perception: Design and experimental validation," *IEEE Trans. Intell. Transp. Syst.*, vol. 16, no. 2, pp. 663–680, Apr. 2015.

[15] H. Li and F. Nashashibi, "Multi-vehicle cooperative perception and augmented reality for driver assistance: A possibility to 'see' through front vehicle," in *Proc. of 2011 14th International IEEE Conference on Intelligent Transportation Systems (ITSC)*, Washington, DC, USA, Oct. 2011, pp. 242–247.

[16] B. Coll-Perales, J. Gozalvez, and M. Gruteser, "Sub-6GHz assisted MAC for millimeter wave vehicular communications," *IEEE Commun. Mag.*, vol. 57, no. 3, pp. 125–131, Mar. 2019.

[17] T. Nguyen, O. Berder, and O. Sentieys, "Energy-efficient cooperative techniques for infrastructure-to-vehicle communications," *IEEE Trans. Intell. Transp. Syst.*, vol. 12, no. 3, pp. 659–668, Sep. 2011.

[18] X. Ge, H. Cheng, G. Mao, Y. Yang, and S. Tu, "Vehicular communications for 5G cooperative small-cell networks," *IEEE Trans. Veh. Technol.*, vol. 65, no. 10, pp. 7882–7894, Oct. 2016.

[19] G. J. Foschini and M. J. Gans, "On limits of wireless communications in a fading environment when using multiple antennas," *Wireless personal communications*, vol. 6, no. 3, pp. 311–335, Mar. 1998.

[20] J. C. Roh and B. D. Rao, "Transmit beamforming in multiple-antenna systems with finite rate feedback: A VQ-based approach," *IEEE Trans. Inf. Theory*, vol. 52, no. 3, pp. 1101–1112, Mar. 2006.

[21] J. Choi, V. Va, N. Gonzalez-Prelcic, R. Daniels, C. R. Bhat, and R. W. Heath, "Millimeter-wave vehicular communication to support massive automotive sensing," *IEEE Commun.s Mag.*, vol. 54, no. 12, pp. 160–167, Dec. 2016.

[22] A. Yamamoto, K. Ogawa, T. Horimatsu, A. Kato, and M. Fujise, "Path-loss prediction models for intervehicle communication at 60 GHz," *IEEE Trans. Veh. Technol.*, vol. 57, no. 1, pp. 65–78, Jan. 2008.

[23] H. Zhou, B. Liu, T. H. Luan, F. Hou, L. Gui, Y. Li, Q. Yu, and X. Shen, "Chaincluster: Engineering a cooperative content distribution framework for highway vehicular communications," *IEEE Trans. Intell. Transp. Syst.*, vol. 15, no. 6, pp. 2644–2657, Dec. 2014.

[24] A. Benslimane, T. Taleb, and R. Sivaraj, "Dynamic clustering-based adaptive mobile gateway management in integrated VANET – 3G heterogeneous wireless networks," *IEEE J. Sel. Areas Commun.*, vol. 29, no. 3, pp. 559–570, Mar. 2011.

[25] P. Salvo, F. Cuomo, A. Baiocchi, and A. Bragagnini, "Road side unit coverage extension for data dissemination in VANETs," in *Proc. of 2012 9th Annual Conference on Wireless On-demand Network Systems and Services (WONS)*, Courmayeur, Italy, Jan. 2012, pp. 47–50.

[26] G. Karagiannis, O. Altintas, E. Ekici, G. Heijenk, B. Jarupan, K. Lin, and T. Weil, "Vehicular networking: A survey and tutorial on requirements, architectures, challenges, standards and solutions," *IEEE Commun. Surveys Tuts.*, vol. 13, no. 4, pp. 584–616, Jul. 2011.

[27] H. Kawai, K. Higuchi, N. Maeda, and M. Sawahashi, "Adaptive control of surviving symbol replica candidates in QRM-MLD for OFDM MIMO multiplexing," *IEEE J. Sel. Areas Commun.*, vol. 24, no. 6, pp. 1130–1140, Jun. 2006.

[28] Y.-S. Song and H.-K. Choi, "Analysis of V2V broadcast performance limit for WAVE communication systems using two-ray path loss model," *ETRI Journal*, vol. 39, no. 2, pp. 213–221, Apr. 2017.

[29] D. Jiang, V. Taliwal, A. Meier, W. Holfelder, and R. Herrtwich, "Design of 5.9 GHz DSRC-based vehicular safety communication," *IEEE Wireless Commun.*, vol. 13, no. 5, Oct. 2006.

[30] "DEDICATED SHORT-RANGE COMMUNICATION SYSTEM," Sep. 2001, ARIB STD-T75.

[31] "700 MHz BAND INTELLIGENT TRANSPORT SYSTEMS," Jul. 2017, ARIB STD-T109.

[32] Q. H. Spencer, A. L. Swindlehurst, and M. Haardt, "Zero-forcing methods for downlink spatial multiplexing in multiuser MIMO channels," *IEEE Trans. Signal Process.*, vol. 52, no. 2, pp. 461–471, Feb. 2004.

[33] H. T. Friis, "A note on a simple transmission formula," *Proceedings of the IRE*, vol. 34, no. 5, pp. 254–256, May 1946.

[34] R. S. Sutton and A. G. Barto, *Reinforcement learning: An introduction*. Cambridge Univ. Press, 1998.

[35] N. D. Nguyen, T. Nguyen, and S. Nahavandi, "System design perspective for human-level agents using deep reinforcement learning: A survey," *IEEE Access*, vol. 5, pp. 27 091–27 102, Nov. 2017.

[36] V. Mnih, K. Kavukcuoglu, D. Silver, A. A. Rusu, J. Veness, M. G. Bellemare, A. Graves, M. Riedmiller, A. K. Fidjeland, G. Ostrovski *et al.*, "Human-level control through deep reinforcement learning," *Nature*, vol. 518, no. 7540, pp. 529–533, Feb. 2015.

[37] D. Silver, A. Huang, C. J. Maddison, A. Guez, L. Sifre, G. Van Den Driessche, J. Schrittwieser, I. Antonoglou, V. Panneershelvam, M. Lanctot *et al.*, "Mastering the game of go with deep neural networks and tree search," *Nature*, vol. 529, no. 7587, pp. 484–489, Jan. 2016.

[38] A. Nair, P. Srinivasan, S. Blackwell, C. Alcicek, R. Fearon, A. D. Maria, V. Panneershelvam, M. Suleyman, C. Beattie, S. Petersen, S. Legg, V. Mnih, K. Kavukcuoglu, and D. Silver, "Massively parallel methods for deep reinforcement learning," in *Proc. of the 32nd International Conference on Machine Learning (ICML) Deep Learning Workshop*, Lille, France, Jul. 2015.

[39] V. Mnih, A. P. Badia, M. Mirza, A. Graves, T. Lillicrap, T. Harley, D. Silver, and K. Kavukcuoglu, "Asynchronous methods for deep reinforcement learning," in *Proc. of the 33rd International Conference on Machine Learning (ICML)*, New York, USA, Jun. 2016, pp. 1928–1937.

[40] J. Imamura, S. Denno, D. Umehara, and M. Morikura, "A virtual layered space-frequency receiver architecture with iterative decoding," *IEICE Trans. Commun.*, vol. E94-B, no. 7, pp. 1994–2002, Jul. 2011.

[41] K.-K. Wong, A. Paulraj, and R. D. Murch, "Efficient high-performance decoding for overloaded MIMO antenna systems," *IEEE Trans. Wireless Commun.*, vol. 6, no. 5, pp. 1833–1843, May 2007.

[42] B. W. Zarikoff, J. K. Cavers, and S. Bavarian, "An iterative groupwise multiuser detector for overloaded MIMO applications," *IEEE Trans. Wireless Commun.*, vol. 6, no. 2, pp. 443–447, Feb. 2007.

[43] S. Denno, H. Maruyama, D. Umehara, and M. Morikura, "A virtual layered space time receiver with maximum likelihood channel detection," in *Proc. of IEEE 69th Vehicular Technology Conference (VTC Spring)*. Barcelona, Spain: IEEE, Apr. 2009, pp. 1–5.

[44] S. Yoshikawa, S. Denno, and M. Morikura, "Complexity reduced lattice-reduction-aided MIMO receiver with virtual channel detection," *IEICE Trans. Commun.*, vol. 96, no. 1, pp. 263–270, Jan. 2013.

[45] C. Berrou and A. Glavieux, "Near optimum error correcting coding and decoding: Turbo-codes," *IEEE Trans. Commun.*, vol. 44, no. 10, pp. 1261–1271, Oct. 1996.

[46] H. Kawai, K. Higuchi, N. Maeda, M. Sawahashi, T. Ito, Y. Kakura, A. Ushirokawa, and H. Seki, "Likelihood function for QRM-MLD suitable for soft-decision Turbo decoding and its performance for OFCDM MIMO multiplexing in multipath fading channel," *IEICE Trans. Commun.*, vol. E88-B, no. 1, pp. 47–57, Jan. 2005.

[47] A. Stefanov and T. M. Duman, "Turbo-coded modulation for systems with transmit and receive antenna diversity over block fading channels: system model, decoding approaches, and practical considerations," *IEEE J. Sel. Areas Commun.*, vol. 19, no. 5, pp. 958–968, May 2001.

[48] B. M. Hochwald and S. Ten Brink, "Achieving near-capacity on a multiple-antenna channel," *IEICE Trans. Commun.*, vol. 51, no. 3, pp. 389–399, Mar. 2003.

[49] J. Ylioinas and M. Juntti, "Iterative joint detection, decoding, and channel estimation in turbo-coded MIMO-OFDM," *IEEE Trans. Veh. Technol.*, vol. 58, no. 4, pp. 1784–1796, May 2009.

[50] E. P. Simon, L. Ros, H. Hijazi, J. Fang, D. P. Gaillot, and M. Berbineau, "Joint carrier frequency offset and fast time-varying channel estimation for MIMO-OFDM systems," *IEEE Trans. Veh. Technol.*, vol. 60, no. 3, pp. 955–965, Mar. 2011.

[51] X. Cheng, Q. Yao, M. Wen, C. X. Wang, L. Y. Song, and B. L. Jiao, "Wideband channel modeling and intercarrier interference cancellation for vehicle-to-vehicle communication systems," *IEEE J. Sel. Areas Commun.*, vol. 31, no. 9, pp. 434–448, Sep. 2013.

[52] G. J. Foschini, "Layered space-time architecture for wireless communication in a fading environment when using multi-element antennas," *Bell Labs Tech. J.*, vol. 1, no. 2, pp. 41–59, 1996.

[53] J. A. Fax and R. M. Murray, "Information flow and cooperative control of vehicle formations," *IEEE Trans. Autom. Control*, vol. 49, no. 9, pp. 1465–1476, Sep. 2004.

[54] R. Olfati-Saber and R. M. Murray, "Distributed cooperative control of multiple vehicle formations using structural potential functions," *IFAC Proceedings Volumes*, vol. 35, no. 1, pp. 495–500, 2002.

[55] P. Basu and J. Redi, "Movement control algorithms for realization of fault-tolerant ad hoc robot networks," *IEEE Network*, vol. 18, no. 4, pp. 36–44, Jul. 2004.

[56] S. Gundry, J. Zou, C. S. Sahin, J. Kusyk, and M. U. Uyar, "Autonomous and fault tolerant vehicular self deployment mechanisms in MANETs," in *Proc. of 2013 IEEE International Conference on Technologies for Homeland Security (HST)*, Waltham, MA, USA, Nov. 2013, pp. 595–600.

[57] A. Taya, T. Nishio, M. Morikura, and K. Yamamoto, "Coverage expansion through dynamic relay vehicle deployment in mmwave V2I communications," in *2018 IEEE 87th Vehicular Technology Conference (VTC Spring)*, Porto, Portugal, Jun. 2018, pp. 1–5.

[58] P. Raja and S. Pugazhenthi, "Optimal path planning of mobile robots: A review," *International Journal of Physical Sciences*, vol. 7, no. 9, pp. 1314–1320, Feb. 2012.

[59] R. Verdone, "Multihop R-ALOHA for intervehicle communications at millimeter waves," *IEEE Trans. Veh. Technol.*, vol. 46, no. 4, pp. 992–1005, Nov. 1997.

[60] C. Wu, T. Yoshinaga, and Y. Ji, "Cooperative content delivery in vehicular networks with integration of sub-6 GHz and mmWave," in *Proc. of 2017 IEEE Globecom Workshops (GC Wkshps)*, Singapore, Dec. 2017, pp. 1–6.

[61] T. Paul, T. R. Krogstad, and J. T. Gravdahl, "Modelling of UAV formation flight using 3D potential field," *Simulation Modelling Practice and Theory*, vol. 16, no. 9, pp. 1453–1462, Oct. 2008.

[62] X. Yu, W. Huang, J. Lan, and X. Qian, "A novel virtual force approach for node deployment in wireless sensor network," in *Proc. of 2012 IEEE 8th International Conference on Distributed Computing in Sensor Systems*, Hangzhou, China, May 2012, pp. 359–363.

[63] J. Chen, S. Li, and Y. Sun, "Novel deployment schemes for mobile sensor networks," *Sensors*, vol. 7, no. 11, pp. 2907–2919, Nov. 2007.

[64] W. Roh, J.-Y. Seol, J. Park, B. Lee, J. Lee, Y. Kim, J. Cho, K. Cheun, and F. Aryanfar, "Millimeter-wave beamforming as an enabling technology for 5G cellular communications: theoretical feasibility and prototype results," *IEEE Commun. Mag.*, vol. 52, no. 2, pp. 106–113, Feb. 2014.

[65] E. M. Mohamed, K. Sakaguchi, and S. Sampei, "Millimeter wave beamforming based on WiFi fingerprinting in indoor environment," in *Proc. of 2015 IEEE International Conference on Communication Workshop (ICCW)*, London, UK, Jun. 2015, pp. 1155–1160.

[66] N. González-Prelcic, R. Méndez-Rial, and R. W. Heath, "Radar aided beam alignment in mmWave V2I communications supporting antenna diversity," in *Proc. of 2016 Information Theory and Applications Workshop (ITA)*, La Jolla, CA, USA, Feb. 2016, pp. 1–7.

[67] R. Jiang and Q.-S. Wu, "The adaptive cruise control vehicles in the cellular automata model," *Physics Letters A*, vol. 359, no. 2, pp. 99–102, Nov. 2006.

[68] Y. Wang, K. Venugopal, A. F. Molisch, and R. W. Heath, "Analysis of urban millimeter wave microcellular networks," in *Proc. of 2016 IEEE 84th Vehicular Technology Conference (VTC Fall)*, Montreal, QC, Canada, Sep. 2016, pp. 1–5.

[69] H. Okamoto, T. Nishio, M. Morikura, K. Yamamoto, D. Murayama, and K. Nakahira, "Machine-learning-based throughput estimation using images for mmWave communications," in *Proc. of 2017 IEEE 85th Vehicular Technology Conference (VTC Spring)*, Sydney, NSW, Australia, Jun. 2017, pp. 1–5.

[70] H. Okamoto, T. Nishio, M. Morikura, and K. Yamamoto, "Recurrent neural network-based received signal strength estimation using depth images for mmWave communications," in *Proc. of 2018 15th IEEE Annual Consumer Communications & Networking Conference (CCNC)*, Las Vegas, NV, USA, Jan. 2018, pp. 1–2.

[71] C. Perfecto, J. Del Ser, and M. Bennis, "Millimeter-wave V2V communications: Distributed association and beam alignment," *IEEE J. Sel. Areas Commun.*, vol. 35, no. 9, pp. 2148–2162, Sep. 2017.

[72] J. Qiao, L. X. Cai, X. Shen, and J. W. Mark, "STDMA-based scheduling algorithm for concurrent transmissions in directional millimeter wave networks," in *Proc. of 2012 IEEE International Conference on Communications (ICC)*, Ottawa, ON, Canada, Jun. 2012, pp. 5221–5225.

[73] Y. Niu, Y. Li, D. Jin, L. Su, and D. Wu, "Blockage robust and efficient scheduling for directional mmwave WPANs," *IEEE Trans. Veh. Technol.*, vol. 64, no. 2, pp. 728–742, Feb. 2015.

[74] Y. Wang, X. Kang, H. K. Garg, M. Motani, and Q. Chen, "Throughput maximization for 60 GHz WPANs via device cooperation," *IEEE Commun. Lett.*, vol. 18, no. 5, pp. 785–788, May 2014.

[75] L. Wischhof, A. Ebner, and H. Rohling, "Information dissemination in self-organizing intervehicle networks," *IEEE Trans. Intell. Transp. Syst.*, vol. 6, no. 1, pp. 90–101, Mar. 2005.

[76] J. Bronsted and L. M. Kristensen, "Specification and performance evaluation of two zone dissemination protocols for vehicular ad-hoc networks," in *Proc. of the 39th Annual Symposium on Simulation (ANSS)*, Huntsville, Alabama, USA, Apr. 2006, pp. 68–79.

[77] A. Yamada and S. Ishihara, "Data exchange strategies for aggregating geographical distribution of demands for location-dependent information using soft-state sketches in VANETs," in *Proc. of 2017 IEEE 31st International Conference on Advanced Information Networking and Applications (AINA)*, Taipei, Taiwan, May 2017, pp. 728–736.

[78] K. Liu, J. K. Ng, V. Lee, S. H. Son, and I. Stojmenovic, "Cooperative data scheduling in hybrid vehicular ad hoc networks: VANET as a software defined network," *IEEE/ACM Trans. Netw.*, vol. 24, no. 3, pp. 1759–1773, Jun. 2016.

[79] Y. Li, Z. Wang, D. Jin, L. Zeng, and S. Chen, "Collaborative vehicular content dissemination with directional antennas," *IEEE Trans. Wireless Commun.*, vol. 11, no. 4, pp. 1301–1306, Apr. 2012.

[80] D. Li, H. Huang, X. Li, M. Li, and F. Tang, "A distance-based directional broadcast protocol for urban vehicular ad hoc network," in *Proc. of 2007 International Conference on Wireless Communications, Networking and Mobile Computing*, Shanghai, China, Oct. 2007, pp. 1520–1523.

[81] S. Sakai, M. Togasaki, and K. Yamazaki, "A note on greedy algorithms for the maximum weighted independent set problem," *Discrete Applied Mathematics*, vol. 126, no. 2-3, pp. 313–322, Mar. 2003.

[82] N. Wisitpongphan, F. Bai, P. Mudalige, V. Sadekar, and O. Tonguz, "Routing in sparse vehicular ad hoc wireless networks," *IEEE J. Sel. Areas Commun.*, vol. 25, no. 8, pp. 1538–1556, Oct. 2007.

[83] World Health Organization, "Speed management: a road safety manual for decision-makers and practitioners," *Global Road Safety Partnership, Geneva*, 2008.

[84] I. Toyoda, T. Seki, K. Iigusa, H. Sawada, Y. Fujita, A. Miura, and N. Orihashi, "Reference antenna model with side lobe for TG3c evaluation," *IEEE 802.15-06/474r0*, Nov. 2006.

[85] A. Maltsev *et al.*, "Channel models for 60 GHz WLAN systems," *IEEE 802.11-09/0334r8*, May 2010.

Publication List

Journal Papers

1. A. Taya, S. Denno, K. Yamamoto, M. Morikura, D. Umehara, H. Murata, and S. Yoshida, "An iterative MIMO receiver employing virtual channels with a turbo decoder for OFDM wireless systems," *IEICE Trans. Commun.*, vol. E98.B, no. 5, pp. 878–889, May 2015.

2. S. Denno, A. Taya, H. Murata, D. Umehara, K. Yamamoto, S. Yoshida, M. Morikura, "Linear precoding with reduced channel state information for base station cooperation," *IEICE Trans. Commun.*, vol. J100-B, no. 3, pp. 270–279, Mar. 2017.

3. A. Taya, T. Nishio, M. Morikura, and K. Yamamoto, "Concurrent transmission scheduling for perceptual data sharing in mmWave vehicular networks," *IEICE Trans. Inf. & Syst.*, vol. E102-D, no. 5, pp. 952–962, May 2019.

4. A. Taya, T. Nishio, M. Morikura, and K. Yamamoto, "Deep-reinforcement-learning-based distributed vehicle position controls for coverage expansion in mmWave V2X," *IEICE Trans. Commun.*, vol. E102-B, no. 10, Oct. 2019 (accepted).

International Conference Papers

1. A. Taya, S. Denno, D. Umehara, M. Morikura, H. Murata, K. Yamamoto, and S. Yoshida, "A virtual layered space-frequency receiver for multiuser MIMO-OFDM systems," in *Proc. of 2011 IEEE 74th Vehicular Technology Conference (VTC Fall)*, San Francisco, USA, Sep. 2011.

2. A. Taya, S. Denno, K. Yamamoto, M. Morikura, D. Umehara, H. Murata, and S. Yoshida, "A virtual successive detection for cooperative MU-MIMO systems with reduced CSI," in *Proc. of 2012 IEEE 75th Vehicular Technology Conference (VTC Spring)*, Yokohama, Japan, May 2012.

3. A. Taya, S. Denno, K. Yamamoto, M. Morikura, D. Umehara, H. Murata, and S. Yoshida, "A successive detector with virtual channel detection for cooperative multiuser MIMO systems," in *Proc. of 9th IEEE Vehicular Technology Society Asia Pacific Wireless Communications Symposium (APWCS)*, Kyoto, Japan, Aug. 2012.

4. A. Taya, S. Denno, K. Yamamoto, M. Morikura, D. Umehara, H. Murata, and S. Yoshida, "Turbo coded successive detector with virtual channels for MIMO-OFDM," in *Proc. of 2012 IEEE International Conference on Wireless Information Technology and Systems (ICWITS)*, Hawaii, USA, Nov. 2012.

5. S. Denno, A. Taya, and M. Morikura, "A virtual channel detector for iterative receiver in overloaded MIMO OFDM systems," in *Proc. of 2014 8th International Conference on Signal Processing and Communication Systems (ICSPCS)*, Gold Coast, QLD, Australia, Dec. 2014.

6. A. Taya, T. Nishio, M. Morikura, and K. Yamamoto, "Coverage expansion through dynamic relay vehicle deployment in mmWave V2I communications," in *Proc. of 2018 IEEE 87th Vehicular Technology Conference (VTC Spring)*, Porto, Portugal, June 2018.

7. A. Taya, T. Nishio, M. Morikura, and K. Yamamoto, "Concurrent data dissemination at intersections in mmWave for cooperative perceptions," in *Proc. of IEEE Connected and Automated Vehicles Symposium (CAVS)*, Chicago, USA, Aug. 2018.

Technical Reports and Local Conference Papers

1. A. Taya, S. Denno, D. Umehara, K. Yamamoto, M. Morikura, H. Murata, and S. Yoshida, "Virtual layered space-frequency receivers for multiuser MIMO-

OFDM systems," *IEICE General Conference.*, B-5-94, Tokyo, Japan, Mar. 2011.

2. A. Taya, S. Denno, D. Umehara, K. Yamamoto, M. Morikura, H. Murata, and S. Yoshida, "Virtual layered space-frequency receivers for multiuser MIMO-OFDM systems," *IEICE Technical Report*, RCS2010-302, pp. 313–318, Yokosuka, Japan, Mar. 2011.

3. A. Taya, S. Denno, D. Umehara, K. Yamamoto, M. Morikura, H. Murata, and S. Yoshida, "Virtual channel detection for base station cooperative multiuser MIMO systems with limited channel state information," *IEICE Technical Report*, RCS2011-78, pp. 19–24, Asahikawa, Japan, Jul. 2011.

4. A. Taya, S. Denno, D. Umehara, K. Yamamoto, M. Morikura, H. Murata, and S. Yoshida, "Diversity gain of multi-band cooperative MU-MIMO systems," *IEICE General Conference*, B-5-34, Okayama, Japan, Mar. 2012.

5. A. Taya, T. Nishio, M. Morikura, and K. Yamamoto, "Received signal strength prediction using image data for mmWave connected vehicles," *IEICE Society Conference*, B-15-4, Tokyo, Japan, Sep. 2017.

6. A. Taya, T. Nishio, M. Morikura, and K. Yamamoto, "Coverage expansion of vehicular millimeter wave communication with multi-hop relaying," *IEICE Technical Report*, IEICE-MoNA2017-17, pp. 13–18, Kitakyushu, Japan, Nov. 2017.

7. A. Taya, T. Nishio, M. Morikura, and K. Yamamoto, "Coverage expansion in mmWave V2I communications by deep reinforcement learning based vehicle re-deployment," *IEICE Technical Report*, IEICE-MoNA2017-69, pp. 317–322, Tokyo, Japan, Feb. 2018.

8. A. Taya, T. Nishio, M. Morikura, and K. Yamamoto, "Coverage expansion in mmWave V2I Communications with deep reinforcement learning based vehicle position control methods," *IEICE General Conference*, B-18-37, Tokyo, Japan, Mar. 2018.

9. A. Taya, T. Nishio, M. Morikura, and K. Yamamoto, "Coverage expansion in mmWave V2I communications by deep reinforcement learning based

vehicle re-deployment," *IEICE Technical Report*, RCS2018-15, pp. 73–78, Yamaguchi, Japan, Apr. 2018.

10. A. Taya, T. Nishio, M. Morikura, and K. Yamamoto, "Image sensor data sharing at intersections in mmWave vehicular networks," *IEICE Society Conference*, B-15-3, Kanazawa, Japan, Sep. 2018.

Awards

1. IEEE VTS Japan 2012 Young Researcher's Encouragement Award.
2. IEICE Young Researcher's Award in 2018.